TITLE:

Ellipsometry

PROJECT PERIOD:
September 1st - December 21st 2004

THEME:
Detection of Nanostructures

PROJECT GROUP:
116

GROUP MEMBERS:
Jesper Jung
Jakob Bork
Tobias Holmgaard
Niels Anker Kortbek

SUPERVISOR:
Kjeld Pedersen

NUMBERS PRINTED: 7

REPORT PAGE NUMBER: 70

TOTAL PAGE NUMBER: 132

SYNOPSIS:

This project concerns measurement of the refractive index of various materials and measurement of the thickness of thin films on silicon substrates by use of ellipsometry. The ellipsometer used in the experiments is the SE 850 photometric rotating analyzer ellipsometer from Sentech.

After an introduction to ellipsometry and a problem description, the subjects of polarization and essential ellipsometry theory are covered.

The index of refraction for silicon, aluminum, copper and silver are modelled using the Drude-Lorentz harmonic oscillator model and afterwards measured by ellipsometry. The results based on the measurements show a tendency towards, but are not adequately close to, the table values. The materials are therefore modelled with a thin layer of oxide, and the refractive indexes are computed. This model yields good results for the refractive index of silicon and copper. For aluminum the result is improved whereas the result for silver is not.

The thickness of a thin film of SiO_2 on a substrate of silicon is measured by use of ellipsometry. The result is 22.9 nm which deviates from the provided information by 6.5 %.

The thickness of two thick (multiple wavelengths) thin polymer films are measured. The polymer films have been spin coated on substrates of silicon and the uniformities of the surfaces are investigated. The two polymer films are measured to be 3.32 and 4.17 μm on average with a maximum deviation from the mean across the surface of 3.0 % and 4.2 % respectively.

Preface

This project is written by group 116 at the Institute of Physics and Nanotechnology, Aalborg University, in the period between September 1st 2004 and December 21st 2004. The theme for the 7th semester project on Applied Physics is "Detection of Nanostructures" under which the project "Ellipsometry" has been chosen.

The main report consists of three parts. The *Preanalysis*, the *Ellipsometry Theory* and the *Simulations and Experiments*. The three parts begins with a short introduction and consists of several chapters each starting with a description of the contents. The main report treats subjects that have direct relevance to ellipsometry and the ellipsometric measurements performed during this project.

In addition to the main report several subjects are treated in appendixes which can be found after the bibliography. The appendixes treat subjects of general theory of light waves, optics and properties of materials. Also included in the appendixes are some of the more extensive calculations and test descriptions of the performed tests.

Enclosed on the inside of the back page is the project CD, containing test data, source code etc. References to files on this CD e.g. Matlab® programs, are written in square brackets containing the path and filename with extension like this: [CD 2004, matlab/polymer_thickness/film_thickness_polymer.m]. References to other sources are written in similar manner, where the author and year of publishing refer to the bibliography, where further information about the source can be found. References to a source can be found at the end of a section, where the use of the source ends. The reference to a source might also contain a page number if necessary, e.g. [Azzam & Bashara 1977, p. 245]. A citation before a punctuation means that the reference is to the sentence only. A citation after a punctuation means that the reference is related to the whole paragraph.

Regarding the notation throughout the report it has been decided to use [Klein & Furtak 1986] as a general guideline, e.g. vectors will be boldfaced $\mathbf{E}$ and matrixes will be boldfaced Arial $\mathbf{A}$. In the cases that [Klein & Furtak 1986] does not cover the notation, the notation of the used source is adapted. The symbol j will be used as the imaginary unit.

Aalborg University, Tuesday 21st 2004

Jesper Jung

Jakob Bork

Tobias Holmgaard

Niels Anker Kortbek

Contents

Introduction

Optical measurement techniques in development and production are of great interest since these techniques are normally non-invasive. Using these techniques involves no physical contact with the surface and does not normally destruct the surface. This is a notable property of a measurement technique on nanoscale. Only surfaces that are sensitive to bleaching can be subject to damage by optical measurements. There are several optical measurement techniques based on the reflection or transmission of light from a surface, among these are interferometry, reflectometry and ellipsometry. There are three different types of ellipsometry, namely scattering, transmission and reflection ellipsometry. This project concerns reflection ellipsometry only.

Ellipsometry normally requires some computer power to get results and therefore, the technique has only recently become widely used, although it has been known and used since Paul Drude proposed it over 115 years ago. [Poksinski 2003, p. 1]

Ellipsometry can be used to measure any physical property of an optical system that will induce a change in polarization state of the incident light wave. This makes ellipsometry a very versatile technology that is useful in many different applications.

One possible application is in the semiconductor industry. This industry often deals with a thin layer of SiO_2 on a silicon wafer used throughout production. In order to keep track and effectively control the thickness of this film, process engineers can use ellipsometry to measure the film thickness of selected sample wafers. Ellipsometry is known for the high accuracy when measuring very thin film, with a thickness in the Ångström scale or below. When measuring thicker films the technique becomes more complex and requires more calculations.

Other possible applications of ellipsometry are determination of the refractive index, the surface roughness or the uniformity of a sample and more. [Jawoollam 2004]

This project addresses the issue of ellipsometry as a way of determining physical properties of an optical system. A Sentech SE 850 ellipsometer has been put at disposal for the group in order to perform test of various samples. This leads to the goal of the project

The goal of this project is to determine the complex index of refraction of several materials and the thickness of films by ellipsometric measurements.

1

Part I

Preanalysis

The first part contains a short introduction to ellipsometry and the different terms used in connection with the technique. All important terms mentioned in this part will be described in depth later in the report. After this introduction, a problem description will line up the purposes and more specific goals within this project.

Introduction to Ellipsometry

<div align="right">

1

</div>

Ellipsometry is generally a non-invasive, non-destructive measurement technique to obtain optical properties of a sample material by means of the reflected light waves. The technique measures a relative change in polarization and is therefore not dependent on absolute intensity as long as the absolute intensity is sufficient. This makes ellipsometric measurement very precise and reproducible.

Ellipsometry uses the fact that linearly polarized light at an oblique incidence to a surface changes polarization state when it is reflected. It becomes elliptically polarized, thereby the name "ellipsometry". In some cases elliptically polarized light is used as the incident light wave. The idea of ellipsometry is shown in general in Figure 1.1.
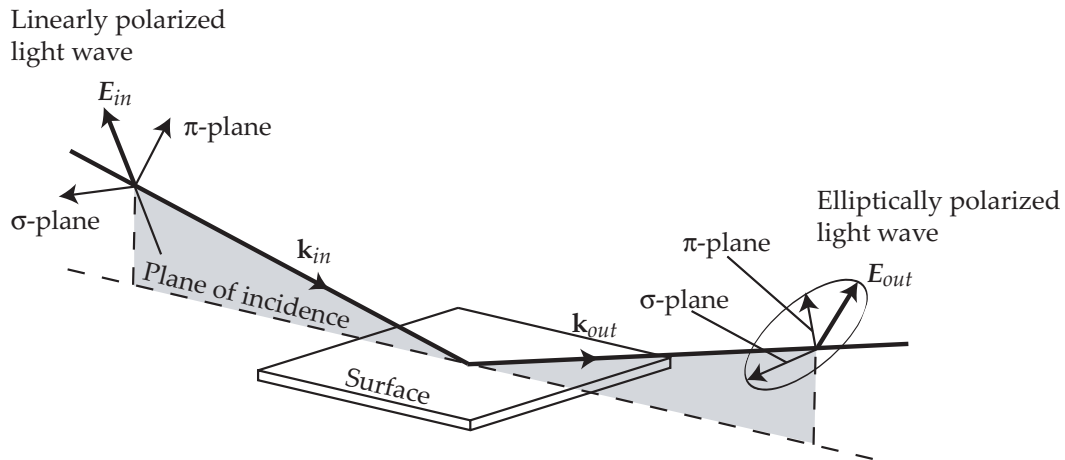
Figure 1.1: The general principle in ellipsometry. [Jawoollam 2004]

When a monochromatic, plane light wave is directed at a surface at oblique incidence, the plane of incidence is defined as a plane perpendicular to the surface and containing the vector which points in the direction of propagation of the light wave. This vector is called the wavevector $\mathbf{k}_{in}$. Perpendicular to $\mathbf{k}_{in}$ are the two mutually perpendicular vectors for the electric field $\mathbf{E}$ and the magnetic field $\mathbf{B}$ of the light wave. The $\mathbf{E}$-vector is chosen as the vector defining the polarization of the light wave and is therefore the only one shown in Figure 1.1. The $\mathbf{E}$-vector is decomposed into two components, which are mutually perpendicular and perpendicular to $\mathbf{k}_{in}$. The two components of $\mathbf{E}$ are respectively parallel and perpendicular to the plane of incidence as seen in Figure 1.1. The vectors are named from their German names, "Parallel" and "Senkrecht", and are from this given the corresponding Greek letters π and σ, respectively.

The incident light wave is linearly polarized. Polarization will be described in depth later, but for now the π- and σ-component of $\mathbf{E}$ can be seen as oscillating with an amplitude

and mutual phase causing the endpoint of **E** to move in a straight line in the plane of the π- and σ-components. When the light wave reflects off the surface, the polarization changes to elliptical polarization. This means that the amplitude and mutual phase of the π- and σ-component of **E** are changed causing the endpoint of **E** to move in an ellipse.

The form of the ellipse can be measured by a detector and data processing can relate this to the ellipsometric parameters ψ and Δ. The ellipsometric parameters can be related to the reflection coefficients of the light polarized parallel and perpendicular to the plane of incidence ρ_π and ρ_σ, respectively. The relation is the basic equation in ellipsometry and is given by the complex ratio ρ of the two reflection coefficients

$$\rho = \frac{\rho_\pi}{\rho_\sigma} = \tan(\psi)e^{j\Delta} \tag{1.1}$$

The ellipsometric parameters ψ and Δ are given by a measurement with an ellipsometer and the two reflection coefficients are functions of the complex refractive index of the material.

Ellipsometry is often used to measure the thickness of thin films on top of a substrate. A simplified model of this is shown in Figure 1.2 where an incident light wave is reflected off and transmitted through the surface of a thin film. If the refractive indexes of the film and the substrate are known, it is possible to calculate the thickness d of the thin film by ellipsometry. This application of ellipsometry is widely used to investigate materials and surfaces.
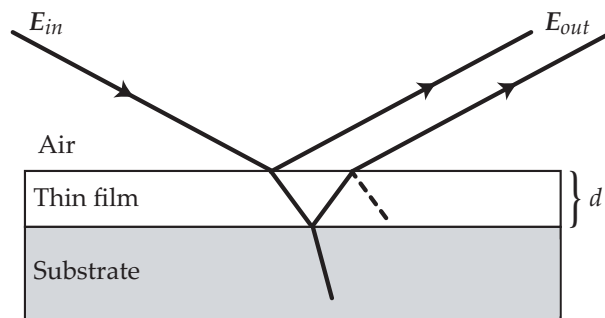
Figure 1.2: Illustration of a thin film on top of a crystal.

Problem Description 2

There are two overall objectives in this project. These are to determine the refractive index of various materials and to determine the thickness of various films by ellipsometry. The materials at hand in this project for measuring the index of refraction are silicon, aluminum, copper and silver. The materials with a film on a substrate are silicon with a silicon dioxide film and silicon with a polymer film.

The following requirements are to be met in this project.

1. **Theoretical**

    (a) Modelling of the optical system under investigation in order to enable calculation of refractive index and film thickness.

2. **Simulation**

    (a) Simulation of the refractive index of silicon, aluminum, copper and silver.

3. **Experiments**

    (a) Refractive Index — Use ellipsometry to measure the refractive index of silicon, aluminum, copper and silver.
    (b) Thickness of thin SiO_2 film — Measurement of the thickness of a thin film of silicon dioxide on a silicon wafer.
    (c) Thickness and uniformity of polymer film — Measurement of the thickness of two optically thick polymer films on substrates of silicon. Furthermore, several measurements of the thickness of the polymers should be performed in order to illustrate the uniformity of the surfaces.

All materials except the SiO_2 and polymer films are provided by the Institute of Physics and Nanotechnology at Aalborg University. The SiO_2 film sample is a test wafer from Sentech. The test wafer has a known film thickness. Two polymer films are imposed on silicon wafers by NanoNord A/S. The polymers are spin coated on the wafers and afterwards baked at high temperature as prescribed by the manufacturer of the polymer. The polymer is manufactured by HD MicroSystems and is called PI-5878G. The two samples differ only in the angular speed of the spin coating which should yield different thicknesses of the polymer. Estimates from NanoNord suggest that the polymers are 2 and 5 μm, but these estimates are very loose.

Part II

Ellipsometry Theory

This part contains three chapters. The first concerns polarization of light, where elliptically polarized light is of special interest. Also treated in this chapter is the correlation between the ellipsometric parameters and the Fresnel reflection coefficients. The second chapter concerns ellipsometer systems. In this chapter a description of different ellipsometer configurations is given. The ellipsometer used in the tests is also described in this chapter. The last chapter in this part concerns calculation of refractive index and film thickness by use of measured ellipsometric parameters.

Polarization of Light

3

This chapter describes the polarization of light. Three types of polarization will be introduced. These are linearly, circularly and elliptically polarized light. The descriptions of these polarization types will be limited to treat monochromatic plane waves only. Apart from this, a description of unpolarized light will be given. Finally, the ellipsometric parameters ψ and Δ will be introduced.

This chapter is mainly based on [Klein & Furtak 1986, pp. 585-596] and the definitions derived in Appendix A.

3.1 Definition of Polarization

From the description of monochromatic plane light waves, treated in Appendix A, it can be seen that light consists of an electric field $\mathbf{E}$ and a magnetic field $\mathbf{B}$. The connection between these and the direction of propagation is given by (A.28) and rewritten here

$$\mathbf{B} = \frac{\mathbf{k} \times \mathbf{E}}{\omega} \tag{3.1}$$

where the direction of propagation is the direction of $\mathbf{k}$. It is seen that electromagnetic waves are transverse waves, i.e. $\mathbf{E}$ and $\mathbf{B}$ are mutually perpendicular and perpendicular to $\mathbf{k}$. As a consequence, $\mathbf{E}$ can point in any direction perpendicular to $\mathbf{k}$. Thus $\mathbf{E}$ has two degrees of freedom, i.e. it is "free" to move in a 2-dimensional coordinate system. This can be seen in opposition to longitudinal waves, which are bound to point in the direction of propagation. This extra degree of freedom implies the existence of different polarization states, which in the following will be divided into some basic types. But first, some general definitions will be stated.

The polarization direction of light is defined as the direction of $\mathbf{E}$. When $\mathbf{E}$ is known, $\mathbf{B}$ can readily be deduced, direct or indirect from Maxwell's equations, e.g. from (3.1).

In the following, a right-handed system of coordinates is used, where the z-axis is defined as the direction of propagation. Thus, the E-field can be described as a linear combination of an x- and y-component

$$\mathbf{E}(z,t) = E_x\hat{\mathbf{x}} + E_y\hat{\mathbf{y}} \tag{3.2}$$

where

$$E_x(z,t) = A_x \cos(\omega t - kz + \phi_x) \tag{3.3a}$$
$$E_y(z,t) = A_y \cos(\omega t - kz + \phi_y) \tag{3.3b}$$

as described in (A.24).

If only the polarization state is of interest, the temporal and spatial dependencies can be omitted. Thus, by using the Jones formalism, which is described in Appendix D, (3.3) can be expressed by a Jones vector

$$\mathbf{E} = \begin{bmatrix} E_x \\ E_y \end{bmatrix} = \begin{bmatrix} A_x e^{j\phi_x} \\ A_y e^{j\phi_y} \end{bmatrix} \tag{3.4}$$

as described in (D.6) and (D.7). (3.4) entirely describes the polarization of light. Whether the light is described using the Jones formalism (3.4) or with the temporal and spatial information included (3.3), the essential parameters are the relative phase ϕ defined as

$$\phi = \phi_y - \phi_x \tag{3.5}$$

and the relative amplitude, which is a relation between A_x and A_y.

3.2 Polarization Types

In the following some basic polarization types will be defined.

3.2.1 Linearly Polarized Light

Linearly polarized (LP) light[1] is the most straightforward example of polarized light. Light is linearly polarized when $\mathbf{E}(z)$ and $\mathbf{E}(t)$ oscillates on a bounded straight line projected in the xy-plane, with the center at $(0,0)$. This occurs when

$$\phi = \pm p\pi \, , \text{ for } p = \{0, 1, 2, \cdots\} \tag{3.6}$$

which imply

$$E_y = \pm \frac{A_y}{A_x} E_x \tag{3.7}$$

Hence, E_y is a linear function of E_x, and vice versa, as both A_x and A_y are constants. An illustration of the projection of LP light in the xy-plane can be found in Figure 3.1(a). A depiction of $\mathbf{E}$ with respect to z, where the time is held constant, can be found in Figure 3.1(b).

Note

The requirement to the phase stated in (3.6) is only requisite when both $A_x \neq 0$ and $A_y \neq 0$. If $A_x = 0$ or $A_y = 0$, the light is linearly polarized.

3.2.2 Circularly Polarized Light

Light is circularly polarized (CP) when $\mathbf{E}$, with respect to t as well as z, defines a circle projected in the xy-plane. Thus, the following phase-relation must hold

$$\phi = \frac{\pi}{2} \pm p\pi \, , \text{ for } p = \{0, 1, 2, \cdots\} \tag{3.8}$$

---

[1]Linearly polarized light is also denoted plane polarized light.

(a) Depiction of **E** in the xy-plane.

(b) Illustration of $\mathbf{E}(z)$.
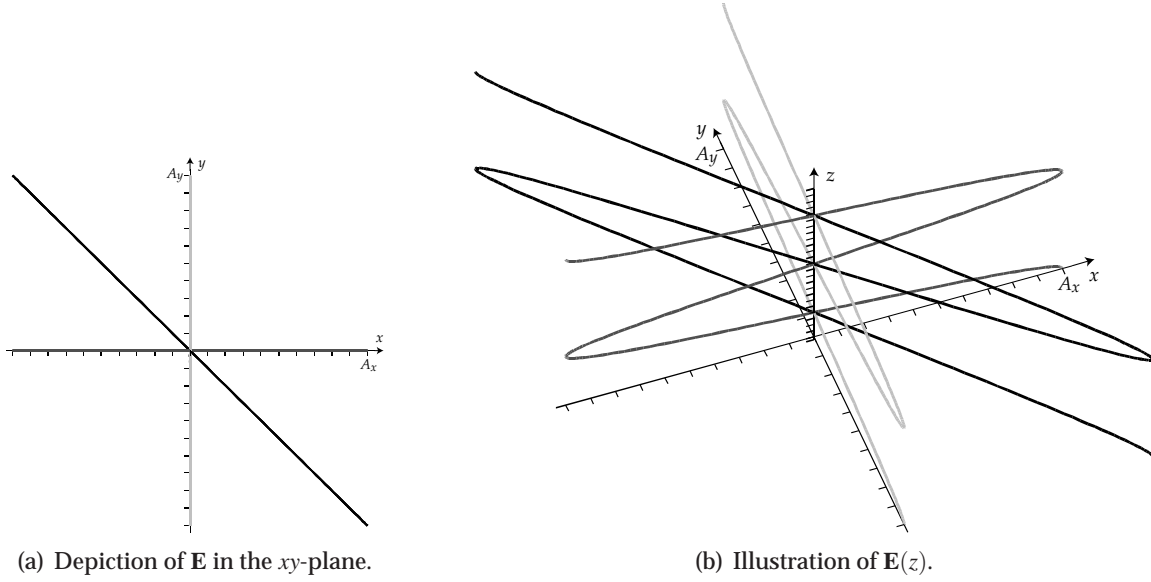
Figure 3.1: Illustration of linearly polarized light for $\phi = \pi$ and $A_x = A_y$. E_x and E_y are illustrated by the dark and light grey curve, whereas the total electric field is illustrated by the black curve.

and the following amplitude relation must be fulfilled

$$A_x = A_y \neq 0 \tag{3.9a}$$

or

$$A_x = -A_y \neq 0 \tag{3.9b}$$

but the latter is not taken into account in the following, as (3.9b) can be expressed using (3.9a) with a extra phase difference of π. It is seen that the direction of rotation projected in the xy-plane depends of ϕ. The two directions are denoted RCP (Right Circularly Polarized)[2] and LCP (Left Circularly Polarized) respectively. LCP occurs when **E** rotates clockwise with respect to z when viewed along the negative direction of the z-axis. This can be seen in Figure 3.2(a). A spatial depiction of LCP light with respect to z can be found in Figure 3.2(b). When LCP light is described with respect to t, the rotation will consequently be in the counterclockwise direction. LCP occurs when $\phi = -\pi/2 \pm 2p\pi$, where $p = \{0, 1, 2, \cdots\}$. Naturally the direction of rotation of RCP is opposite to LCP both with respect to z and t. RCP occur when $\phi = \pi/2 \pm 2p\pi$, where $p = \{0, 1, 2, \cdots\}$.

The fact that **E** defines a circle in the xy-plane when (3.8) and (3.9) are met, can be seen from the following. If $\phi = \pm\pi/2$, and $A_x = A_y = A$, then (3.3) can be expressed as

$$E_x = A\cos(\omega t - kz + \phi_x) \tag{3.10a}$$

$$E_y = A\cos(\omega t - kz + \phi_x \pm \frac{\pi}{2})$$

$$= \mp A\sin(\omega t - kz + \phi_x) \tag{3.10b}$$

---

[2]The name RCP origins from the appearance of a normal screw, where the spiral groove has the same shape as RCP light with respect to z if the screw is placed in the z-axis [Klein & Furtak 1986, p. 588].

(a) Depiction of $\mathbf{E}(z)$ in the xy-plane.

(b) Illustration of $\mathbf{E}(z)$.
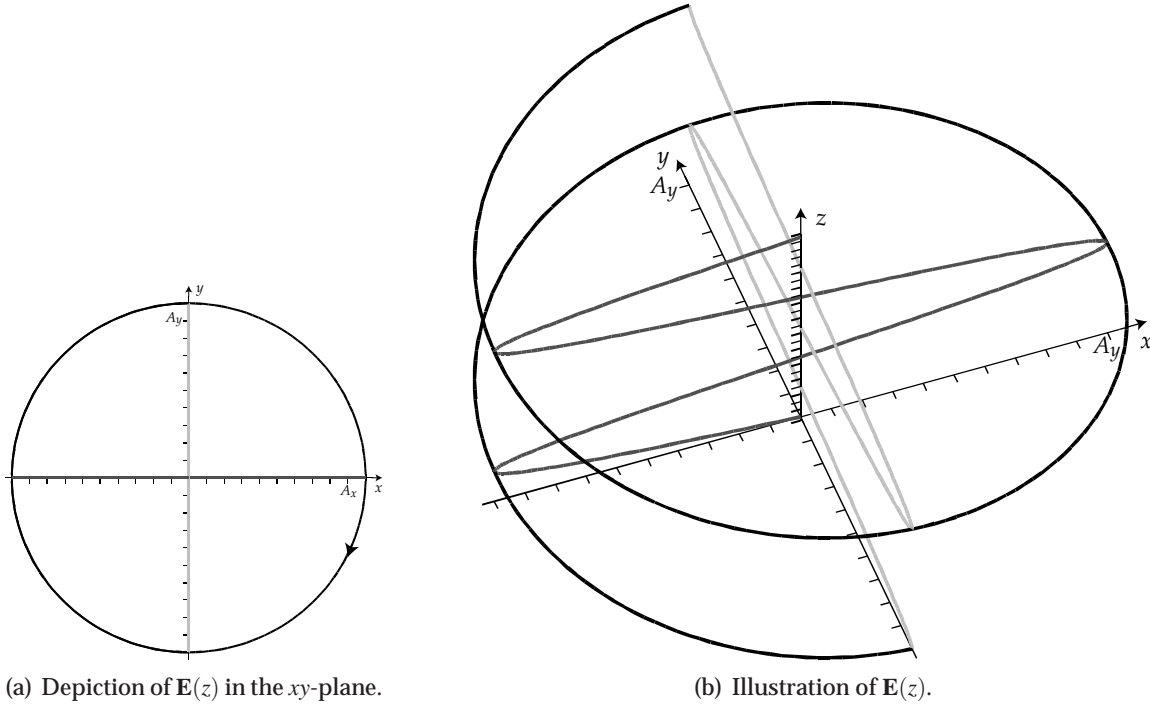
Figure 3.2: Illustration of LCP light ($\phi = -\pi/2$) and $A_x = A_y$. E_x and E_y are illustrated by the dark and light grey curve, whereas the total electric field are illustrated by the black curve.

Adding the squared of (3.10a) to the squared of (3.10b) yields

$$E_x^2 + E_y^2 = (A\cos(\omega t - kz + \phi_x))^2 + (\mp A\sin(\omega t - kz + \phi_x))^2$$
$$= A^2(\cos^2(\omega t - kz + \phi_x) + \sin^2(\omega t - kz + \phi_x))$$
$$= A^2 \tag{3.11}$$

where it is observed that (3.11) is the representation of a circle with the center in $(0,0)$.

3.2.3 Elliptically Polarized Light

If $\mathbf{E}$ with respect to z and t describes an ellipse projected in the xy-plane, the light is denoted elliptically polarized (EP). First, a simple description of EP light is considered.

Description of Elliptically Polarized Light Starting From Circularly Polarized Light

Starting from the description of CP light, the restriction to the phase given by (3.8) is kept, whereas the amplitude relation given by (3.9) is discarded. This is done in order to allow $A_x \neq A_y$. A_x and A_y must however still be nonzero. Similarly as in (3.11) it is seen that

$$\frac{E_x^2}{A_x^2} + \frac{E_y^2}{A_y^2} = 1 \tag{3.12}$$

which is the description of an ellipse with the major and minor axis along the x- and y-axis.

General description of Elliptically Polarized Light

In general, no restrictions to the relation between the amplitudes A_x and A_y or the phase difference ϕ exist for EP light. The general case of EP light can then be stated using (3.3) as

$$E_x = A_x \cos(\omega t - kz) \tag{3.13a}$$
$$E_y = A_y \cos(\omega t - kz + \phi) \tag{3.13b}$$

which can be written as

$$\frac{E_x}{A_x} = \cos(\omega t - kz) \tag{3.14a}$$
$$\frac{E_y}{A_y} = \cos(\omega t - kz)\cos(\phi) - \sin(\omega t - kz)\sin(\phi) \tag{3.14b}$$

Multiplying (3.14a) with $\cos(\phi)$ and subtracting the result from (3.14b) yields

$$\frac{E_y}{A_y} + \frac{E_x}{A_x}\cos(\phi) = -\sin(\omega t - kz)\sin(\phi) \tag{3.15}$$

$$= -\sin(\phi)\sqrt{1 - \cos^2(\omega t - kz)} \tag{3.16}$$

Squaring this, results in

$$\frac{E_y^2}{A_y^2} + \frac{E_x^2}{A_x^2}\cos^2(\phi) - 2\frac{E_x E_y}{A_x A_y}\cos(\phi) = [1 - \cos^2(\omega t - kz)]\sin^2(\phi) \tag{3.17}$$

Substituting the squared of (3.14a) into (3.17) yields

$$\frac{E_y^2}{A_y^2} + \frac{E_x^2}{A_x^2}\cos^2(\phi) - 2\frac{E_x E_y}{A_x A_y}\cos(\phi) = \left[1 - \left(\frac{E_x}{A_x}\right)^2\right]\sin^2(\phi) \tag{3.18}$$

or

$$\frac{E_y^2}{A_y^2} + \frac{E_x^2}{A_x^2} - 2\frac{E_x E_y}{A_x A_y}\cos(\phi) + \cos^2(\phi) = 1 \tag{3.19}$$

which defines an ellipse in the xy-plane. It is seen from (3.19) that if $\phi = p\pi$, for $p = \{\cdots, -2, -1, 0, 1, 2, \cdots\}$, then

$$E_y = ((-1)^p)\frac{A_y}{A_x}E_x \tag{3.20}$$

which, as expected results in the definition of LP light. Similarly if $\phi = p\pi/2$, then

$$\frac{E_y^2}{A_y^2} + \frac{E_x^2}{A_x^2} = 1 \tag{3.21}$$

which is EP light with the major axis along the x- or y-axis; or if $A_x = A_y$ it is CP light. Thus, LP and CP light are both special cases of EP light. It is clear that the ellipse described in the xy-plane will be inscribed in a rectangle given by A_x and A_y. An illustration of EP light projected in the xy-plane can be seen in Figure 3.3.
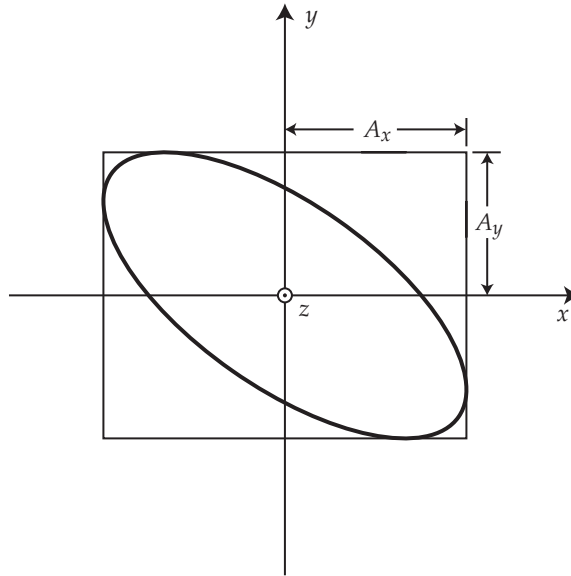
Figure 3.3: Illustration of elliptically polarized light.

3.2.4 Unpolarized Light

Unpolarized light is the term used for light that is not polarized in any defined pattern as the ones stated above. For unpolarized light, the electric field vector fluctuates in a random pattern. If **E** is divided into components described as in (3.2), E_x and E_y will be incoherent. That is, the phase relation of the components will be random. Furthermore, as the field vector fluctuates randomly, the mean value of the magnitude of the field will be the same in all directions perpendicular to the direction of propagation. Thus $\langle A_x^2 \rangle = \langle A_y^2 \rangle$.

3.3 Definition of the ellipsometric parameters ψ and Δ

ψ and Δ angles will in the following be defined as quantities describing the reflected light, when linearly polarized light is incident on a surface. A depiction of the orientations of the coordinate systems for the incident and the reflected E-field in relation to the surface can be seen in Figure 3.4. Using the definition of the Jones vector, a new term χ is defined as the ratio between the components in the Jones vector, namely

$$\chi = \frac{E_y}{E_x} \tag{3.22}$$

The surface can be viewed as a system with the incident E-field $\mathbf{E_i}$ as the input and the reflected E-field $\mathbf{E_o}$ as the output. This is illustrated in Figure 3.5 in terms of χ. The term of interest is the relation describing the optical system S, which is given as χ_i/χ_o, thus

$$\frac{\chi_i}{\chi_o} = \frac{\frac{E_{iy}}{E_{ix}}}{\frac{E_{oy}}{E_{ox}}} = \frac{E_{iy}E_{ox}}{E_{ix}E_{oy}} \tag{3.23}$$
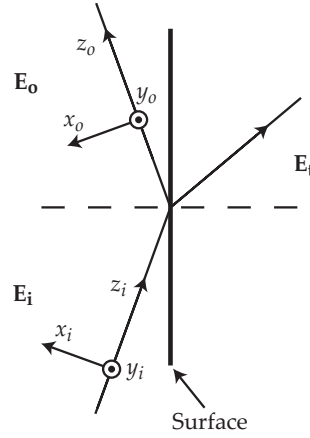
Figure 3.4: Illustration showing the orientation of the coordinate systems relative to the sample surface. $\mathbf{E_i}$ is the incident or input E-field, $\mathbf{E_o}$ is the reflected or output E-field and $\mathbf{E_t}$ is the transmitted E-field. y is parallel with the surface.
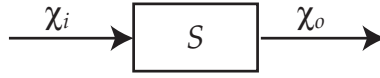
Figure 3.5: Input χ_i and output χ_o to an optical system S.

Rewriting this expression using the Jones vector, (3.4) yields

$$\frac{\chi_i}{\chi_o} = \frac{A_{iy}e^{j\phi_{iy}}}{A_{ix}e^{j\phi_{ix}}} \frac{A_{ox}e^{j\phi_{ox}}}{A_{oy}e^{j\phi_{oy}}} \tag{3.24}$$

$$= \frac{A_{iy}}{A_{ix}}e^{j(\phi_{iy}-\phi_{ix})}\frac{A_{ox}}{A_{oy}}e^{j(\phi_{ox}-\phi_{oy})} \tag{3.25}$$

If the incident light is linearly polarized with $\phi_i = 0$ and $A_{ix} = A_{iy}$, then (3.25) is given as

$$\frac{\chi_i}{\chi_o} = \frac{A_{ox}}{A_{oy}}e^{j(\phi_{ox}-\phi_{oy})} \tag{3.26}$$

which only contains information for the elliptically polarized reflected light. For the reflected light, the parameter ψ is defined in order to satisfy the following

$$\tan\psi = \frac{A_{ox}}{A_{oy}} \tag{3.27}$$

This is illustrated in Figure 3.6.
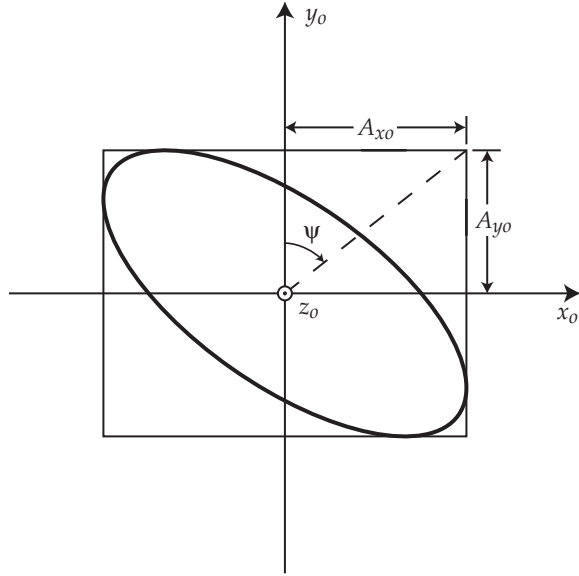
Figure 3.6: Illustration of ψ, which is defined for reflected elliptically polarized light.

Furthermore, the parameter Δ is defined as

$$\Delta = \phi_{ox} - \phi_{oy} \tag{3.28}$$

Using (3.27) and (3.28), (3.26) can be expressed as

$$\frac{\chi_i}{\chi_o} = \tan(\psi)e^{j\Delta} \tag{3.29}$$

which is a general ellipsometer equation [Azzam & Bashara 1977, p. 259].

3.3.1 Connecting ψ and Δ to ρ_π and ρ_σ

The Fresnel reflection coefficients are introduced in Appendix B as the reflected amount of the E-field in proportion to the incident amount. This is viewed either parallel (π) or perpendicular (σ) to the plane of incidence as

$$\rho_\pi = \left| \frac{\mathbf{E}_{o\pi}}{\mathbf{E}_{i\pi}} \right| \tag{3.30a}$$

$$\rho_\sigma = \left| \frac{\mathbf{E}_{o\sigma}}{\mathbf{E}_{i\sigma}} \right| \tag{3.30b}$$

where all $\mathbf{E}$-vectors are Jones vectors. By fixing the xy-coordinate system to the sample surface so that x is parallel to the plane of incidence and y is perpendicular to the plane of

incidence, (3.23) can be rewritten to

$$\frac{\chi_i}{\chi_o} = \frac{E_{iy}E_{ox}}{E_{ix}E_{oy}} \tag{3.31}$$

$$= \frac{|\mathbf{E}_{i\sigma}|\,|\mathbf{E}_{o\pi}|}{|\mathbf{E}_{i\pi}|\,|\mathbf{E}_{o\sigma}|} \tag{3.32}$$

$$= \frac{\frac{|\mathbf{E}_{o\pi}|}{|\mathbf{E}_{i\pi}|}}{\frac{|\mathbf{E}_{o\sigma}|}{|\mathbf{E}_{i\sigma}|}} \tag{3.33}$$

$$= \frac{\rho_\pi}{\rho_\sigma} \tag{3.34}$$

Inserting this expression into (3.29) yields

$$\frac{\rho_\pi}{\rho_\sigma} = \tan(\psi)e^{j\Delta} \tag{3.35}$$

which correlates the ellipsometric parameters to the Fresnel reflection coefficient of a surface. This correlation is utilized throughout the rest of the report to derive expressions for e.g. the refractive index of a material as a function of ψ and Δ.

Ellipsometer Systems

<div style="text-align: right">4</div>

This chapter concerns the operational principle of ellipsometers. First a general introduction to ellipsometers is given which explains the different components encountered in an ellipsometer. After this introduction to ellipsometers, two different ellipsometer configurations are described, namely the null and the photometric ellipsometer. After this, the problem of measuring the ellipsometric parameters ψ and Δ with a photometric rotating analyzer ellipsometer is treated. Finally a description of the Sentech SE 850 ellipsometer used in this project is given.

4.1 Description of an Ellipsometer

Ellipsometry is generally defined as the task of measuring the state of polarization of a wave. In the case of an optical system the wave of interest would be a light wave. Although the polarization state of a light wave itself can be of interest, in reflection ellipsometry the change in polarization is the essential issue. This change in polarization as the light is reflected at a surface boundary is caused by difference in Fresnel reflection coefficients as described in Appendix B. These coefficients are different for π and σ polarized light. A general ellipsometer configuration is depicted in Figure 4.1. As can be seen from the figure an ellipsometer
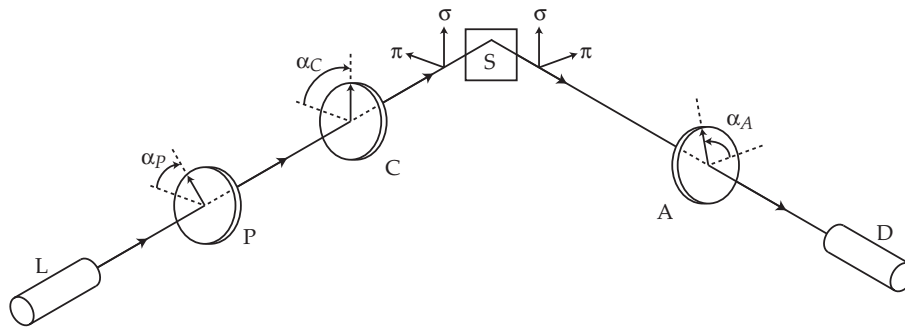
Figure 4.1: Illustration of a general ellipsometer setup. Light is emitted from the source L, passes through the linear polarizer P and the compensator C before it is reflected at the surface boundary S. After reflection the light again passes a linear polarizer denoted the analyzer A before it reaches the detector D. [Azzam & Bashara 1977, p. 159]

generally consists of six parts:

The light source which emits circularly or unpolarized light. This can be either a laser or some type of lamp. A laser has the advantage of emitting very intense and well collimated light which produces a very small spot size on the sample. It is however not possible to use a laser to perform spectroscopic measurements as the laser contains

only one wavelength. However a lamp made of e.g. Xenon emits light at many different wavelengths enabling spectroscopic measurement.

The linear polarizer which converts the incoming light to linearly polarized light. The rotational azimuth angle of the polarizer relative to the direction of the π linear eigenpolarization is denoted α_P in the figure. This angle is the angle from the plane of incidence to the transmission axis of the polarizer.

The compensator or linear retarder, retards the two perpendicular components of the electrical vector by different amounts thus alternating the polarization state of the wave. The azimuth angle of the compensator α_C is measured relative to the direction of the π eigenpolarization.

The surface where a fraction of the light wave is transmitted and another is reflected due to the Fresnel reflection and transmission coefficients ρ_π, ρ_σ, τ_π and τ_σ as described in Appendix B.

The analyzer is a linear polarizer at a rotational azimuth angle α_A relative to the π direction of the linear eigenpolarization.

The detector measures the intensity of the light from the analyzer. The detector can be any device able to measure the intensity of a light wave.

Upon making ellipsometric measurements of a surface the rotational angles of the polarizer, the compensator and the analyzer and the degree of retardation in the compensator must be known in order to determine the ellipsometric parameters ψ and Δ. There exists a variety of ways to perform the task of determining the ellipsometric parameters. In the next section the principles behind two such methods are described.

4.2 Different Ellipsometer Configurations

In this section two general ellipsometer configurations are described; the null and the photometric ellipsometer.

4.2.1 Null Ellipsometer

The null ellipsometer was historically the first ellipsometer, to be constructed. An illustration of the general structure of the null ellipsometer and the polarization state of the light between the components is shown in Figure 4.2. The principle behind this ellipsometer type is to minimize the intensity of the light wave at the detector. This is done by adjusting the rotational azimuth angle of the polarizer P, the compensator C and the analyzer A. As illustrated in the figure the source emits unpolarized light, which is made linearly polarized by the polarizer. By adjusting the azimuth angle of the polarizer and compensator the light can be made linearly polarized after reflection at the surface boundary. By adjusting the azimuth angle of the analyzer in order to achieve a perpendicular orientation relative to the linearly polarized wave the light intensity at the detector is minimized or "nulled". The ellipsometric parameters can then be calculated. As the degree of retardation in the compensator
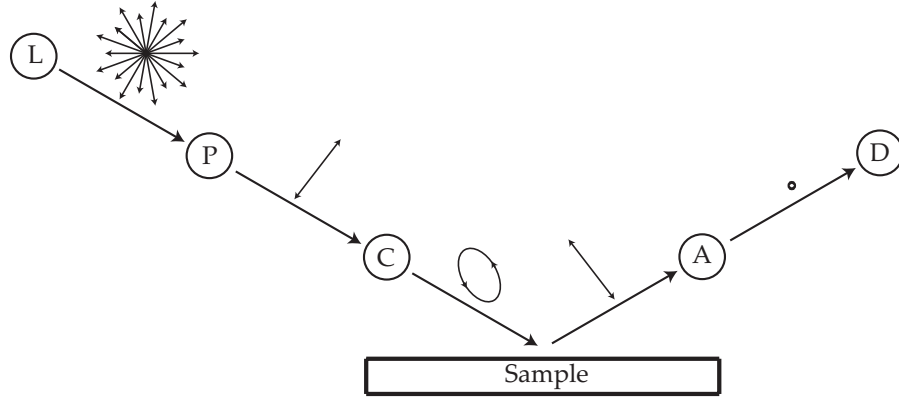
Figure 4.2: A null ellipsometer. The components of the ellipsometer are illustrated by encircled letters. The polarization state between the components is illustrated above. The black dot between the analyzer and the detector illustrates that the light wave intensity has been nulled.

is dependent on wavelength it is not possible to perform spectroscopic measurements in a large range of wavelengths with a null ellipsometer.

By use of the Jones matrix formalism the system matrix for a null ellipsometer can be found.[1] The input to this system matrix must be a Jones vector describing the light wave at the source $\mathbf{E}_{Lo}^{\pi\sigma}$. The superscript shows that the Jones vector is defined relative to the π and σ directions i.e. parallel and perpendicular to the plane of incidence and perpendicular to the direction of propagation. The subscript shows that it is the Jones vector at the light source output. The output Jones vector of the source is the same as the input Jones vector to the polarizer i.e. $\mathbf{E}_{Pi}^{\pi\sigma} = \mathbf{E}_{Lo}^{\pi\sigma}$. The Jones vector at the output of the polarizer is then given as

$$\mathbf{E}_{Po}^{\pi\sigma} = \mathbf{R}(-P)\mathbf{T}_P^{te}\mathbf{R}(P)\mathbf{E}_{Lo}^{\pi\sigma} \tag{4.1}$$

where $\mathbf{R}(P)$ is a Jones matrix that rotates coordinate system from $\pi\sigma$ to te, which is an abbreviation for transmission extinction referring to the fact that a polarizer has a transmission and an extinction axis. $\mathbf{T}_P^{te}$ is the Jones matrix for the polarizer. $\mathbf{R}(-P)$ rotates the Jones vector back to the $\pi\sigma$-coordinate system.

With the Jones vector at the output of the polarizer given, the Jones vector at the output of the compensator is expressed as

$$\mathbf{E}_{Co}^{\pi\sigma} = \mathbf{R}(-C)\mathbf{T}_C^{fs}\mathbf{R}(C)\mathbf{E}_{Po}^{\pi\sigma} \tag{4.2}$$

where $\mathbf{T}_C^{fs}$ is the Jones matrix of the compensator. Again the Jones vector is rotated to the coordinate system of the compensator, which is denoted fs for fast-slow, referring to the fact that a compensator has a fast and a slow axis. The Jones vector at the output side of the surface can be expressed as

$$\mathbf{E}_{So}^{\pi\sigma} = \mathbf{T}_S^{\pi\sigma}\mathbf{E}_{Co}^{\pi\sigma} \tag{4.3}$$

---

[1]See Appendix D for an explanation of the Jones matrix formalism.

where $\mathbf{T}_S^{\pi\sigma}$ is the Jones matrix of the surface. Finally the Jones vector at the output of the analyzer and hence at the detector is given as

$$\mathbf{E}_{Ao}^{te} = \mathbf{T}_A^{te}\mathbf{R}(A)\mathbf{E}_{So}^{\pi\sigma} \tag{4.4}$$

where $\mathbf{T}_A^{te}$ is the Jones matrix of the analyzer. There is no rotational matrix after the analyzer that transforms the Jones vector back to the π, σ system of coordinates. This is because the light detector, in the absence of errors is insensitive to polarization. Thus $\mathbf{E}_o = \mathbf{E}_{Ao}^{te}$

By combining (4.1), (4.2), (4.3) and (4.4), an expression for the Jones vector of the light wave at the detector as a function of the Jones vector of the light wave at the source can be derived

$$\mathbf{E}_o = \mathbf{T}_A^{te}\mathbf{R}(A)\mathbf{T}_S^{\pi\sigma}\mathbf{R}(-C)\mathbf{T}_C^{fs}\mathbf{R}(C-P)\mathbf{T}_P^{te}\mathbf{R}(P)\mathbf{E}_{Lo}^{\pi\sigma} \tag{4.5}$$

This equation describes a null ellipsometer where a compensator has been placed before the surface, but a compensator can also be placed after the surface. In that case the equation describing the system will be

$$\mathbf{E}_o = \mathbf{T}_A^{te}\mathbf{R}(A-C)\mathbf{T}_C^{fs}\mathbf{R}(C)\mathbf{T}_S^{\pi\sigma}\mathbf{R}(-P)\mathbf{T}_P^{te}\mathbf{R}(P)\mathbf{E}_{Lo}^{\pi\sigma} \tag{4.6}$$

The light wave intensity measured at the detector I_o is then given as the multiplication of $\mathbf{E}_o$ with its Hermitian adjoint $\mathbf{E}_o^\dagger$ [Röseler 1990, p. 60]. The Hermitian adjoint of a matrix is defined as the complex conjugate of the transpose of the matrix i.e.

$$I_o = \mathbf{E}^\dagger\mathbf{E} \tag{4.7}$$

In both cases the only unknown is the Jones matrix for the surface $\mathbf{T}_S^{\pi\sigma}$, which can be found if the output intensity is "nulled" and the rotational angles of the polarizer, compensator, analyzer, the relative phase retardation of the compensator and the angle of incidence are known.

4.2.2 Photometric Ellipsometer

In photometric ellipsometry one or more conditions are varied while the light intensity at the detector is measured. This is unlike null ellipsometry, as it is not the means of a photometric ellipsometer to have zero light intensity at the detector. Thus the output of photometric ellipsometry measurements are light intensity values at a number of prescribed conditions. The varied conditions could be the rotational azimuth angle of the polarizer, compensator or analyzer, the relative retardation of the compensator or the angle of incidence. In most cases the varied condition is the angle of the polarizer or analyzer, and thus only these two cases are considered in the following.

Unlike the null ellipsometer the photometric ellipsometer does not necessarily include a retarding element. This has the apparent advantage of making spectroscopic measurements possible as the polarizers generally are achromatic over a wider spectral range than retarders. Other advantages include that polarizers are relatively easy to construct compared to compensators and that they are easy to align within a system. On the other hand a disadvantage is that the system looses sensitivity when Δ is near 0 or $180°$, which will be described further in the next section.
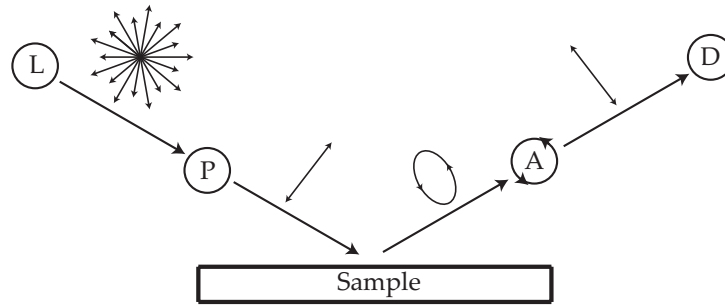
Figure 4.3: A photometric ellipsometer. The components of the ellipsometer are illustrated by encircled letters. The polarization state between the components is illustrated above. The arrows on the circle that illustrates the analyzer shows that it is rotating.

The general structure of a photometric rotating analyzer ellipsometer (RAE) is shown in Figure 4.3. Also shown in the figure is the polarization state between the different components of the ellipsometer. The light source emits unpolarized light, which is linearly polarized by the polarizer. After reflection at the surface boundary the polarization state of the light wave is changed from linearly polarized to elliptical polarized. The analyzer is rotated and the light intensity is measured at different rotational azimuth angles of the analyzer. The general principle behind a rotating analyzer photometric ellipsometer is thus to measure the intensity at different analyzer rotational angles, and from these measurements calculate the ellipsometric parameters ψ, Δ. It is also possible to vary the angle of the polarizer in which case the ellipsometer will be denoted a photometric rotating polarizer ellipsometer (RPE). The operation characteristics of the RAE and the RPE are basically the same, but some disadvantages/disadvantages exist for both configurations. The RPE requires the source to be totally unpolarized in order to perform accurate measurements. Correspondingly the RAE requires photodetectors that are insensitive to polarization in order to minimize errors. [Röseler 1990], [Jawoollam 2004]

Static and Dynamic Photometric Ellipsometers

As mentioned the light intensity is measured when either the angle of the polarizer or the analyzer is varied in a photometric ellipsometer in order to measure the ellipsometric parameters ψ and Δ. This variation can be done in one of two different ways. One is to measure the light intensity at predetermined fixed azimuthal positions. This method is denoted static photometric ellipsometry. The other is to periodically vary the azimuth angle of either or both the analyzer and polarizer with time. The detected signal is then Fourier-analyzed in order to determine ψ and Δ. In the next section a description of a photometric RAE is given by use of the Jones matrix formalism. [Azzam & Bashara 1977, pp. 255-260]

4.3 Determination of ψ and Δ with a Static Photometric RAE

The ellipsometer available in this project is a photometric RAE ellipsometer and thus this section concerns this type of ellipsometer only. This ellipsometer utilizes static analyzer an-

gles in the determination of the ellipsometric parameters in the ultra violet (UV) and visible (VIS) region. As the tests performed in this project are done in the UV-VIS area the static method of determining ψ and Δ is treated. The determination of the ellipsometric parameters ψ and Δ with a photometric RAE is performed by measuring the intensity of the reflected light at three or more analyzer angles and making a calculation of the ellipsometric parameters from these light intensity values. The principles underlying these calculations are explained in this section. In the following the light waves are considered being monochromatic plane waves.

4.3.1 Description of an RAE by use of the Jones Matrix Formalism

Measurement of the ellipsometric parameters of a sample is illustrated in Figure 4.4. The
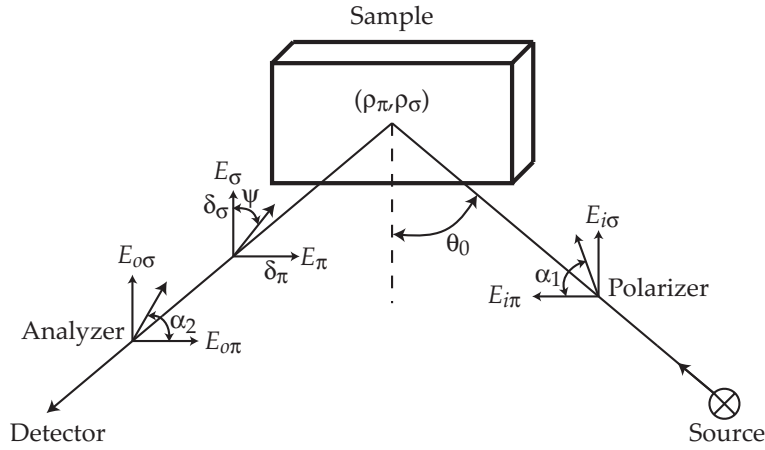
Figure 4.4: Illustration of ellipsometry performed with a photometric RAE without a compensator. [Röseler 1990, p. 73]

light from the source becomes linearly polarized at the fixed polarizer. The Jones vector of the light wave after the polarizer $\mathbf{E}_i^{\pi\sigma}$ is

$$\mathbf{E}_i^{\pi\sigma} = \begin{bmatrix} E_{i\pi} \\ E_{i\sigma} \end{bmatrix} = \begin{bmatrix} E_i\cos(\alpha_1) \\ E_i\sin(\alpha_1) \end{bmatrix} \tag{4.8}$$

where E_i is the magnitude of the Jones vector $\mathbf{E}_i^{\pi\sigma}$ and α_1 is the azimuth angle of the polarizer measured from the direction of the π eigenpolarization.

The light is reflected by the surface, which in Jones notation corresponds to multiplication by the Jones matrix of the surface

$$\mathbf{T}_s^{\pi\sigma} = \begin{bmatrix} \rho_\pi & 0 \\ 0 & \rho_\sigma \end{bmatrix} \tag{4.9}$$

Next the Jones vector of the light wave after the surface must be rotated to the coordinate system of the analyzer by the Jones transform matrix

$$\mathbf{R}(\alpha_2) = \begin{bmatrix} \cos(\alpha_2) & \sin(\alpha_2) \\ -\sin(\alpha_2) & \cos(\alpha_2) \end{bmatrix} \tag{4.10}$$

26

With the Jones vector given in the coordinates system of the analyzer the Jones matrix of the analyzer is given by

$$\mathbf{T}_A^{te} = \begin{bmatrix} 1 & 0 \\ 0 & 0 \end{bmatrix} \tag{4.11}$$

as the analyzer is considered ideal. [Röseler 1990, pp. 60-63], [Azzam & Bashara 1977, p. 76]

The Jones vector at the detector $\mathbf{E}_o^{te}$ can be expressed as

$$\mathbf{E}_o^{te} = \mathbf{T}_A^{te} \mathbf{R}(\alpha_2) \mathbf{T}_s^{\pi\sigma} \mathbf{E}_i^{\pi\sigma} \tag{4.12}$$

$$= \begin{bmatrix} 1 & 0 \\ 0 & 0 \end{bmatrix} \begin{bmatrix} \cos(\alpha_2) & \sin(\alpha_2) \\ -\sin(\alpha_2) & \cos(\alpha_2) \end{bmatrix} \begin{bmatrix} \rho_\pi & 0 \\ 0 & \rho_\sigma \end{bmatrix} \begin{bmatrix} E_i \cos(\alpha_1) \\ E_i \sin(\alpha_1) \end{bmatrix} \tag{4.13}$$

$$= \begin{bmatrix} \cos(\alpha_2)\rho_\pi \cos(\alpha_1)E_i + \sin(\alpha_2)\rho_\sigma \sin(\alpha_1)E_i \\ 0 \end{bmatrix} \tag{4.14}$$

$$= \begin{bmatrix} \cos(\alpha_2)E_\pi + \sin(\alpha_2)E_\sigma \\ 0 \end{bmatrix} \tag{4.15}$$

where $E_\pi = \rho_\pi \cos(\alpha_1)E_i$ and $E_\sigma = \rho_\sigma \sin(\alpha_1)E_i$.

4.3.2 Light Wave Intensity at the Detector

The light wave intensity at the detector I_o is given as

$$I_o = \mathbf{E}_o^\dagger \mathbf{E}_o \tag{4.16}$$

$$= \begin{bmatrix} \cos(\alpha_2)E_\pi^* + \sin(\alpha_2)E_\sigma^* & 0 \end{bmatrix} \begin{bmatrix} \cos(\alpha_2)E_\pi + \sin(\alpha_2)E_\sigma \\ 0 \end{bmatrix} \tag{4.17}$$

$$= \cos^2(\alpha_2)E_\pi E_\pi^* + \sin^2(\alpha_2)E_\sigma E_\sigma^* + \cos(\alpha_2)\sin(\alpha_2)(E_\pi E_\sigma^* + E_\sigma E_\pi^*) \tag{4.18}$$

where the *te* notation is omitted. This expression for the intensity can be rewritten by utilizing the following trigonometric identities [Råde & Westergren 1998, p.124]

$$\cos(\alpha_2)\sin(\alpha_2) = \frac{1}{2}\sin(2\alpha_2) \tag{4.19a}$$

$$\sin^2(\alpha_2) = \frac{1 - \cos(2\alpha_2)}{2} \tag{4.19b}$$

$$\cos^2(\alpha_2) = \frac{1 + \cos(2\alpha_2)}{2} \tag{4.19c}$$

The intensity is then given as

$$I_o = \frac{1}{2}\left(E_\pi E_\pi^* + E_\pi E_\pi^* \cos(2\alpha_2)\right) + \frac{1}{2}\left(E_\sigma E_\sigma^* - E_\sigma E_\sigma^* \cos(2\alpha_2)\right) + \frac{1}{2}\left(E_\pi E_\sigma^* + E_\sigma E_\pi^*\right)\sin(2\alpha_2) \tag{4.20}$$

$$= \frac{1}{2}\left[E_\pi E_\pi^* + E_\sigma E_\sigma^* + \left(E_\pi E_\pi^* - E_\sigma E_\sigma^*\right)\cos(2\alpha_2) + \left(E_\pi E_\sigma^* + E_\sigma E_\pi^*\right)\sin(2\alpha_2)\right] \tag{4.21}$$

$$= \frac{1}{2}\left[s_0 + s_1 \cos(2\alpha_2) + s_2 \sin(2\alpha_2)\right] \tag{4.22}$$

where the three Stokes parameters $s_0 = E_\pi E_\pi^* + E_\sigma E_\sigma^*$, $s_1 = E_\pi E_\pi^* - E_\sigma E_\sigma^*$ and $s_2 = E_\pi E_\sigma^* + E_\sigma E_\pi^*$ are introduced. [Röseler 1990, p. 74]

4.3.3   Determination of ψ and Δ with a Static Photometric RAE

From (4.22) expressions for the light wave intensity at different analyzer angles can be calculated. The light intensity at four specific values of α_2 in steps of $45°$ is

$$I_o(0°) = \frac{1}{2}(s_0 + s_1) \tag{4.23a}$$

$$I_o(45°) = \frac{1}{2}(s_0 + s_2) \tag{4.23b}$$

$$I_o(90°) = \frac{1}{2}(s_0 - s_1) \tag{4.23c}$$

$$I_o(-45°) = \frac{1}{2}(s_0 - s_2) \tag{4.23d}$$

The determination of the ellipsometric parameters ψ and Δ requires only three analyzer angle setting e.g. $\alpha_2 = 0°$, $\alpha_2 = 45°$ and $\alpha_2 = 90°$. Additional measurements would be redundant, but due to practical imperfections in the ellipsometer they might increase the precision of the determined parameter values.

The Stokes parameters are connected to the measured light wave intensities at the detector due to (4.23). The Stokes parameters are furthermore connected to the ellipsometric parameters in Appendix E due to (E.26). Combining these equations yields

$$\cos(2\psi') = \frac{-s_1}{s_0} = \frac{\frac{1}{2}(s_0 - s_1) - \frac{1}{2}(s_0 + s_1)}{\frac{1}{2}(s_0 - s_1) + \frac{1}{2}(s_0 + s_1)} = \frac{I_o(90°) - I_o(0°)}{I_o(90°) + I_o(0°)} \tag{4.24}$$

and

$$\sin(2\psi')\cos(\Delta) = \frac{s_2}{s_0} = \frac{s_0 + s_2}{s_0} = \frac{2I_o(45°)}{I_o(90°) + I_o(0°)} \tag{4.25}$$

where the new variable ψ' is given by the relation

$$\tan(\psi') = \frac{\tan(\psi)}{\tan(\alpha_1)} \tag{4.26}$$

In the case where the polarizer angle is $45°$ i.e. $\alpha_1 = 45°$ the relation reduces to

$$\tan(\psi') = \tan(\psi) \tag{4.27}$$

and hence $\psi' = \psi$.

As can be seen from (4.24) and (4.25) the ellipsometric parameters can, as mentioned above, be calculated from only three measurements of the light wave intensity, however some limitations are present. Δ is determined in the region $0° \leq \Delta \leq 180°$ only. In the region of $\cos(\Delta) \approx 1$ the determined Δ can be very inaccurate because a small variation in $\cos(\Delta)$ causes a large variation in the determined Δ. These problems can be minimized by introducing a retarder in the system. [Röseler 1990, p. 76]

4.4 Description of the Sentech SE 850 Ellipsometer

The ellipsometer used for experiments in this project is the spectroscopic ellipsometer SE 850 from Sentech. This is a photometric RAE ellipsometer that utilizes both static and dynamic measurements. The SE 850 is computer controlled via the Sentech software "Spectraray". The ellipsometer has a range of wavelength from 350 nm to 1700 nm.

During this project it has not been possible to use the NIR part of the ellipsometer due to software failure. This means that the range of wavelength is limited to 350 nm - 850 nm in all measurements.

4.4.1 Functional Description

A block scheme showing the structure of the SE 850 is depicted in Figure 4.5. The ellip-
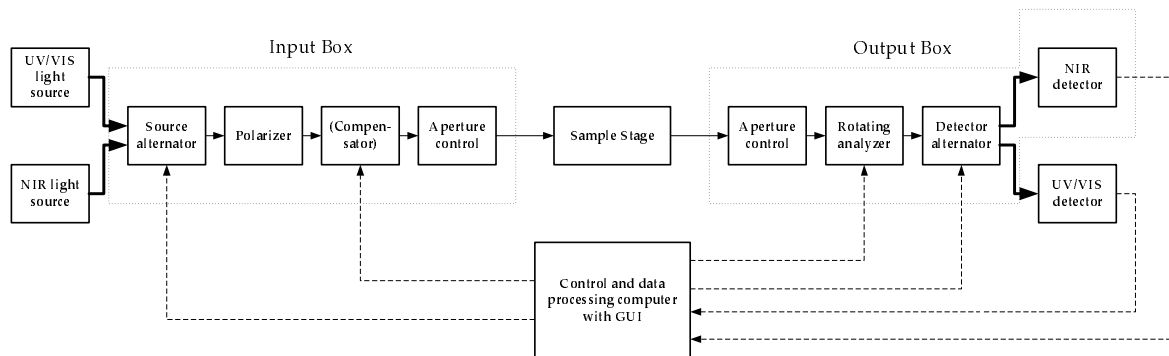
Figure 4.5: A block scheme of the SE 850. Control signals are illustrated with dashed lines, the light waves travelling through air are illustrated by fully drawn lines, and the light waves travelling through optical fibers are illustrated by thick fully drawn lines.

someter is centered around the control and data processing computer. This computer also has a graphical user interface (GUI) in order for the user to initiate the ellipsometric measurement and perform data processing of the measured data. The control signals from and to the computer are shown as dashed lines. These output signals are control signals for the choice of source and detector, control signal for the compensator if this is to be used in the measurement and a control signal for the rotating analyzer. The input signals are the measured intensities from the detectors. The fully drawn lines in the figure illustrate light waves travelling through air. The light wave is propagated through an optical fiber between the sources and the source alternator. The same is the case between the detector alternator and the detectors. The optical fibers are illustrated by thick fully drawn lines. Note that the compensator is enclosed by brackets as this component only is utilized in some special cases. Further specifications of the SE 850 are listed below.

4.4.2 Specifications

The specifications for the SE 850 are found at Sentech's web page [Spectroscopic Ellipsometer SE 850 2004].

UV/VIS Light Source: The light source used for UltraViolet/Visible (UV/VIS) measurements is a 75 W xenon lamp. With this light source measurements in the spectrum from 350 nm to 850 nm can be performed.

NIR Light Source: A halogen lamb is used for measurements in the Near InfraRed (NIR) range between 850 nm to 1700 nm.

UV/VIS Detector: A photodiode array with 1024 elements is used to detect the light intensity in the UV/VIS range. This unit is placed in the control computer cabinet.

NIR Detector: A Fourier Transform InfraRed (FT-IR) photodetector is used in the NIR range. This unit is placed in the output box of the ellipsometer after the source alternator.

Polarizer: The polarizer is fixed at a rotational azimuth angle of $45°$.

Analyzer: The azimuth angle of the analyzer is variable and is controlled by the spectraray software running on the computer.

Compensators: Computer controlled super achromatic retarder for UV/VIS spectral range. (Optional)

Goniometer: The angle of incidence is controlled by a manual goniometer which has a range from $30°$ to $90°$ with a step size of $5°$.

Sample Stage: The sample stage is manually controlled. Possible adjustment parameters are the height and inclination of the sample stage. Furthermore it is possible to control the azimuth angle of the sample stage with a resolution of $1°$ and the translational position in one dimension of the sample in the plane of incidence with a resolution of $10\ \mu$m.

Apertures A manual aperture control is placed on the input and output side of the sample stage. With this component it is possible to adjust the spot size and hence the intensity of the light wave.

A picture of the SE 850 ellipsometer is shown in Figure 4.6. The box to the left is the input box with the source alternator, the polarizer, the compensator and the aperture control. The box to the right is the output box with the aperture control, the analyzer, detector alternator and the NIR detector. A picture of the two boxes without the cover can be seen in Figure 4.7.
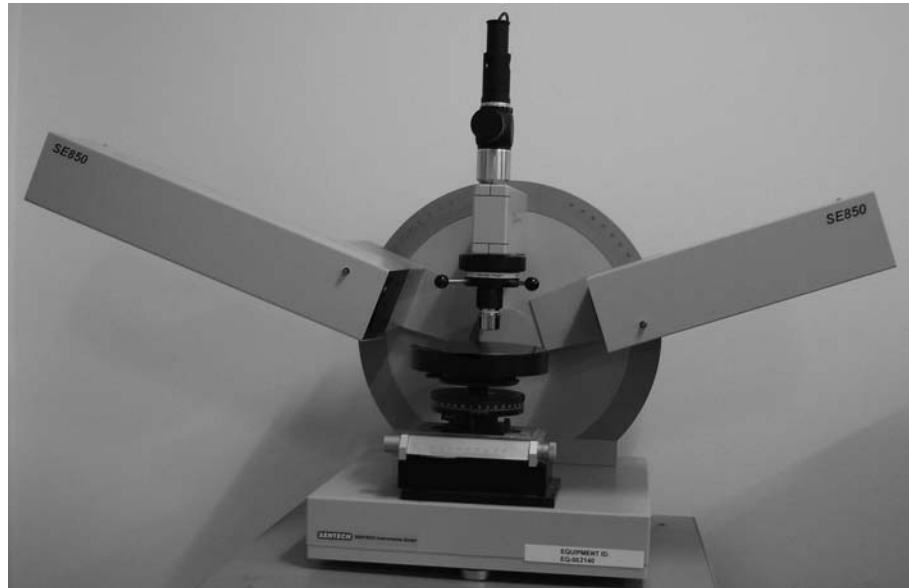
Figure 4.6: The Sentech SE 850 ellipsometer.

(a) The input box of the ellipsometer..

(b) The output box of the ellipsometer.

Figure 4.7: The input and output units of the ellipsometer without the covers.

Calculations of Physical Properties

<div style="text-align:right">5</div>

This chapter describes the calculation of the complex refractive index and the film thickness of a thin film. Furthermore, the method of calculating the thickness of an optically thick film is described.

5.1 Index of Refraction

This section describes the relation between the ellipsometric parameters ψ and Δ measured with the ellipsometer and the complex index of refraction $\tilde{n}_1$. Figure 5.1 shows the basic setup in order to calculate the refractive index. The basic equation for an ellipsometer found
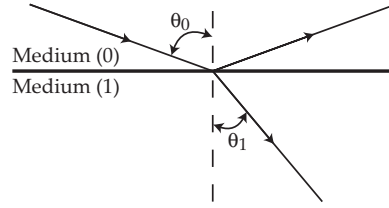
Figure 5.1: Reflection and transmission of an incident light wave at a surface boundary.

in (3.35) on page 19 contains the Fresnel reflection coefficients ρ_π and ρ_σ which are deduced in Appendix B. In this appendix, they are given by (B.30a) and (B.25) as

$$\rho_\pi = \frac{\tilde{n}_1 \cos(\theta_0) - \tilde{n}_0 \cos(\theta_1)}{\tilde{n}_1 \cos(\theta_0) + \tilde{n}_0 \cos(\theta_1)} \tag{5.1}$$

$$\rho_\sigma = \frac{\tilde{n}_0 \cos(\theta_0) - \tilde{n}_1 \cos(\theta_1)}{\tilde{n}_0 \cos(\theta_0) + \tilde{n}_1 \cos(\theta_1)} \tag{5.2}$$

where $\cos(\theta_1)$ can be found via Snell's law and the trigonometric identity as

$$\cos(\theta_1) = \sqrt{1 - \left(\frac{\tilde{n}_0}{\tilde{n}_1}\right)^2 \sin^2(\theta_0)} \tag{5.3}$$

Here, $\tilde{n}_1$ is the complex refractive index of medium 1, $\tilde{n}_0$ is the complex refractive index of the ambient, θ_0 is the angle of incidence and θ_1 is the unknown angle of transmission. Inserting (5.1), (5.2) and (5.3) into (3.35) and solving for $\tilde{n}_1$ yields

$$\tilde{n}_1 = \frac{\left[\sqrt{1 - 4\sin^2(\theta_0)\tan(\psi)\,e^{j\Delta} + 2\tan(\psi)\,e^{j\Delta} + \tan^2(\psi)\,e^{j\Delta}}\right]\tilde{n}_0 \sin(\theta_0)}{\cos(\theta_0)\left[1 + \tan(\psi)\,e^{j\Delta}\right]} \tag{5.4}$$

The data from the ellipsometer are values of ψ and Δ as a function of wavelength. Using (5.4), these data can be used to calculate the complex index of refraction as a function of wavelength.

5.2 Film Thickness

When ellipsometric measurements are performed on a three phase optical system consisting of an ambient-film-substrate structure, it is possible to determine the thickness of the film, if the refractive indexes for the three media are known. This section concerns relating the film thickness to the ellipsometric parameters ψ and Δ. An ambient-film-substrate optical system is depicted in Figure 5.2 The incident light wave from the ellipsometer strikes the surface
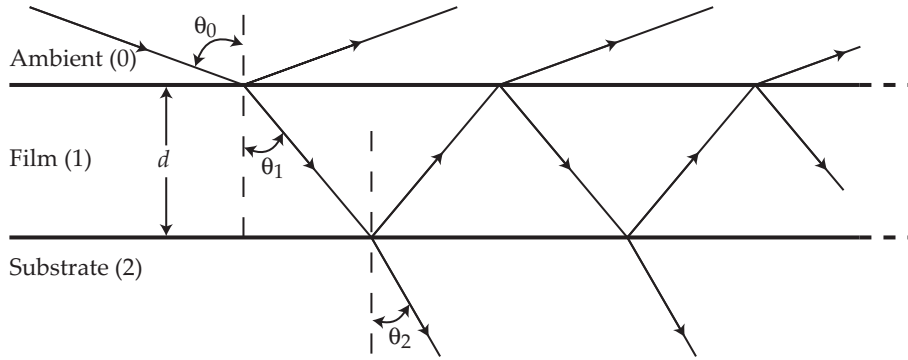
Figure 5.2: Illustration of an ambient-film-substrate optical system. The incident wave is partially reflected and partially transmitted.

boundary between ambient and the film at an angle of θ_0, which will also be the angle of the reflected wave due to Snell's law. Reflection and transmission of a polarized wave due to the surface boundaries in a three phase optical system is treated in Appendix C. In this appendix the total reflection coefficients of σ and π polarized light are found to be

$$P_\sigma = \frac{\rho_{01,\sigma} + \rho_{12,\sigma} e^{-j2\beta}}{1 + \rho_{01,\sigma} \rho_{12,\sigma} e^{-j2\beta}} \tag{5.5a}$$

$$P_\pi = \frac{\rho_{01,\pi} + \rho_{12,\pi} e^{-j2\beta}}{1 + \rho_{01,\pi} \rho_{12,\pi} e^{-j2\beta}} \tag{5.5b}$$

due to (C.29a) and (C.29b). P is the Greek letter capital ρ. The reflection coefficients in these equations are given in (C.30). An expression for β is given in (C.16).

5.2.1 Relation Between Ellipsometric Parameters and Film Thickness

(5.5a) and (5.5b) can be related to the ellipsometric parameters due to (3.35) where the reflection coefficients in a two-phase optical system ρ_π and ρ_σ are replaced by the reflection coefficients of a three-phase optical system P_π and P_σ

$$P = \frac{P_\pi}{P_\sigma} = \tan(\psi) e^{j\Delta} \tag{5.6}$$

where the parameter P is introduced as the complex reflection ratio [Azzam & Bashara 1977, p. 288]. By inserting the expressions for P_σ and P_π the following is given

$$P = P_\pi \cdot \frac{1}{P_\sigma} = \frac{\rho_{01,\pi} + \rho_{12,\pi} e^{-j2\beta}}{1 + \rho_{01,\pi}\rho_{12,\pi} e^{-j2\beta}} \cdot \frac{1 + \rho_{01,\sigma}\rho_{12,\sigma} e^{-j2\beta}}{\rho_{01,\sigma} + \rho_{12,\sigma} e^{-j2\beta}} \tag{5.7}$$

$$= \frac{\rho_{12,\pi}\rho_{01,\sigma}\rho_{12,\sigma} e^{-j4\beta} + (\rho_{01,\pi}\rho_{01,\sigma}\rho_{12,\sigma} + \rho_{12,\pi}) e^{-j2\beta} + \rho_{01,\pi}}{\rho_{01,\pi}\rho_{12,\pi}\rho_{12,\sigma} e^{-j4\beta} + (\rho_{01,\pi}\rho_{12,\pi}\rho_{01,\sigma} + \rho_{12,\sigma}) e^{-j2\beta} + \rho_{01,\sigma}} \tag{5.8}$$

This is an equation of 11 parameters, where the two ellipsometric parameters ψ and Δ are related to nine real parameters. These parameters are the real and imaginary parts of the complex refractive indexes, $\tilde{n}_0$, $\tilde{n}_1$, $\tilde{n}_2$, the angle of incidence θ_0, the free-space wavelength of the incident light wave λ and the film thickness d. If a set of ellipsometric parameters are measured at a given angle of incidence and a given wavelength the thickness of the film is the only unknown, assuming that the refractive indexes of the ambient, film and substrate are known. Thus by solving (5.8) for d, the film thickness of a sample can be determined.

5.2.2 Solving for the Film Thickness

(5.8) can be rewritten to

$$P = \frac{AX^2 + BX + C}{DX^2 + EX + F} \tag{5.9}$$

where $A = \rho_{12,\pi}\rho_{01,\sigma}\rho_{12,\sigma}$, $B = \rho_{01,\pi}\rho_{01,\sigma}\rho_{12,\sigma} + \rho_{12,\pi}$, $C = \rho_{01,\pi}$, $D = \rho_{01,\pi}\rho_{12,\pi}\rho_{12,\sigma}$, $E = \rho_{01,\pi}\rho_{12,\pi}\rho_{01,\sigma} + \rho_{12,\sigma}$, $F = \rho_{01,\sigma}$ and $X = e^{-j2\beta}$. Rearrangement of this equation yields

$$(PD - A)X^2 + (PE - B)X + (PF - C) = 0 \tag{5.10}$$

which is a complex quadratic equation with the solution

$$X = \frac{-(PE - B) \pm \sqrt{(PE - B)^2 - 4(PD - A)(PF - C)}}{2(PD - A)} \tag{5.11}$$

If the refractive index for the film is known, two analytical solutions to this equation exist, namely X_1 and X_2.

If the refractive index for the film is not known, but is assumed real i.e. $\tilde{n}_1 = n_1$, solutions to (5.11) can be found by iteration. In this iteration procedure n_1 is varied until the condition $|X| = 1$ is satisfied. As $X = e^{-j2\beta}$, where β is given by (C.16) on page 87 it is given that $|X|$ must equal 1. With the determined value of n_1 a value for X is also given.

With X determined from either of the methods, it is possible to calculate the film thickness due to

$$X = e^{-j2\beta} \tag{5.12}$$

$$\ln(X) = -j4\pi \frac{d}{\lambda} \tilde{n}_1 \cos(\theta_1) \tag{5.13}$$

$$d = \frac{j \ln(X)\lambda}{4\pi \tilde{n}_1 \cos(\theta_1)} \tag{5.14}$$

where X is either of the previously calculated solutions to (5.11). Obviously only one solution for the film thickness is valid, which should be real and positive. In the presence of errors the calculated thickness may be complex. In this case the solution with the smaller imaginary part should be chosen.

5.3 Film Thickness of a Thick Thin Film

In cases where the film is transparent i.e. the refractive index is purely real, multiple solutions for the film thickness exist. This can be seen from (5.12) which can be rewritten to

$$X = e^{-j4\pi \frac{d}{\lambda} \tilde{n}_1 \cos(\theta_1)} = e^{-j2\pi \left(\frac{d}{D}\right)} \tag{5.15}$$

where

$$D = \frac{\lambda}{2\tilde{n}_1 \cos(\theta_1)} \tag{5.16}$$

. From this equation it can be seen that X is a periodic function of d with a period of D, thus D is denoted the film thickness period. The film thickness period is a function of the angle of incidence, the wavelength of the light in free-space and the refractive indexes of the ambient and the film. The complete solution for the film thickness is then given as

$$d = d_0 + mD \tag{5.17}$$

where d_0 is the solution found in (5.14), which is called the standard solution and m is either 0 or a natural number i.e. $m = \{0, 1, 2, ..\}$. Without knowledge of the range of the thickness in advance it can thus prove difficult to explicitly determine the film thickness if the film is non-absorbing. The next section treats this subject. [Azzam & Bashara 1977, pp. 283-317]

5.3.1 Solving for the Film Thickness of a Thick Thin Film

When the film thickness d exceeds the film thickness period D, interference in the reflected light will appear, as the different components[1] of the reflected wave will be in phase at some wavelengths and in counter phase at other wavelengths. This will result in ψ and Δ angles that vary between positive and negative interference with a period that is dependent on wavelength. An example of this is given in Figure 5.3 where Δ is plotted as a function of wavelength. It is emphasized that the graph serves as an illustration only, and that it is not an actual experimental result. From a Δ-spectrum as this, it is possible to calculate the film thickness, as the distance between the local maxima are determined by the angle of incidence θ_0, the refractive index of the ambient $\tilde{n}_0$, the film $\tilde{n}_1$, the substrate $\tilde{n}_2$, the wavelength of the light λ and the film thickness d. Usually the only unknown is the film thickness which can then be calculated. This is done by determining the wavelengths of two adjacent peaks. At these two wavelengths the standard solution d_0 and the thickness period D can be calculated as described above. Two expressions for the film thickness can be set up due to (5.17). One at the first maximum at $\lambda = \lambda_0$

$$d = d_{00} + m_0 D_0 \tag{5.18}$$

and one at the next at $\lambda = \lambda_1$.

$$d = d_{01} + m_1 D_1 \tag{5.19}$$

---

[1]See Figure 5.2
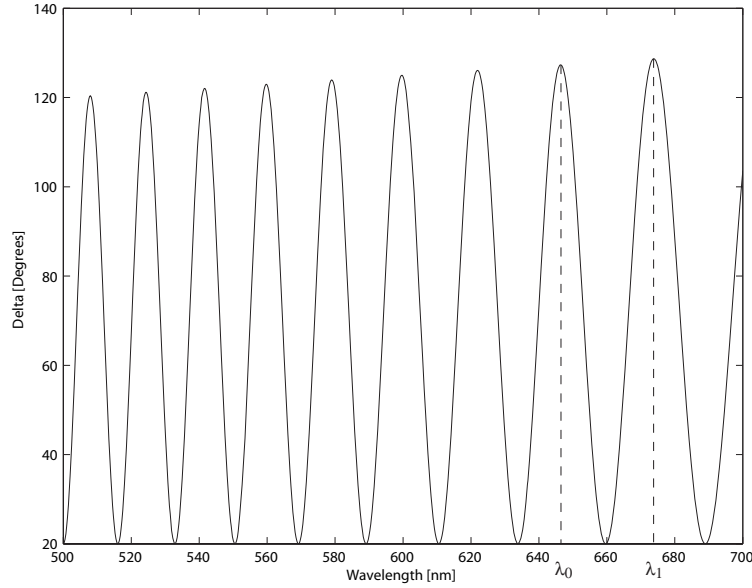
Figure 5.3: Illustration of interference as the film thickness exceeds the film thickness period. It can be seen that the distance between to adjacent peaks increases as the wavelength increases. Two adjacent peaks has been marked as λ_0 and λ_1.

As the thickness of the film is not dependent of wavelength, d must be the same in both equations. Subtraction of (5.18) from (5.19) yields

$$0 = d_{01} - d_{00} + m_1 D_1 - m_0 D_0 \tag{5.20}$$

The factors m_0 and m_1 are then the only unknowns. If the measured Δ spectrum has sufficient resolution to enable determination of all peaks, i.e. it is certain that there are no peaks between λ_0 and λ_1 it can be reasoned that

$$m_0 = m_1 + 1 \tag{5.21}$$

With a relation between m_0 and m_1 (5.20) can be rewritten to

$$0 = d_{01} - d_{00} + m_1 D_1 - (m_1 + 1) D_0 \tag{5.22}$$

$$m_1 = \frac{D_0 + d_{00} - d_{01}}{D_1 - D_0} \tag{5.23}$$

The only unknown parameter in (5.23) is m_1 and thus the value for this can be calculated. In the absence of errors m_1 is a natural number. Inserting the expression for m_1 into (5.19) yields

$$d = d_{01} + \frac{D_0 + d_{00} - d_{01}}{D_1 - D_0} D_1 \tag{5.24}$$

from which the film thickness can be directly calculated.

Part III

Simulations and Experiments

This part contains simulations of the refractive index of silicon, aluminum, copper and silver. It also describes the results of the tests performed with the SE 850 ellipsometer. These tests include measurement of the refractive index of the same four materials that were simulated, measurement of the film thickness of a silicon dioxide film coated on a silicon wafer and measurement of the thickness and uniformity of an optically thick polymer film coated on a silicon wafer.

Simulation of the Refractive Index of Crystals

<div style="text-align: right; font-size: 3em;">6</div>

This chapter contains simulations of the refractive index of silicon, copper, aluminum and silver derived from the Drude-Lorentz harmonic oscillator model in Appendix F. There are unknown parameters in some of the simulations, which are then found by fitting to table values shown in Appendix H.

The simulations are performed with wavelengths between 350 nm and 820 nm, which corresponds to the spectrum of the experiments.

The Drude-Lorentz model for a classical, forced, damped harmonic oscillator is explained in depth in Appendix F. The model sees the electrons in the material as oscillating with regard to the nucleus. This yields a mathematical expression for the complex dielectric coefficient $\tilde{\varepsilon}(\omega)$ given as

$$\tilde{\varepsilon}(\omega) = 1 + \frac{\omega_p^2}{\omega_0^2 - \omega^2 - j\gamma\omega} \tag{6.1}$$

from (F.40). ω_0 is the resonance frequency of the undamped oscillator, γ is the damping coefficient given as $\gamma = 1/\tau$ where τ is a table value for the specific material yielding the mean time between collisions of the electrons and ω_p is the plasma frequency defined as

$$\omega_p = \sqrt{\frac{Ne^2}{\varepsilon_0 m}} \tag{6.2}$$

where N is a table value for the electron density in the material, e is the electron charge, ε_0 is the free-space permittivity and m is the mass of the electron. The relation between (6.1) and the complex refractive index $\tilde{n}(\omega)$ is given as

$$\tilde{n}(\omega) = \sqrt{\tilde{\varepsilon}(\omega)} \tag{6.3}$$

The Drude-Lorentz model is used to simulate resonance phenomena in the refractive index, where ω_0 is the frequency corresponding to the resonance. When simulating these resonance peaks, it is necessary to use another amplification factor instead of ω_p in order to achieve a proper fit to the table values of the refractive index. This amplification factor is in the following Drude-Lorentz models denoted A.

In case of metals, Drude's free-electron model is used to simulate the refractive index of the materials. This model is given as the Drude-Lorentz model with $\omega_0 = 0$ yielding

$$\tilde{\varepsilon}(\omega) = 1 - \frac{\omega_p^2}{\omega(\omega + j\gamma)} \tag{6.4}$$

from (F.43).

If the refractive index of the simulated material contains several resonance peaks, a model that is made up of a sum of several dielectric coefficients must be used. When simulating metals with resonance peaks, a model that is made up of a sum of Drude's free-electron model and the Drude-Lorentz model must be used.

6.1 Silicon

Silicon is a semiconductor and the simulation of n and K is done only by means of the Drude-Lorentz model. The intrinsic electron concentration for silicon at room temperature is estimated from [Kittel 1986, p. 184] to 10^{10} electrons per cm^3. This is very low considering that there are approximately $5.0 \cdot 10^{22}$ Si-atoms per cm^3. This entails that the effect from the plasma frequency can be entirely neglected in this model. Instead, the amplification-factor A is used to fit the amplitude of the resonant peak to the table values. To further fit the amplitude of the resonance peak, a phase factor is introduced in A. The phase factor can move the peak upwards or downwards in the spectrum and determines if the peak is positive or negative in relation to the original curve.

Table values and [Palik 1998, III: p. 531-534] suggest that there are two oscillators affecting the index of refraction in the vicinity of the simulation spectrum due to the two band gaps on 3.38 eV and 4.27 eV. The resonance peak at ω_0 related to the band gap on 3.38 eV can be seen in the simulation spectrum, whereas the other band gap is outside the spectrum and therefore not affecting the simulation. The frequency corresponding to the band gap affecting the spectrum can be found as

$$\omega_0 = \frac{E_g}{\hbar} \tag{6.5}$$

where $\hbar$ is Planck's constant divided by 2π and ω_0 is the resonance frequency for the un-damped oscillator related to the band gap from E_g. The relation between any frequency ω and the wavelength λ is given by

$$\omega = \frac{2\pi c}{\lambda} \tag{6.6}$$

where c is the speed of light in vacuum. This yields a resonance peak in the model at $\lambda = 366.9$ nm. The model then becomes

$$\tilde{n} = \sqrt{1 + \frac{A}{\omega_0^2 - \omega^2 - j\gamma\omega}} \tag{6.7}$$

where the damping coefficient γ will be estimated. The effect of γ is related to the height and width of the resonance peak. It is stated that $\gamma \ll \omega_0$ [Reitz et al. 1993, p. 500] but by manual iteration, the peak of the simulation is fitted to the table values of the refractive index of silicon. The values of A, γ and ω_0 are given as

$$A = 1.2 \cdot 10^{32} e^{-j44.8} \text{ s}^{-2}$$

$$\gamma = 7.4 \cdot 10^{14} \text{ s}^{-1}$$

$$\omega_0 = 5.13 \cdot 10^{15} \text{ s}^{-1}$$

The simulation of (6.7) with the parameters given can be seen in Figure 6.1. n is the real part of (6.7) and k is the imaginary.

The model provides a simple understanding of the effect of the band gap yielding the given resonance frequency.
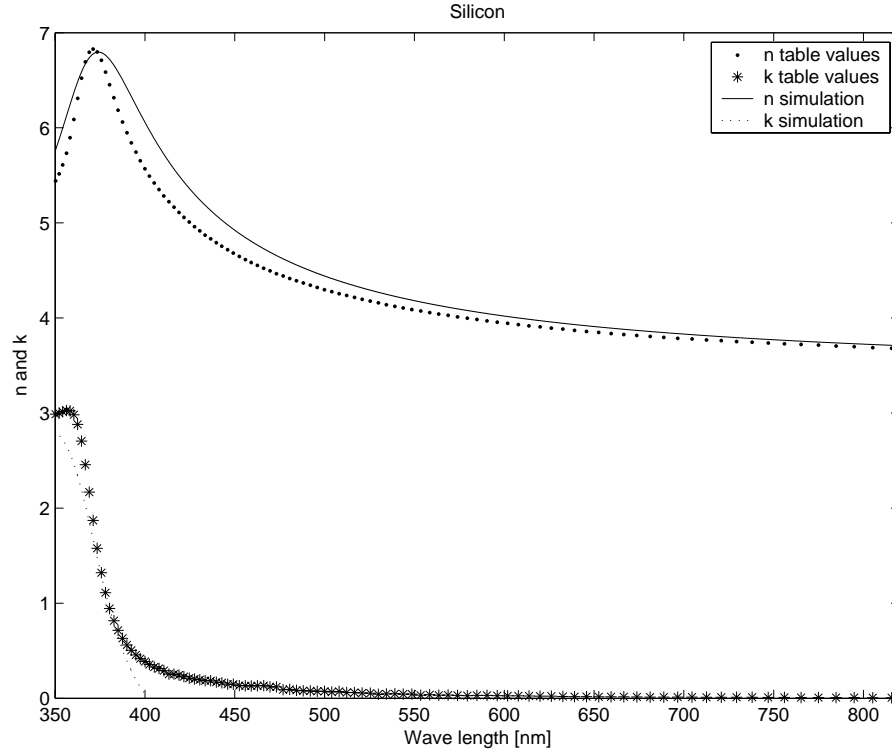
Figure 6.1: A manual fit to table values of *n* and *k* for silicon. [CD 2004, matlab/refractive_index_simulation/drude_free_electron_model.m]

6.2 Copper

Copper is the first of the metals which are simulated. For the metals, Drude's free-electron model is mainly used to simulate the index of refraction due to the free electrons in the material. For copper, there is however also an effect from two resonance peaks.

The plasma frequency for copper is located outside the simulation spectrum at 115 nm. There is resonance at 5 eV due to interband transition in the conduction bands and resonance due to a transition from the d-band to the conduction band is yielding a peak at approximately 2 eV. This can be seen in Appendix G. The resonance at 5 eV mainly affects the real part of the refractive index in wavelengths up to approximately 600 nm. The resonance at 2 eV can be seen as a little "flip" in the imaginary part of the complex index of refraction around 580 nm in Figure 6.2.

The simulation model used for copper is then given as the square root of the sum of a free-electron model and two resonance models

$$\tilde{n} = \sqrt{A_1 \left(1 - \frac{\omega_p}{\omega(\omega + j\gamma_1)} \right) + 2 + \frac{A_2}{\omega_{0,2}^2 - \omega^2 - j\gamma_2\omega} + \frac{A_3}{\omega_{0,3}^2 - \omega^2 - j\gamma_3\omega}} \qquad (6.8)$$

The values of the parameters are shown in Table 6.1. To fit the amplitude of the resonance peaks, phase factors are introduced in A_2 and A_3.
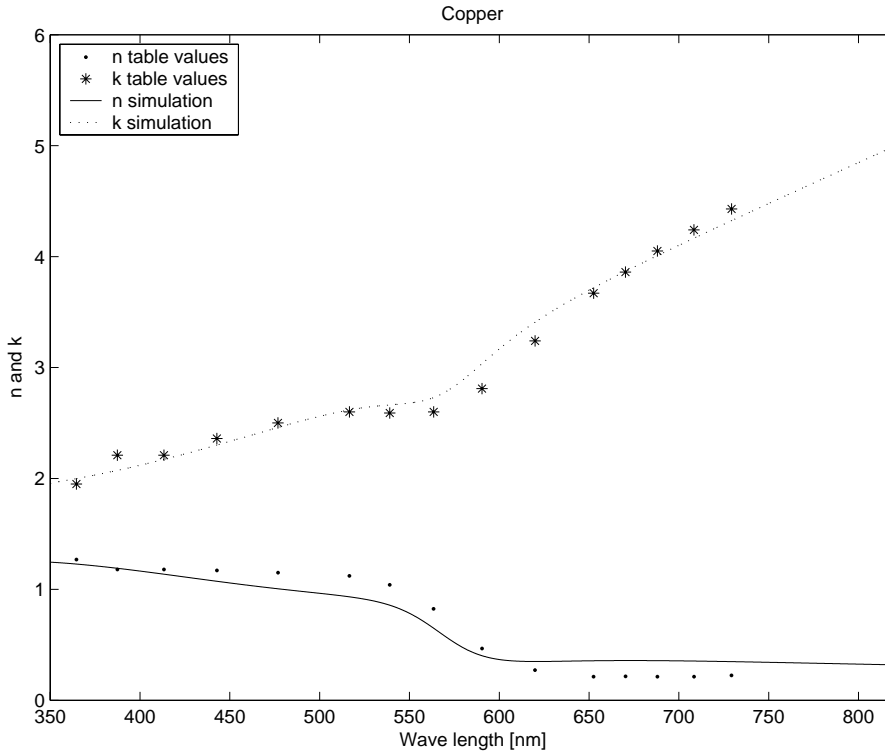
Figure 6.2: A manual fit to table values of n and k for copper. [CD 2004, matlab/refractive_index_simulation/drude_free_electron_model.m]

	1	**2**	**2**
A [s^{-2}]	0.60	$4.0 \cdot 10^{30} e^{-j90}$	$2.7 \cdot 10^{32} e^{j0.4}$
γ [s^{-1}]	$3.70 \cdot 10^{13}$	$5.2 \cdot 10^{14}$	$9.3 \cdot 10^{15}$
ω_0 [s^{-1}]	0	$3.30 \cdot 10^{15}$	$7.60 \cdot 10^{15}$
ω_p [s^{-1}]	$1.64 \cdot 10^{16}$	.	.

Table 6.1: Estimated values for the parameters involved in the simulation of the refractive index of copper. A_1 is without unit.

6.3 Aluminum

Aluminum is also a metal and Drude's free-electron model is mainly used to simulate the index of refraction due to the free electrons in the material. There is however also a small effect from a resonance peak at 1.55 eV. This implies that a square root of the sum of two complex dielectric functions should be taken. One accounting for the plasma frequency without resonance and one relating to the resonance

$$\tilde{n} = \sqrt{A_1 \left(1 - \frac{\omega_p}{\omega(\omega + j\gamma_1)}\right) + 1 + \frac{A_2}{\omega_0^2 - \omega^2 - j\gamma_2\omega}} \tag{6.9}$$

First, an estimate for the plasma frequency can be found by inserting the number of electrons per unit volume $N = 18.1 \cdot 10^{22} \text{cm}^{-3}$ into (F.36) which yields a plasma frequency

at $\omega_p = 2.40 \cdot 10^{16} \text{s}^{-1}$. This corresponds to a wavelength of $\lambda_p = 78.5$ nm, which is outside the spectrum range of the simulation. The plasma frequency does however still influence the spectrum. A scaling factor A_1 is introduced in order to achieve a proper fit to the table values of the index of refraction.

Next, an estimate of the damping coefficient γ must be calculated. For aluminum τ is given as $\tau = 0.8 \cdot 10^{-14}$ s. The corresponding damping can be used in the free-electron model, but must be larger when used in the expression for the resonance peak.

The amplification-factor A_2 used in the resonance model is also manually fitted to the table values of the index of refraction. The values used in the simulation of the refractive index of aluminum can be seen in Table 6.2.

	1	2
A [s^{-2}]	0.65	$9.0 \cdot 10^{31}$
γ [s^{-1}]	$1.25 \cdot 10^{14}$	$8.75 \cdot 10^{14}$
ω_0 [s^{-1}]	0	$2.35 \cdot 10^{15}$
ω_p [s^{-1}]	$2.40 \cdot 10^{16}$	$\cdot$

Table 6.2: Estimated values for the parameters involved in the simulation of the refractive index of aluminum. A_1 is without unit.

The simulation is seen in Figure 6.3 together with the table values of n and k. Again, the
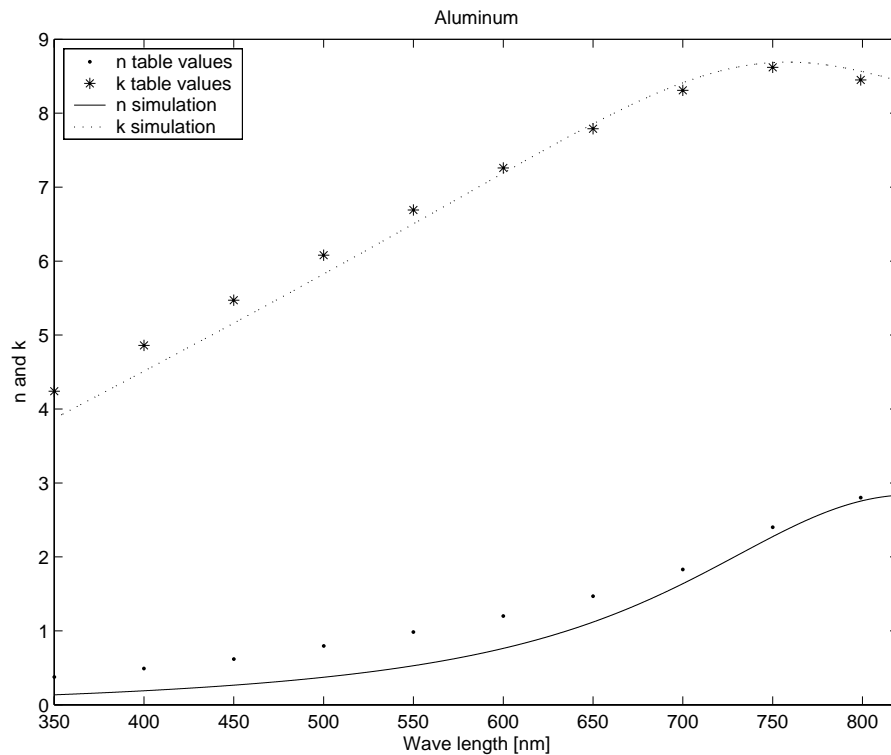
Figure 6.3: A manual fit to table values of n and k for aluminum. [CD 2004, matlab/refractive_index_simulation/drude_free_electron_model.m]

small derivation in especially n implies other effects that are not accounted for in the model or simply just that the manual fit is not optimal. The model does however explain the form and to some extend the size of the curve.

6.4 Silver

The simulation of the index of refraction of silver can be done fairly simple. There are no resonance peaks that affect the simulation spectrum, so the model is simply described by means of the free-electron model as

$$\tilde{n} = \sqrt{A\left(1 - \frac{\omega_p}{\omega(\omega + j\gamma)}\right)} \qquad (6.10)$$

Using a normal table value of the electron density yields a plasma frequency that does not fit the model of the refractive index to the table values. This is because the effective electron density becomes lower because the d-electrons are shielding the free electrons. Taking this effect into account causes a plasma frequency at the wavelength $\lambda = 326$ nm. The damping coefficient can be found by using the table value $\tau = 4.0 \cdot 10^{-14}$. An amplification factor is used to fit the simulation to the table values. The values of the parameters are given as

$$A = 5.3$$

$$\gamma = 2.5 \cdot 10^{13} \text{ s}^{-1}$$

$$\omega_p = 5.77 \cdot 10^{15} \text{ s}^{-1}$$

The simulation graph is shown in Figure 6.4.
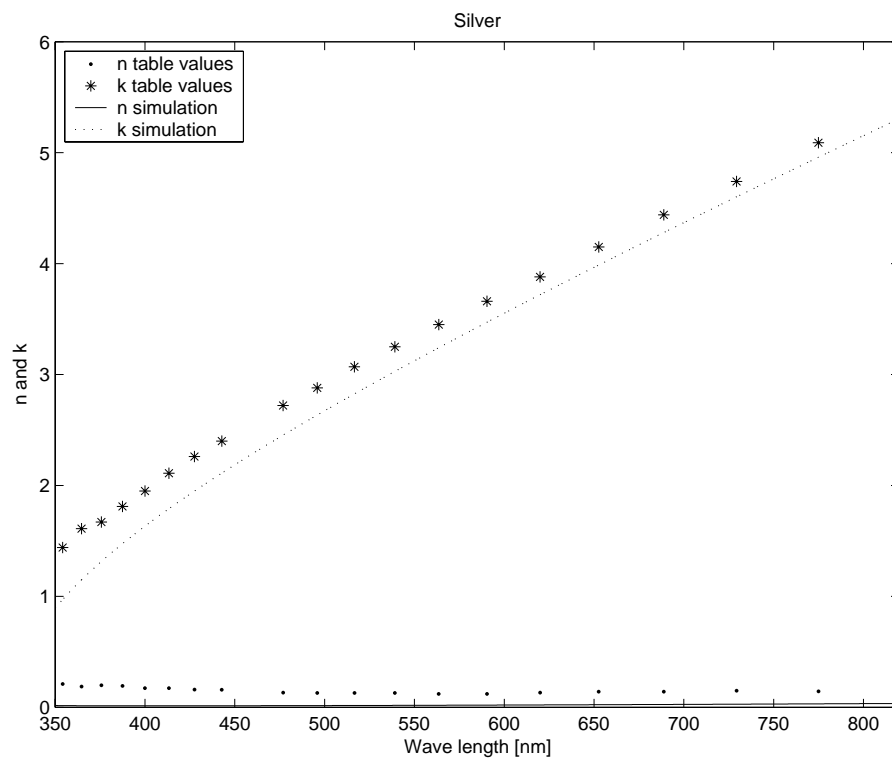
Figure 6.4: A manual fit to table values of *n* and *k* for silver. [CD 2004, matlab/refractive_index_simulation/drude_free_electron_model.m]

Discussion of Crystal Measurements

7

This chapter presents the data processing and the discussion of the measurements performed with the ellipsometer on the silicon, copper, aluminum and silver crystal. The purpose of the experiment is to determine the refractive index of the crystals.

Figure 7.1 and 7.2 depicts the real and the imaginary part of the calculated refractive index as a function of wavelength together with table values for the four crystals. For further reference on the measurement procedure see Appendix H. By contemplating Figure 7.1(a) it can be seen that there is a relatively good correspondence between the table values and the calculated values of the refractive index of silicon. However it can be seen that the imaginary part of refractive index is higher than the table values and the real is lower over the measured spectrum.

Figure 7.1(b) depicts the calculated values of the refractive index of copper together with the table values. The figure shows that the calculated values of both the real and the imaginary part are lower than the table values. The figure furthermore shows that even though the calculated values are lower than the table values they still have the same tendency, over the measured spectrum, as the table values.

In Figure 7.2(a) the calculated refractive index of aluminum together with the table values are depicted. It can be seen that the calculated values are relatively far from the table values but that they have the same tendency as a function of wavelength.

Figure 7.2(b) shows the table and the calculated values in the case of silver. In this case the calculated values are also relatively far from the table values. The imaginary part of the calculated refractive index for silver has the same tendency as the table values. In the lower part of the spectrum the calculated values fit the table values well. The real part however, does not have the same tendency as a function of wavelength. This is because the table values decreases as the wavelength is increasing and the calculated values increases as the wavelength is increasing.

In order to improve these results a new model of calculation is considered. The new model of calculation will used the same measured data as the old. In the new model it is assumed that the surfaces of the crystals are oxidized. It is assumed that there is a thin layer of silicon dioxide SiO_2 on the silicon surface, a thin layer of cuprous oxide Cu_2O on the copper surface, a thin layer of aluminum oxide Al_2O_3 on the aluminum surface and a thin layer of silver oxide Ag_2O on the silver surface. It is required that the indexes of refraction of the four oxide layers are known. The index of refraction of silicon dioxide, cuprous oxide and aluminum oxide are found in [Palik 1998]. The index of refraction of silver oxide is found in [Yin et al. 2001]. The unknown variables in the new model are the index of refraction of the crystal below the oxide layer and the thickness of the oxide layer. As it is the refractive index of the crystal below the oxide layer which is to be determined, the calculations will be made as an iterative process where the thickness of the oxide layer is changed. In order to calculate the refractive index of a material below a thin film where the
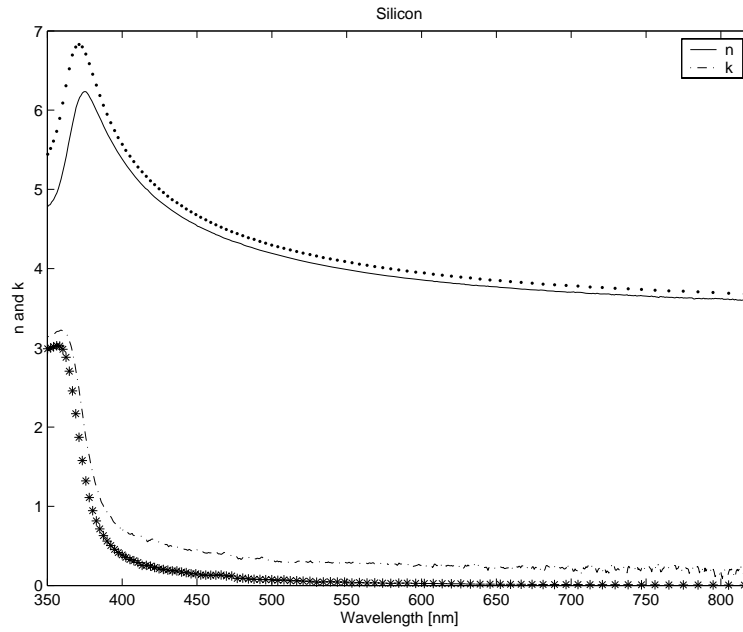
(a)
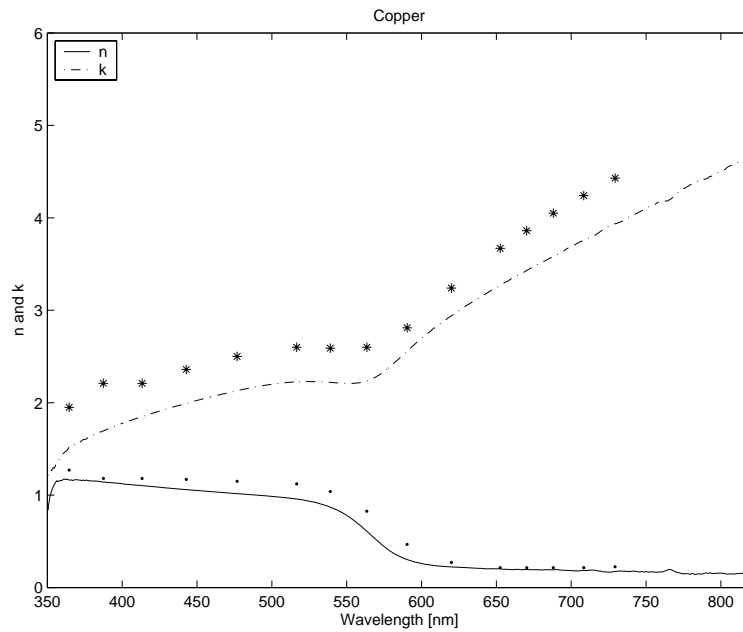
(b)

Figure 7.1: The calculated real n and imaginary k part of the refractive index as a function of wavelength together with table values of the refractive index of silicon and copper. The real part of the table values are dots and the imaginary part are asterisks. Table values are found in [Palik 1998] and in [Klein & Furtak 1986]. [CD 2004, matlab/surface_test/RefractiveIndex.m]
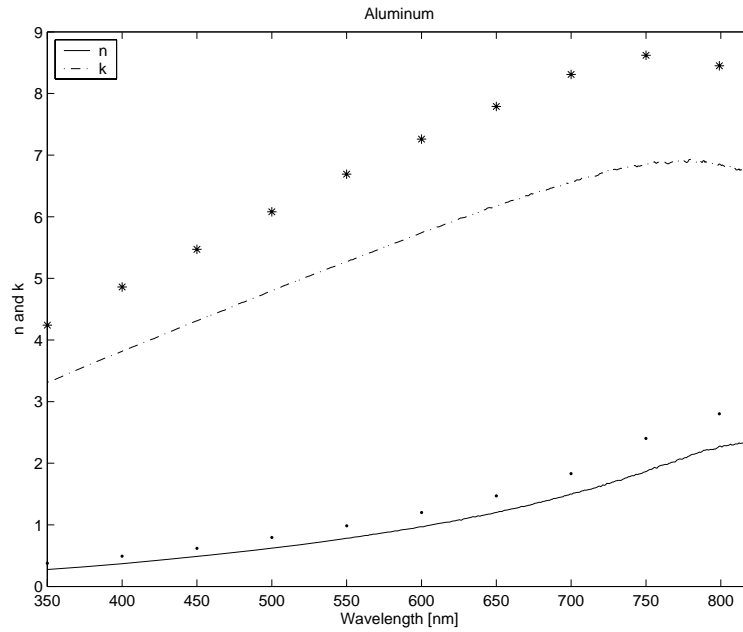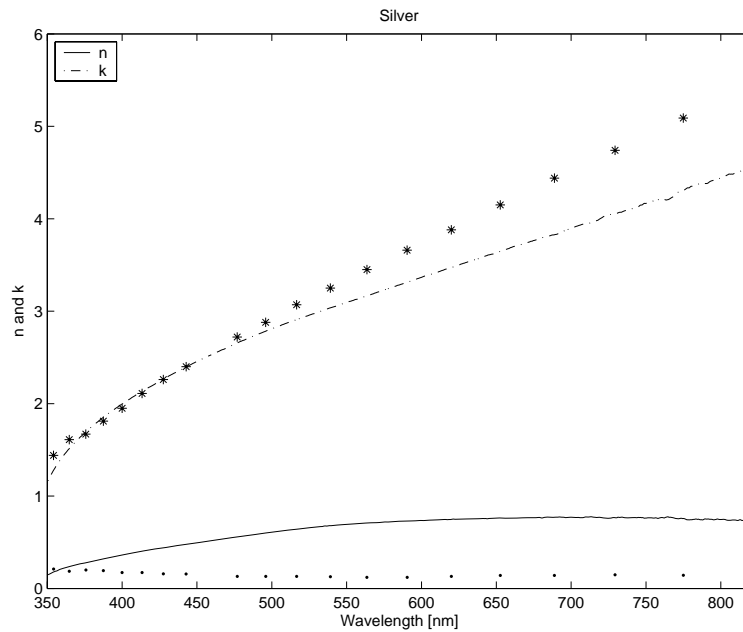
Figure 7.2: The calculated real n and imaginary k part of the refractive index as a function of wavelength together with table values of the refractive index of aluminum and silver. The real part of the table values are dots and the imaginary part are asterisks. Table values are found in [Palik 1998]. [CD 2004, matlab/surface_test/RefractiveIndex.m]

refractive index and thickness of the film are known, (5.6) and (5.8) are combined to yield

$$\tan(\psi)e^{j\Delta} = \frac{\rho_{12,\pi}\rho_{01,\sigma}\rho_{12,\sigma}e^{-j4\beta} + (\rho_{01,\pi}\rho_{01,\sigma}\rho_{12,\sigma} + \rho_{12,\pi})e^{-j2\beta} + \rho_{01,\pi}}{\rho_{01,\pi}\rho_{12,\pi}\rho_{12,\sigma}e^{-j4\beta} + (\rho_{01,\pi}\rho_{12,\pi}\rho_{01,\sigma} + \rho_{12,\sigma})e^{-j2\beta} + \rho_{01,\sigma}} \qquad (7.1)$$

Given the refractive indexes of air n_0 and of the oxide layer $\tilde{n}_1$, the angle of incidence θ_0, the wavelength of the light in free-space λ and Snell's law it is possible to calculate $\rho_{01,\sigma}$ and $\rho_{01,\pi}$ for the given wavelength. From the measurements, ψ and Δ are connected to the wavelength λ. Substituting the expressions for $\rho_{12,\pi}$ and $\rho_{12,\sigma}$ and β given in Appendix C into (7.1) yields an equation in two variables, namely the thickness d of the oxide layer and the index of refraction of the crystal below the oxide layer $\tilde{n}_2$. In order to solve this equation for $\tilde{n}_2$ the thickness of the oxide layer must be guessed or an iterative calculation, where the thickness is changed, must be performed. When a thickness is decided upon, (7.1) can be solved in order to find the refractive index of the crystal below the film for a given wavelength.

7.1 Silicon

A series of calculations where ten different thicknesses of a silicon dioxide film are imposed on the silicon surface and (7.1) is solved for $\tilde{n}_2$ over a wide range of wavelengths are performed. The interval of the thickness is from 1 nm to 10 nm with a jump in thickness of 1 nm. Only the best fit of the ten different thicknesses is depicted in Figure 7.3. The figure shows the real and imaginary part of the calculated refractive index of silicon without a film and with a 4 nm silicon dioxide film imposed on the silicon surface together with the table values. It can be seen from the figure that in order to move the refractive index of silicon closer to the table values, a 4 nm silicon dioxide film can be imposed on the silicon surface. This indicates that there indeed is a film of silicon dioxide or a material with similar refractive index on the silicon surface. From the figure it can be seen that, due to the low resolution of points where the refractive index is calculated, the curve of the real part of the calculated refractive index is edged and non-fluctuating.
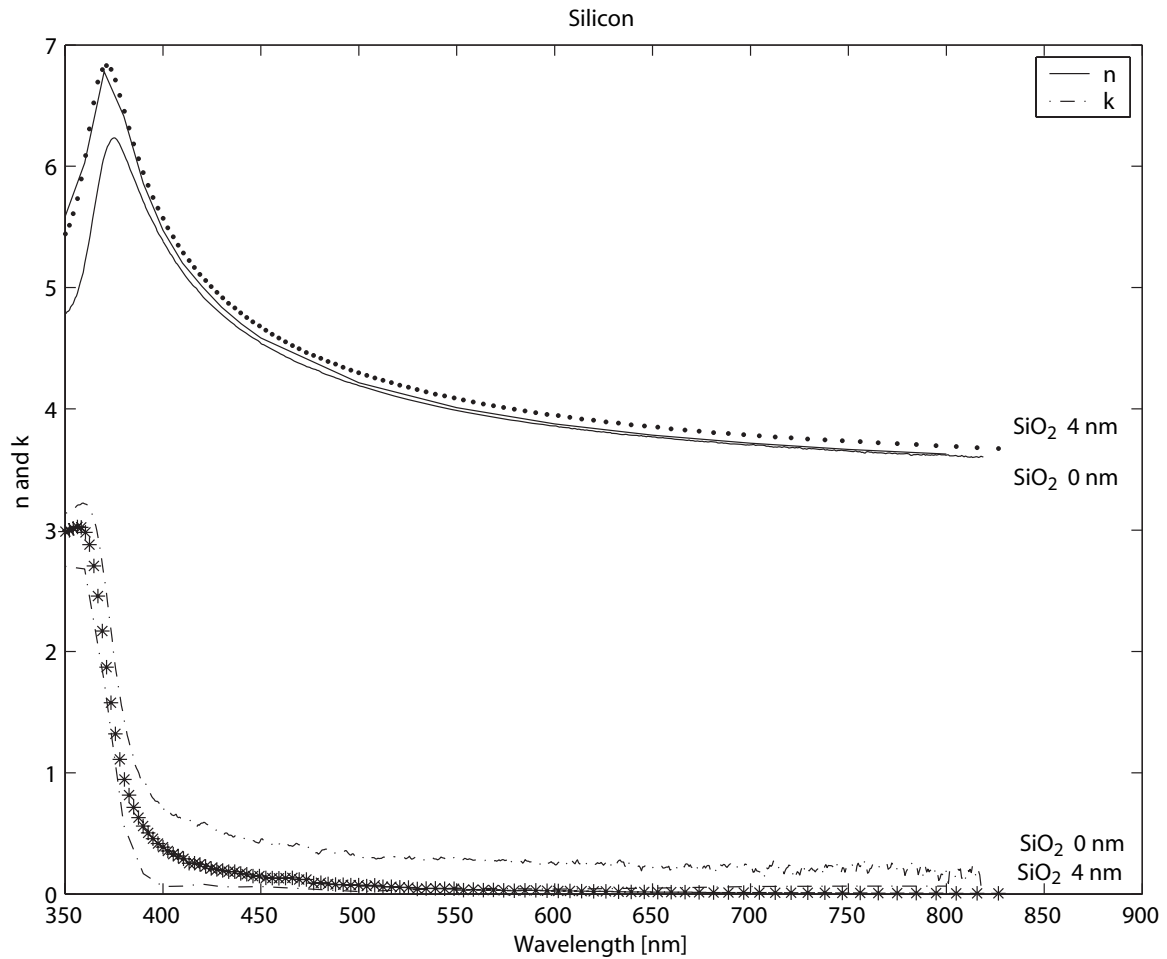
Figure 7.3: Real and imaginary part of the calculated refractive index of silicon without a film and with a 4 nm silicon dioxide film imposed on the silicon surface together with the table values. [CD 2004, matlab/refractive_index_si/refractive_index_si.m]

7.2   Copper

A series of calculations where ten different thicknesses of a cuprous oxide film are imposed on the copper surface and (7.1) is solved for $\tilde{n}_2$ over a wide range of wavelengths are performed. The interval of the thickness is from 1 nm to 10 nm with a jump in thickness of 1 nm. Only the best fit of the ten different thicknesses is depicted in Figure 7.4. The figure
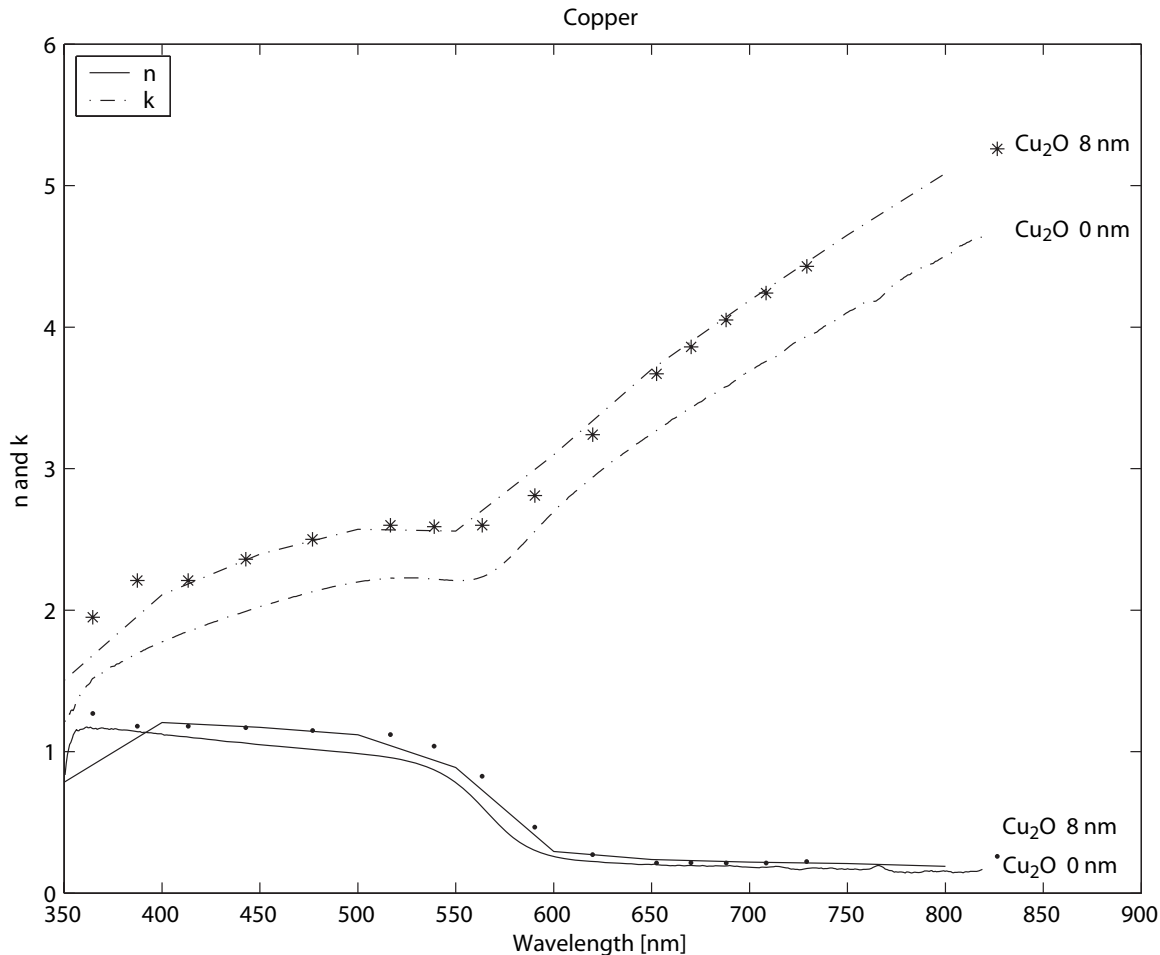
Figure 7.4: Real and imaginary part of the calculated refractive index of copper without a film and with an 8 nm cuprous oxide film imposed on the copper surface together with the table values. [CD 2004, matlab/refractive_index_cu/refractive_index_cu.m]

shows the real and imaginary part of the calculated refractive index of copper without a film and with an 8 nm cuprous oxide film imposed on the copper surface together with the table values. The calculated refractive index of copper without a film is drawn in order to compare the new model with the old model. It can be seen from the figure that in order to move the refractive index of copper closer to the table values, an 8 nm cuprous oxide film can be imposed on the copper surface. This indicates that there indeed is a film of cuprous oxide or a material with similar refractive index on the copper surface.

7.3 Aluminum

A series of calculations where ten different thicknesses of an aluminum oxide film are imposed on the aluminum surface and (7.1) is solved for $\tilde{n}_2$ over a wide range of wavelengths are performed. The interval of the thickness is from 1 nm to 10 nm with a jump in thickness of 1 nm. The results for three essential thicknesses besides the model without film are depicted in Figure 7.5. The figure shows the results of the calculations where no film and
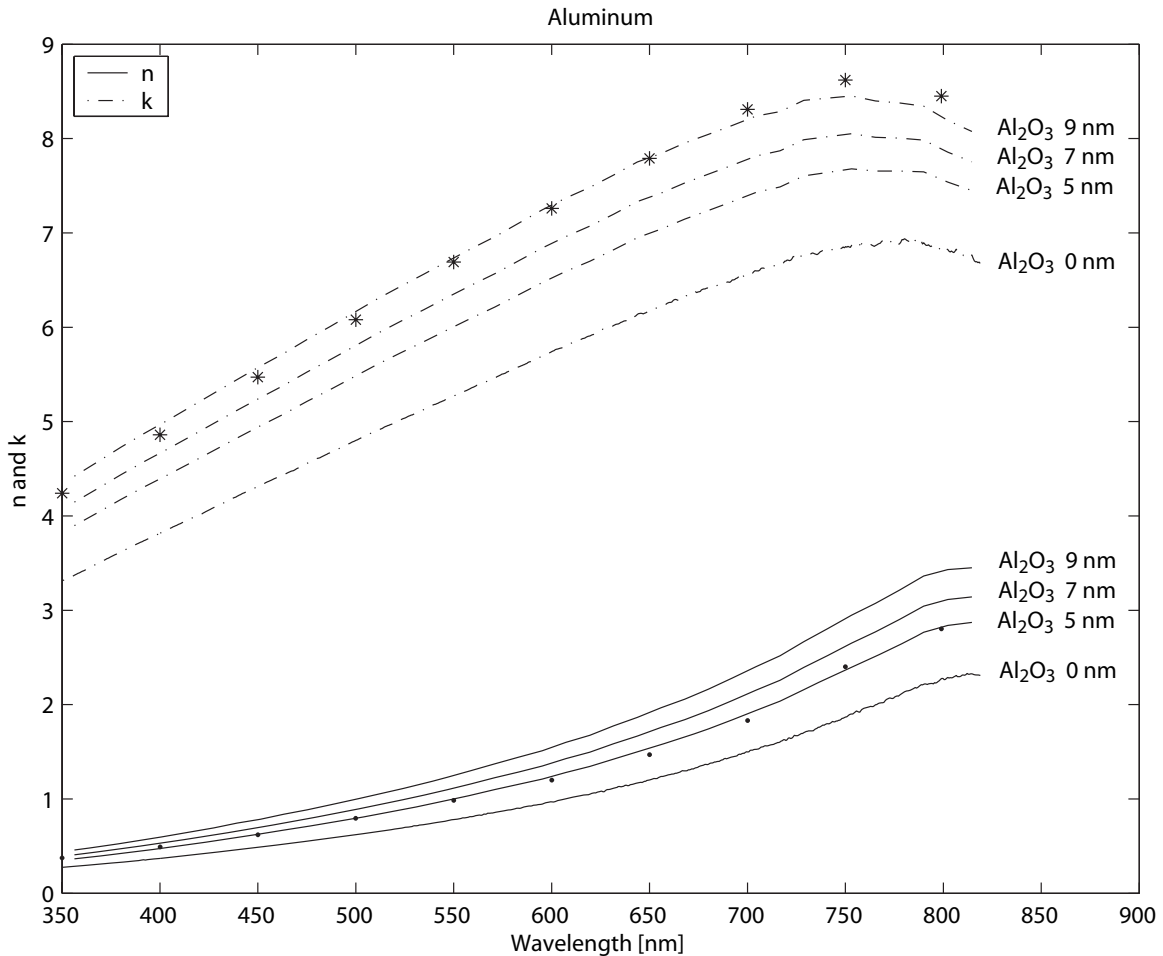
Figure 7.5: Real and imaginary part of the calculated refractive index of aluminum without a film, with a 5, 7 and 9 nm aluminum oxide film on top of the aluminum surface together with the table values. [CD 2004, matlab/refractive_index_al/refractive_index_al.m]

a 5, 7 and 9 nm thick aluminum oxide layer are imposed on the aluminum surface. As can be seen from the figure there is a clear tendency of a better result when an aluminum oxide film is imposed on the surface. In order to fit the real part best it can be seen that a 5 nm aluminum oxide film must be imposed on the aluminum surface. However in order to fit the imaginary part of the refractive index best, a 9 nm aluminum oxide film must be imposed. This indicates that the new model is still not sufficient to get a good fit of both the real and

the imaginary part of the refractive index of aluminum.

An explanation could be that it is not pure aluminum oxide that forms on the aluminum surface. Thus the refractive index of the film currently used in the calculations is not correct.

7.4 Silver

Figure 7.6 depicts the result of the calculation of $\tilde{n}_2$ where the thickness of a silver oxide layer is 0, 5 and 10 nm. Only the result of a 10 nm, a 5 nm and a 0 nm thick silver oxide
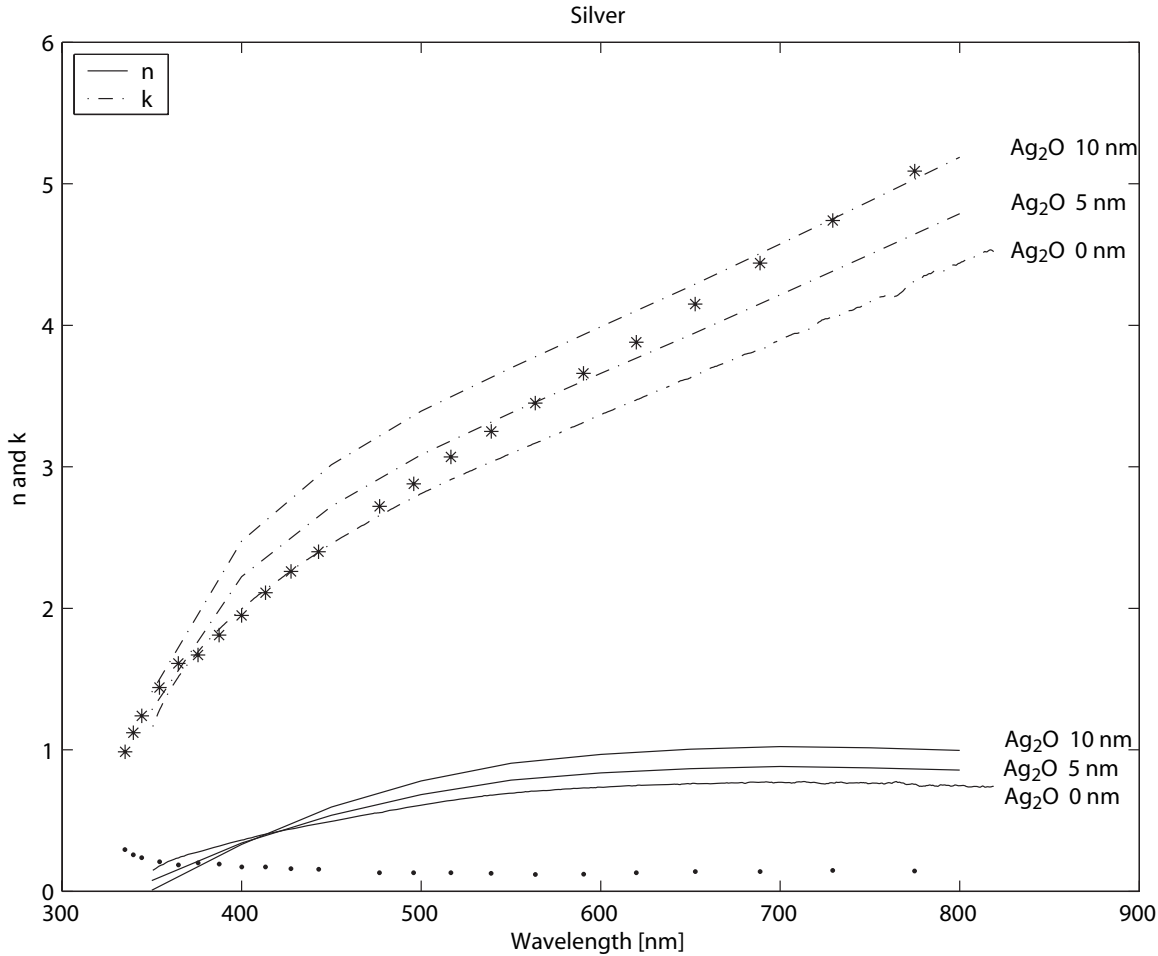
Figure 7.6: Real and imaginary part of the calculated refractive index of silver without a film, with a 5 and 10 nm silver oxide film on top of the aluminum surface together with the table values. [CD 2004, matlab/refractive_index_ag/refractive_index_ag.m]

film are depicted in the figure. It can be seen from the figure that when a silver oxide layer is imposed there is a lower correspondence between the calculated values and the table values. The best fit to the table value of the refractive index is when no silver oxide film is imposed on the surface of the crystal.

The assumption that it is only Ag$_2$O is probably not adequate. Using another refractive index could to some extend remedy the problem. Generally, a silver crystal structure tends to grow argentite Ag$_2$S which has a different refractive index.

7.5 Summary

In general it can be observed that there is a better fit when the new model is used instead of the old model, where no oxide layer is imposed on the surface. The best fits are in the case of silicon and copper, which indicates that it is in fact a good approximation to assume that it is silicon dioxide and cuprous oxide that forms on the respective surfaces. The small deviations from the table values are considered within the range of test uncertainties. In the case of the aluminum, the model with the oxide layer makes a better fit, but a deviation from the table values still exists.

From the result of silver, it can be concluded that neither the model with pure silver nor the model with a layer of Ag$_2$O imposed on the silver surface are correct. A model with a different film layer, e.g. Ag$_2$S must be tested. Due to difficulties obtaining table values of the refractive index of Ag$_2$S, this has not been tested.

Discussion of SiO$_2$ Film Measurements

<div style="text-align: right">8</div>

This chapter presents and discusses the measurement of film thickness of an SiO$_2$ film on an Si surface using the SE 850 ellipsometer. The procedure of making the measurements are presented in Appendix I, and the method of calculating the thickness of the film is presented in Chapter 5.

The measurements that underlie the calculation of film thickness are the same type as in Chapter 7. That is, it is based on measurements of ψ and Δ angles. A depiction of ψ and Δ angles as a function of wavelength for a measurement on the Si wafer with an SiO$_2$ film can be found in Figure I.1 on page 124. It is noted that the Δ angles fluctuate in the higher wavelength region.

8.1 Film Thickness

The thickness is calculated by means of the method described in Section 5.2.

As the ellipsometer measure ψ and Δ angles for approximately every 1 nm within the described spectrum, it is necessary to have the corresponding values of the refractive index for Si and SiO$_2$ in order to be able to calculate the thickness for each measured wavelength. Thus, an interpolation of table values is performed. Table values for Si and SiO$_2$ are from [Palik 1998, I: pp. 563-565] and [Index of Refraction Values and Photonics Calculations 2004] respectively. The interpolation is carried out as a simple linear interpolation and the returned curves are generally smooth.

Graphical illustrations of the calculated thicknesses of the film as functions of the wavelength can be found in Figure 8.1(a) and Figure 8.1(b). The first figure presents the thickness result in a large scale, whereas the second figure zooms in, in order to reveal the curvature of the results.

The actual thickness does obviously not alter with respect to the wavelength. Hence, the calculated thickness would ideally be a constant. This is however not the case. Generally, some fluctuations, which are most pronounced for the larger wavelength, can be seen in Figure 8.1(a) and 8.1(b). This can be traced back to the fluctuations in the measurement of Δ angles in the same wavelength area, as this is the only parameter that does fluctuate. This is similar to Si which is seen in Figure H.2(a) on page 121 and the fluctuations are caused by low light intensities for the mentioned wavelengths. For a graphical confirmation, comparison between Figure I.1 and 8.1(a) can be made.

The appearance of the curve for the small wavelength region is affected by fluctuations in the table values of the imaginary part of the refractive index for Si. Si fluctuates slightly especially in the region from approximately 400 to 500 nm.

It is estimated that the result is most reliable in the region where the measured parameters and the table values are most stable. Thus, it should be in the region from approximately 500 to 600 nm. In this region, the thickness does however have a tendency to increase
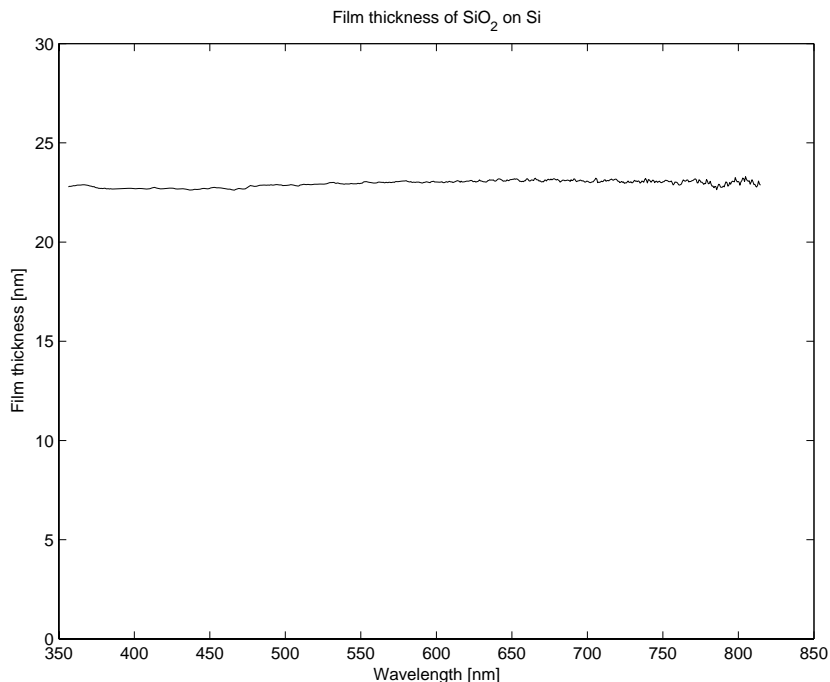
(a) Plot showing the uniformity
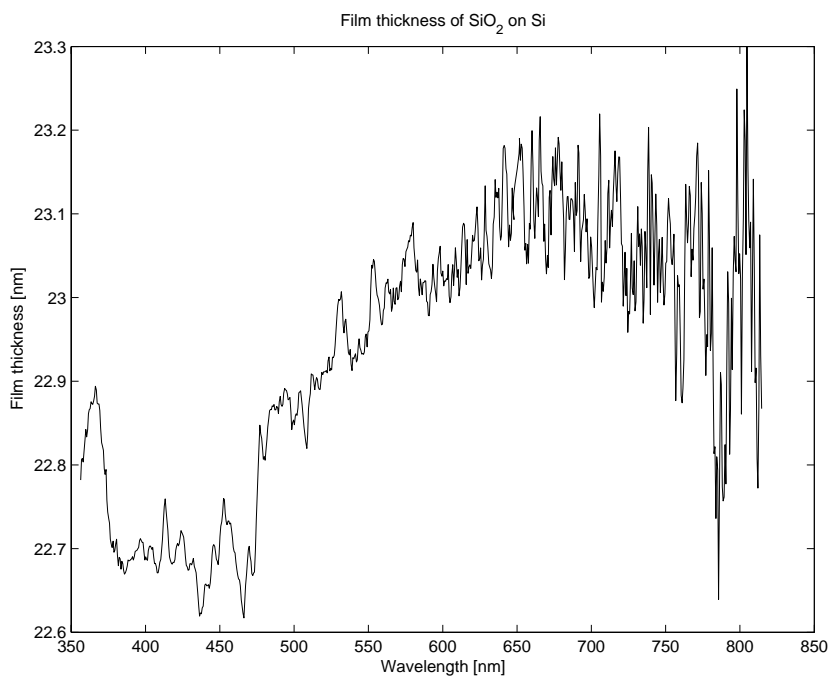
(b) Plot showing the heterogeneity

Figure 8.1: the thickness of the SiO$_2$ film on a Si surface as a function of wavelength. Note that the fluctuations in the larger wavelength region resemble the fluctuation in the values for Δ. [CD 2004, matlab/thickness/-film_thickness_sio_2.m]

slightly. Nevertheless, it is estimated that a thickness of approximately 22.9 nm is a good estimate of the actual thickness. This value does also coincide with an average over the entire spectrum. Furthermore, this estimated value coincides with the automatic fit of the thickness by the Spectraray II software, which yields a thickness of 22.8 nm. From this, it can be concluded that the model is adequate. The manufacturer of the film does however state that the thickness of the film is 21.5±0.3 nm. This corresponds to a deviation of the measured value from this value of 6.5 %. An explanation to the difference between the thickness stated by the manufacturer and the measured/calculated value can be that either the ellipsometer is not calibrated accurately or the thickness of the film is not as specified by the manufacturer.

Discussion of Polymer Film Measurements

<div align="right">9</div>

This chapter presents the discussion of the measurements performed on the two wafers with a PI-5878G polymer film imposed on the surface. The test report of the experiments is found in Appendix J. The first subject of the discussion will be the experiment where the thickness of the two polymer films is calculated as a function of wavelength. The second subject of discussion is the experiment where the uniformity of the thickness of the polymer films is investigated.

In the following it should be possible to distinguish between the two polymer films. They are spin coated with the same angular velocity, but for different time intervals. The wafer where the polymer is spin coated for the shortest time interval will be the thickest and will therefore in the following be referred to as the thick polymer. The wafer where the polymer is spin coated in the longest time interval will be the thinnest and will therefore in the following be referred to as the thin polymer.

Both polymers are optically thick, that is, they are several times thicker than the wavelength of the incident light.

9.1 Film Thickness

Figure 9.1 shows the calculated thickness as a function of wavelength for the thick and the thin polymer. In the ideal case the thicknesses of the two polymer films should be inde-
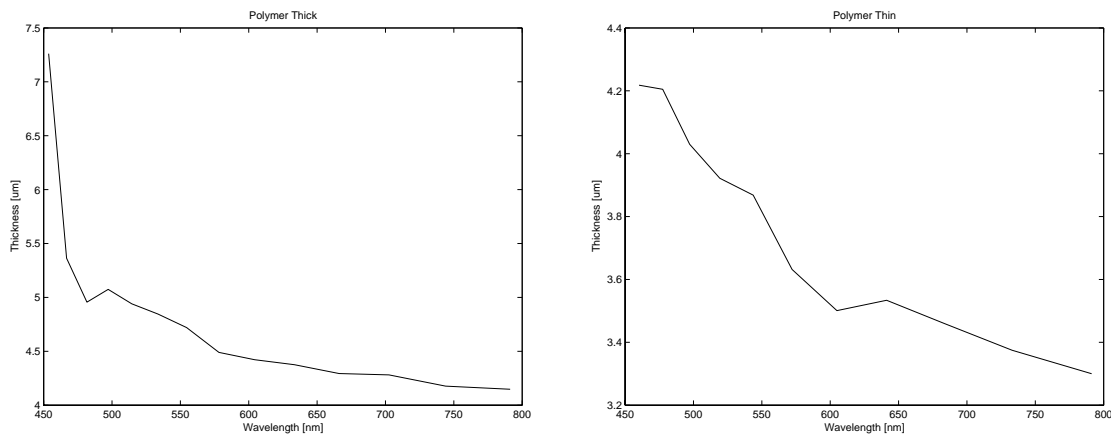
(a) Thickness of the thick polymer at the middle, as a function of wavelength.

(b) Thickness of the thin polymer at the middle, as a function of wavelength.

Figure 9.1: Polymer thickness at the middle of the wafer, as a function of wavelength. [CD 2004, matlab/polymer_thickness/film_thickness_polymer_spectrum.m]

pendent of the wavelength λ. That is, the thickness of the film should be constant for all wavelengths. By contemplating Figure 9.1 it can be seen that the calculated film thickness of both the thick and the thin polymer film is not constant over wavelength. The figures show that the calculated polymer film thickness is larger in the lower part of the wavelength range. The thicknesses of the films are calculated by means of the interference pattern in the ψ-Δ spectrum. By contemplating the ψ-Δ spectrums of the polymer films in Appendix J, it is observed that the interference patterns in the lower part of the wavelength interval are not as ambiguous as in the upper part. This is a possible reason for the larger thickness in the lower part of the wavelength interval. A possible explanation of the variations in the calculated thickness could be that the value of the refractive index of the polymer is not constant 1.78 as specified in [MicroSystems 2003][1]. If white light is incident on an isolated part of the film, i.e. a part without the wafer, it can be observed that the transmitted part of the light has a tendency to contain a greater part of yellow, compared to the rest of the spectrum. The reflected part does however not contain a relative larger part of the blue and red spectrum, i.e. the red and blue part of the spectrum is not reflected more than the yellow part. Thus, light in the red and blue part of the spectrum is absorbed more than it is for the yellow part. This again results in the existence of an imaginary part of the refractive index different from zero and dependent of the wavelength.

9.2 Uniformity of Film Thickness

Figure 9.2 shows the calculated thickness over the axes, as defined in Appendix J, for both the thin and the thick polymer film. The figure shows the thickness of the two polymer
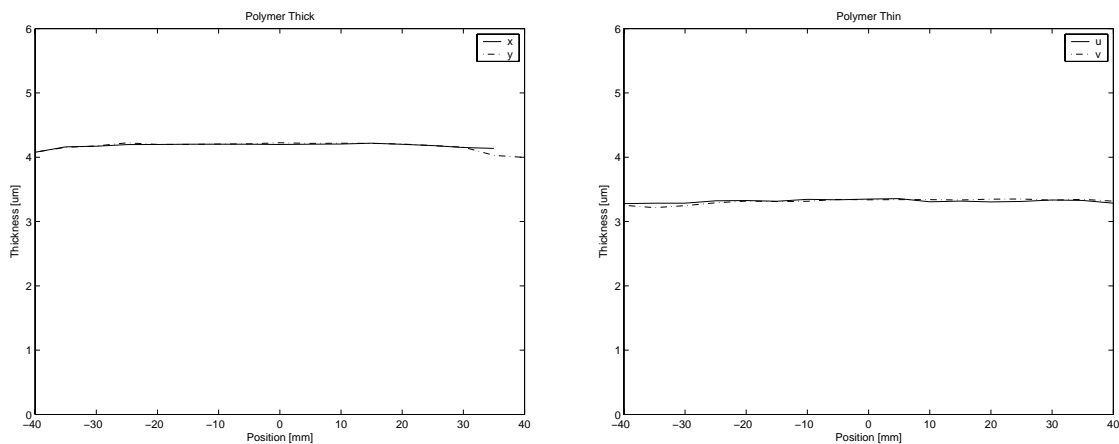
(a) Thickness of the thick polymer film measured over the x- and the y-axis as depicted in Appendix J

(b) Thickness of the thin polymer film measured over the u- and the v-axis as depicted in Appendix J

Figure 9.2: Uniformity of thickness of the two polymer films. [CD 2004, matlab/polymer_thickness/film_thickness_polymer.m]

films in a full scale. It can be seen from the figures that there are no notable variations in the thickness as a function of place on the surface. It is furthermore seen that, as expected the

---

[1]This is the only available material stating the refractive index of the polymer

thick polymer film is thicker than the thin polymer film. Zooming in on the thick polymer film yields the plot shown in Figure 9.3. The figure shows the variations in the thickness as
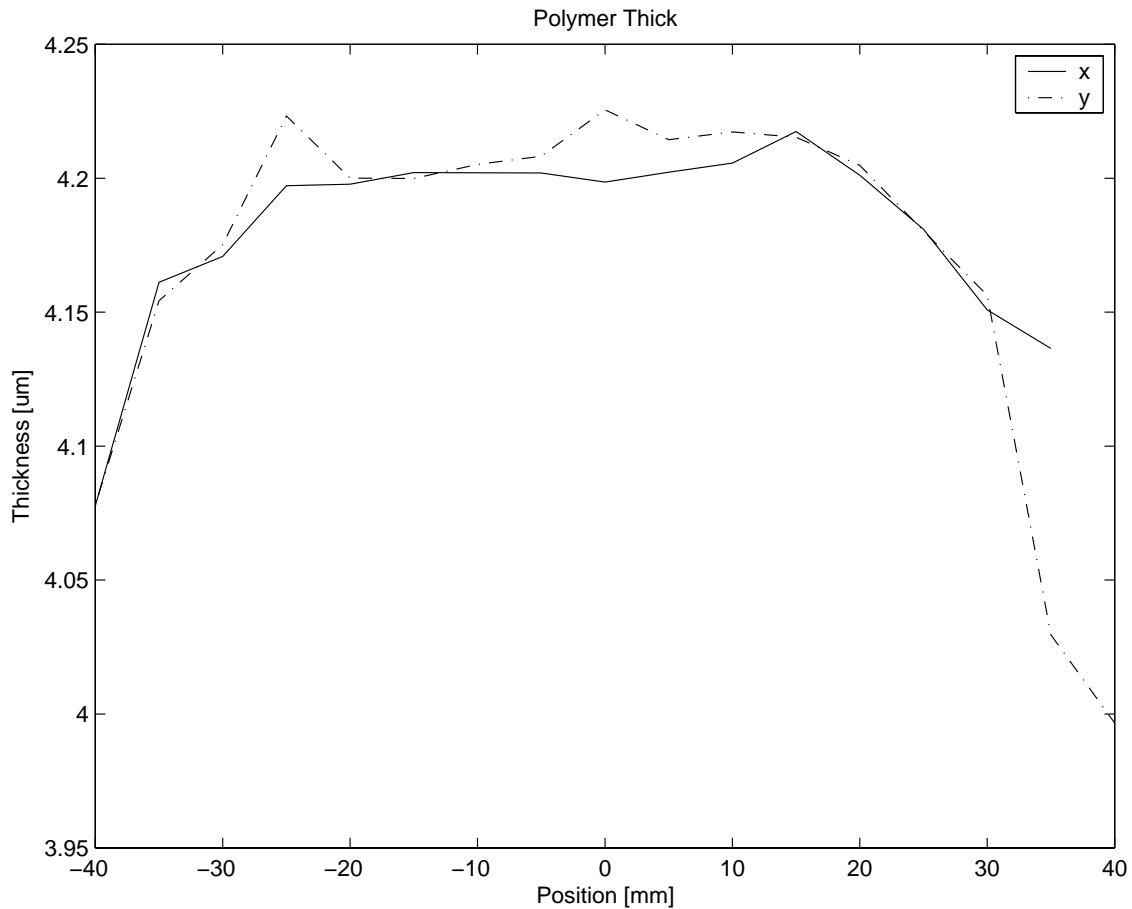
Figure 9.3: Thickness of the thick polymer, zoomed in. [CD 2004, matlab/polymer_thickness/film_thickness_polymer.m]

a function of the position. It can be seen that the film is thickest at the middle of the wafer and gets thinner at the edge. This makes sense because the polymer film is spin coated on the wafer. This is because the velocity of the edge of the wafer is higher than the velocity near the center of the wafer during the spin coating. The mean value of the thickness of the thick polymer film E_{thick} is calculated to

$$E_{thick} = 4.17 \, \mu\text{m} \tag{9.1}$$

The maximum deviation from the mean value for the thick polymer film is calculated to

$$S_{max,thick} = 4.2 \, \% \tag{9.2}$$

Zooming in on the thin film yields the plot in Figure 9.4. Furthermore it can be seen that the thin polymer film has a vague tendency of being thickest at the middle of the wafer and thinner towards the edge of the wafer. This is however not as noticeable as it is for the thick

65
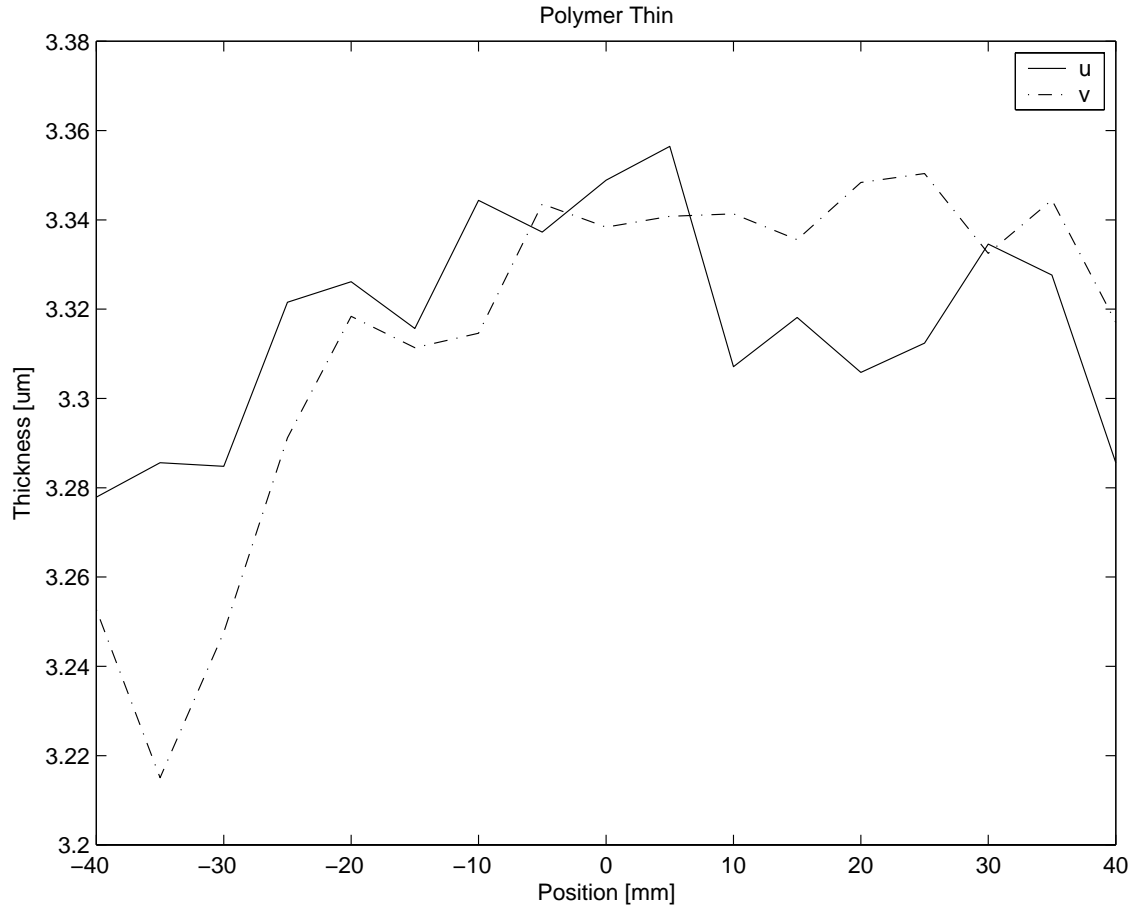
Figure 9.4: Thickness of the thin polymer, zoomed in.[CD 2004, mat-lab/polymer_thickness/film_thickness_polymer_thin.m]

film. The mean value of the thickness of the thin polymer film E_{thin} is calculated to

$$E_{thin} = 3.32 \ \mu m \tag{9.3}$$

The maximum deviation from the mean value for the thin polymer film is calculated to

$$S_{max,thin} = 3.0 \ \% \tag{9.4}$$

It is noted that both the wafers, with the imposed film, show a ring interference pattern. This indicates that the thickness of the film is a function of the distance from the center.

9.3 Summary

In general the calculated polymer film thickness changes as a function of wavelength, where the thickness is larger in the lower part of the wavelength spectrum. The polymer film thickness as a function of position on the wafer is almost constant with a maximum deviation of 4.2 % from the mean. Both wafers tend to be slightly thicker at the middle than at the edge.

Conclusion

The purpose of this project is to determine the complex index of refraction and the film thickness of different materials by use of ellipsometry.

The index of refraction as a function of wavelength is determined for four crystals from ellipsometric measurements of ψ and Δ. The crystals are silicon, copper, aluminum and silver. First, the index of refraction is calculated from a model where the crystals are considered pure. This gives results which are more or less equal to the respective table values. For silicon, copper and aluminum the tendency for the refractive index depicted as a function of the wavelength is the same as for the table values, but displaced slightly in magnitude. Silver has a different tendency for the real part of the refractive index.

In order to improve the results, the models are expanded to include thin layers of oxide. This improves the individual results considerably. Especially the refractive indexes for silicon and copper are hereafter very close to the table values. The small deviation from the table values is considered to be within a margin of experimental uncertainty. For aluminum and silver the results still do not coincide with table values. Optimizing the ambient-film-substrate model by changing the film material could improve the result of the calculated refractive indexes of the substrates. A silver surface tends to grow argentite and not silver oxide. This is not treated due to difficulties retrieving table values for the refractive index.

The tendency in the refractive index of the materials is theoretically explained by Drude-Lorentz models and band gap structures of the crystals. By using these models it has proven possible to simulate the refractive index of the four crystals within a reasonable margin.

The thickness of three films is calculated from measurements of ψ and Δ. The thickness of a layer of silicon dioxide on a substrate of silicon is determined from ψ-Δ measurements to be 22.9 nm. This value coincides with the automatic fit of the thickness by the Spectraray II software, which yields 22.8 nm. From this it can be concluded that the model is adequate. The manufacturer of the film states however that it is 21.5 ± 0.3 nm. An explanation to the difference can be that either the ellipsometer is not calibrated accurately or the thickness of the film is not as specified.

The thickness of two polymer films is calculated. The two films consist of the same type of polymer, but with different thickness. Compared to the silicon dioxide film, the calculations of the polymer film are made by use of additional considerations due to the interference pattern of ψ and Δ. These calculations yield a film thickness of 3.32 and 4.17 μm. There are no table values to confirm these results, but the results are accepted by NanoNord A/S. The results are therefore considered to be satisfying.

The uniformity of the polymer film is calculated by means of 34 individual measurements on each of the two films. The maximum deviations from the mean values of the thickness are 3.0 % and 4.2 % for the thin and the thick polymer film, respectively. The thick polymer film shows a slight tendency to decrease in thickness towards the edge, which can be explained by the higher speed at the edge during the spin coating of the film. Generally, the two films can be taken as uniform.

The goal of this project has been to measure the refractive index of several materials and the thickness of films imposed on a substrate. This goal is achieved with satisfying results.

Bibliography

Azzam, R. M. A. & Bashara, N. M. [1977], *Ellipsometry and Polarized Light*, 1st ed, North-Holland Publishing company. ISBN 0-7204-0694-3.

CD [2004], 'Enclosed cd by group 116'.

Classical Light [2004], http://www-gap.dcs.st-and.ac.uk/~history/HistTopics/Light_1.html.

Ehrenreich, H. & Philipp, H. R. [1962], *Optical Properties of Ag and Cu*, General Electric Research Laboratory Schenectady, New York.

Eric W. Weisstein, Geometric Series [2004], http://mathworld.wolfram.com/GeometricSeries.html. Geometric Series. From MathWorld–A Wolfram Web Resource.

Index of Refraction Values and Photonics Calculations [2004], http://www.luxpop.com/.

Jawoollam [2004], http://www.jawoollam.com/Tutorial_index.html.

Kittel, C. [1986], *Introduction to Solid State Physics*, 6th ed, John Wiley and Sons Inc. ISBN 0-471-87474-4.

Klein, M. V. & Furtak, T. E. [1986], *Optics*, 2nd ed, John Wiley and Sons Inc. ISBN 0-471-87287-0.

Kreyszig, E. [1999], *Advanced Engineering Mathematics*, 8th ed, John Wiley and Sons Inc. ISBN 0-471-33328-0.

Merriam-Webster Online [2004], http://www.m-w.com/.

MicroSystems, H. [2003], *PI-5878G Wet Etch Polyimide*, 1st ed, HD MicroSystems.

Palik, E. D. [1998], *Handbook of Optical Constants of Solids*, Academic Press. ISBN 0-12-544420-6.

Poksinski, M. [2003], *Total Internal Reflection Ellipsometry*, 1st ed, Institute of Technology, Linköping University. Licentiate Thesis No. 1016.

Råde, L. & Westergren, B. [1998], *Mathematics Handbook for Science and Engineering*, 4th ed, Studentlitteratur. ISBN 91-44-00839-2.

Reitz, J. R., Milford, F. J. & Christy, R. W. [1993], *Foundations of Electromagnetic Theory*, 4th ed, Addison-Wesley Publishing Company. ISBN 0-201-52624-7.

Rohlfing, M., Krüger, P. & Pollmann, J. [1993], *Quasiparticle Band-Structure for C, Si, Ge, GeAs and SiC using Gaussian-Orbital Sets*, Institut für Theoretische Physik II - Festkörperphysik, Universität Münster Germany.

Röseler, A. [1990], *Infrared Spectroscopic Ellipsometry*, 1st ed, Akademie-Verlag Berlin. ISBN 3-05-500623-2.

Spectroscopic Ellipsometer SE 850 [2004], `http://www.sentech.com/se850.htm`.

Yin, Y., Li, Z.-Y., Zhong, Z. & Gates, B. [2001], *Synthesis and Charactization of stable aqueous dispersions of silver nanoparticles through the Tollens process*, 1st ed, Journal of Materials Chemistry.

The Electromagnetic Wave Model of Light

A

The purpose of this appendix is to show that light can be described as electromagnetic waves through Maxwell's equations. Furthermore this appendix presents a solution to the wave equations describing light.

It has been known for a long time that light has wave properties, but it was not before Maxwell published his equations that the question of "what was waving ?" was solved. In 1862 Maxwell found out that electromagnetic waves are related to light when he realized that they travel at the same speed in free-space. In 1864 Maxwell wrote a paper in which he stated: *"This velocity is so nearly that of light that it seems we have strong reason to conclude that light itself is an electromagnetic disturbance in the form of waves propagated through the electromagnetic field according to electromagnetic laws"* [Classical Light 2004]. It was then that Maxwell realized that light itself can be described as an electromagnetic field in form of waves propagating through space and time. In 1873 Maxwell published his paper, *Electricity and Magnetism*, where he had developed four partial differential equations, know as Maxwell's equations, which completely describes the classical electromagnetic wave theory. It was therefore assumed that light could be described through Maxwell's equations.

Maxwell's Equations of Light

Maxwell's equations are four partial differential equations, which describes how the electric and the magnetic fields are coupled in an electromagnetic field waving through space and time. Maxwell's equations are in general given as

$$\nabla \cdot \mathbf{D} = \rho \tag{A.1a}$$

$$\nabla \cdot \mathbf{B} = 0 \tag{A.1b}$$

$$\nabla \times \mathbf{E} = -\frac{\partial \mathbf{B}}{\partial t} \tag{A.1c}$$

$$\nabla \times \mathbf{H} = (\mathbf{J} + \frac{\partial \mathbf{D}}{\partial t}) \tag{A.1d}$$

where

$$\mathbf{D} = \varepsilon_0 \mathbf{E} + \mathbf{P} \tag{A.2a}$$

$$\mathbf{B} = \mu_0 (\mathbf{M} + \mathbf{H}) \tag{A.2b}$$

where $\mathbf{D}$ is the electric displacement, $\mathbf{H}$ is the magnetic intensity, $\mathbf{E}$ is the electric field, $\mathbf{B}$ is the magnetic field, $\mathbf{J}$ is the current density, $\mathbf{P}$ is the polarization, $\mathbf{M}$ is the magnetization, ρ is the charge density, ε_0 is the electric permittivity of free-space (vacuum) and μ_0 is the magnetic permeability of free-space.

In order to show that light is an electromagnetic wave, it is assumed that light is propagating through free-space. In free-space there are no charge distributions and therefore no charges which can be polarized or magnetized. That is, $\mathbf{P} = 0$, $\mathbf{M} = 0$, $\mathbf{J} = 0$ and $\rho = 0$. This yields

$$\mathbf{D} = \varepsilon_0 \mathbf{E} \tag{A.3a}$$

$$\mathbf{H} = \frac{\mathbf{B}}{\mu_0} \tag{A.3b}$$

which reduces Maxwell's equations for light propagating through free-space to

$$\nabla \cdot \mathbf{E} = 0 \tag{A.4a}$$

$$\nabla \cdot \mathbf{B} = 0 \tag{A.4b}$$

$$\nabla \times \mathbf{E} = -\frac{\partial \mathbf{B}}{\partial t} \tag{A.4c}$$

$$\nabla \times \mathbf{B} = \mu_0 \varepsilon_0 \frac{\partial \mathbf{E}}{\partial t} \tag{A.4d}$$

Maxwell's equations for light can also be written in integral form which has the form

$$\int_s \mathbf{E} \cdot d\mathbf{A} = 0 \tag{A.5a}$$

$$\int_s \mathbf{B} \cdot d\mathbf{A} = 0 \tag{A.5b}$$

$$\int_k \mathbf{E} \cdot d\mathbf{r} = \frac{-\partial}{\partial t} \int \mathbf{B} \cdot d\mathbf{A} \tag{A.5c}$$

$$\int_k \mathbf{B} \cdot d\mathbf{r} = \mu_0 \varepsilon_0 \frac{\partial}{\partial t} \int \mathbf{E} \cdot d\mathbf{A} \tag{A.5d}$$

To show that Maxwell's equations of light leads to wave equations, the curl is taken of both sides of (A.4d)

$$\nabla \times \nabla \times \mathbf{B} = \nabla \times \left(\varepsilon_0 \mu_0 \frac{\partial \mathbf{E}}{\partial t} \right) \tag{A.6}$$

Using a vector identity [Reitz et al. 1993, p. 20] on the left side and rearranging terms of the right side of (A.6) yields

$$\nabla(\nabla \cdot \mathbf{B}) - \nabla \cdot \nabla \mathbf{B} = \mu_0 \varepsilon_0 \frac{\partial}{\partial t} (\nabla \times \mathbf{E}) \tag{A.7}$$

Now using (A.4b) and (A.4c)

$$\nabla^2 \mathbf{B} - \mu_0 \varepsilon_0 \frac{\partial^2 \mathbf{B}}{\partial t^2} = 0 \tag{A.8}$$

or

$$\nabla^2 \mathbf{B} - \frac{1}{c^2} \frac{\partial^2 \mathbf{B}}{\partial t^2} = 0 \tag{A.9}$$

where c, the speed of light, is given as $c = (\mu_0 \varepsilon_0)^{-1/2}$. With similar manipulations an equation describing the electric field can be obtained as

$$\nabla^2 \mathbf{E} - \frac{1}{c^2} \frac{\partial^2 \mathbf{E}}{\partial t^2} = 0 \tag{A.10}$$

From (A.9) and (A.10) it is seen that Maxwell's equations for light leads to two 3-dimensional wave equations; one for the magnetic field and one for the electric field, both propagating through space and time with the speed of light c in free-space.

Solving the Wave Equations of Light

In general the solutions of the wave equations of light, (A.9) and (A.10), are vector functions of four variables namely, x, y, z and t. That is

$$\mathbf{E} = \mathbf{E}(\mathbf{r}, t) \tag{A.11}$$
$$\mathbf{B} = \mathbf{B}(\mathbf{r}, t) \tag{A.12}$$

where $\mathbf{r}$ is a 3-dimensional vector $\mathbf{r} = x\hat{\mathbf{x}} + y\hat{\mathbf{y}} + z\hat{\mathbf{z}}$ where $\hat{\mathbf{x}}$, $\hat{\mathbf{y}}$ and $\hat{\mathbf{z}}$ are the unit vectors along the respective coordinate axes. These general solutions are rather complex to calculate and the problem is therefore simplified by assuming a plane wave and by placing the system of coordinates such that the wave propagates along the z-axis. For a plane wave propagating along the z-axis the disturbance over each xy-plane is constant and the wave equation of the electric field in (A.10) [1] is therefore reduced to

$$\frac{\partial^2 \mathbf{E}(z,t)}{\partial z^2} - \frac{1}{c^2} \frac{\partial^2 \mathbf{E}(z,t)}{\partial t^2} = 0 \tag{A.13}$$

or

$$\frac{\partial^2 \mathbf{E}(z,t)}{\partial t^2} = c^2 \frac{\partial^2 \mathbf{E}(z,t)}{\partial z^2} \tag{A.14}$$

From (A.13) or (A.14) it can be seen that the equation for a plane wave propagating along the z-axis is a 1-dimensional wave equation, which is a second order partial differential equation in two variables namely z and t. This partial differential equation can be solved be means of the Laplace transformation if the initial conditions are given. It is assumed that the electric field at $t = 0$ is zero and that the derivative of the electric field with respect to time at $t = 0$ is zero. [2] That is the initial conditions are

$$\mathbf{E}(z, 0) = \mathbf{0} \tag{A.15a}$$
$$\left. \frac{\partial \mathbf{E}}{\partial t} \right|_{t=0} = \mathbf{0} \tag{A.15b}$$

---

[1] The wave equation of the magnetic field is reduced in a similar way.
[2] The solution of the partial differential of a plane wave propagating along the z-axis is given for the electric field but can easily be found for the magnetic field by interchanging E with B.

Taking the Laplace transform with respect to t of (A.14) yields with reference to [Kreyszig 1999, p. 259 (2)]

$$L\left\{\frac{\partial^2 \mathbf{E}(z,t)}{\partial t^2}\right\} = s^2 L\{\mathbf{E}(z,t)\} - sE(z,0) - \left.\frac{\partial \mathbf{E}}{\partial t}\right|_{t=0} = c^2 L\left\{\frac{\partial^2 \mathbf{E}(z,t)}{\partial z^2}\right\} \quad \text{(A.16)}$$

where s is the complex Laplace variable. The Laplace transform with respect to t of the partial second order derivative of the electric field with respect to z is given as

$$L\left\{\frac{\partial^2 \mathbf{E}(z,t)}{\partial z^2}\right\} = \int_0^\infty e^{-st}\frac{\partial^2 \mathbf{E}(z,t)}{\partial z^2}dt = \frac{\partial^2}{\partial z^2}\int_0^\infty e^{-st}\mathbf{E}(z,t)dt = \frac{\partial^2}{\partial z^2}L\{E(z,t)\} \quad \text{(A.17)}$$

Comparing (A.16), (A.17) and using the initial conditions from (A.15) yields

$$\frac{\partial^2}{\partial z^2}\mathbf{E}_L(z,s) - \frac{s^2}{c^2}\mathbf{E}_L(z,s) = 0 \quad \text{(A.18)}$$

where $\mathbf{E}_L(z,s) = L\{\mathbf{E}(z,t)\}$. Since this equation only contain derivatives with respect to z it can be considered as an ordinary differential equation of $\mathbf{E}_L(z,s)$, which has a general solution given as

$$\mathbf{E}_L(z,s) = \mathbf{F}(s)e^{-sz/c} + \mathbf{G}(s)e^{sz/c} \quad \text{(A.19)}$$

Taking the inverse Laplace transform of (A.19) and making use of the Laplace shifting theorem yields

$$\mathbf{E}(z,t) = f\left(t - \frac{z}{c}\right) + g\left(t + \frac{z}{c}\right) \quad \text{(A.20)}$$

Thus the general solution for a plane wave propagating along the z-axis is given by (A.20). A special case of (A.20) is a harmonic traveling plane light wave where $g = 0$

$$\mathbf{E}(z,t) = f\left(t - \frac{z}{c}\right) = \mathbf{E}_0 \cos\left[\omega\left(t - \frac{z}{c}\right) + \phi\right] \quad \text{(A.21)}$$

where $\mathbf{E}_0$ is a constant vector associated with the maximum size of the oscillation, ϕ is the phase at $z = 0$ and $t = 0$, $\omega = 2\pi\nu$ and ν is the frequency in hertz. If the normal of the waveplan is not along the z-axis but pointing in an arbitrary direction along the unit vector $\hat{\mathbf{s}}$ the monochromatic[3] plane wave yields

$$\mathbf{E}(\mathbf{r},t) = f\left(t - \frac{\mathbf{r}\cdot\hat{\mathbf{s}}}{c}\right) = \mathbf{E}_0 \cos\left[\omega\left(t - \frac{\mathbf{r}\cdot\hat{\mathbf{s}}}{c}\right) + \phi\right] \quad \text{(A.22)}$$

where $\mathbf{r}$ is a vector pointing from the origin of the coordinate system to an arbitrary point on the plan with the normal vector $\hat{\mathbf{s}}$ and $\mathbf{E}_0$ is a constant vector equal to the maximum oscillation. If the wavevector $\mathbf{k}$ is introduced as

$$\mathbf{k} = \frac{\omega}{c}\hat{\mathbf{s}} \quad \text{(A.23)}$$

---

[3]Radiation of a single wavelength, that is ω is constant over time.

the monochromatic plane wave is given as

$$\mathbf{E}(\mathbf{r},t) = \mathbf{E_0}\cos\left[\omega t - \mathbf{k}\cdot\mathbf{r} + \phi\right] = \mathbf{E_0}\text{Re}\left\{e^{j(\omega t - \mathbf{k}\cdot\mathbf{r} + \phi)}\right\} \tag{A.24}$$

In similar ways the solution to (A.9), the wave equation for the magnetic field, can be found as

$$\mathbf{B}(\mathbf{r},t) = \mathbf{B_0}\text{Re}\left\{e^{j(\omega t - \mathbf{k}\cdot\mathbf{r} + \phi)}\right\} \tag{A.25}$$

Thus the solution to Maxwell's equations for monochromatic plane light waves are given as

$$\mathbf{E} = \mathbf{E_0}e^{j(\omega t - \mathbf{k}\cdot\mathbf{r} + \phi)} \tag{A.26a}$$

$$\mathbf{B} = \mathbf{B_0}e^{j(\omega t - \mathbf{k}\cdot\mathbf{r} + \phi)} \tag{A.26b}$$

where $\mathbf{k}$ is the wavevector, defined as in (A.23), along which the light waves propagates. The "Re" notation is dropped knowing that the physical fields are the real part of (A.26). [Klein & Furtak 1986, pp. 22-23], [Kreyszig 1999, pp. 251-273]

Monochromatic Plane Light Waves

Substituting the solution of the monochromatic plane light wave from (A.26) into Maxwell's equation (A.4c) yields

$$-j\mathbf{k}\times\mathbf{E} = -j\omega\mathbf{B} \tag{A.27}$$

or

$$\mathbf{B} = \frac{\mathbf{k}\times\mathbf{E}}{\omega} \tag{A.28}$$

or by substituting with (A.23)

$$\mathbf{B} = \frac{1}{c}\hat{\mathbf{s}}\times\mathbf{E} \tag{A.29}$$

Thus by (A.28) a monochromatic plane light wave has an electric field perpendicular to a magnetic fields which again propagates along a wavevector perpendicular to both the electric and magnetic field. Furthermore by (A.29) the electric field and the magnetic field are in phase. [Klein & Furtak 1986, pp. 46-47]

Fresnel Reflection and Transmission Coefficients

B

The purpose of this appendix is to describe the reflection and transmission of light waves at an interface between two media. The interface is assumed to be smooth and abrupt, and the two media at the interface are assumed homogeneous, linear and isotropic. The incident light is divided into two different polarization states, of which one is analyzed further using among other things Maxwell's equations. This appendix is based on [Klein & Furtak 1986, pp. 71-80].

When an electromagnetic wave of light is incident on a boundary between two materials with different index of refraction, a situation as the one depicted in Figure B.1 occur. The
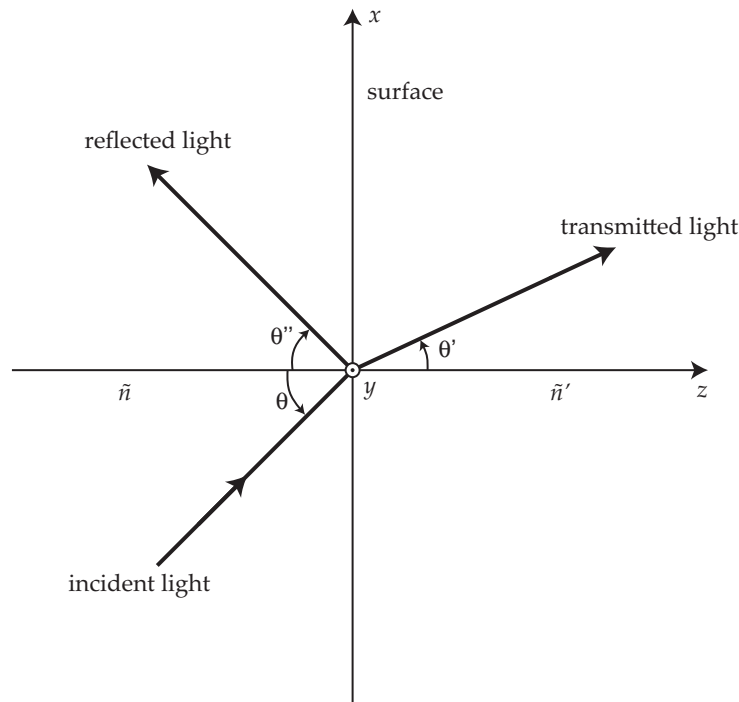
Figure B.1: Situation where incident light, in the *xz*-plane is propagating towards a surface, in the *xy*-plane. After interaction with the surface, part of the light is transmitted and part of it is reflected.

surface lies in the *xy*-plane and the plane of incident is the *xz*-plane. Part of the wave is transmitted and part of it is reflected. It can readily be proven which direction the reflected and transmitted wave will have by use of Fermat's principle or Huygens' construction.

The focus in this appendix will, however, be on a derivation of the reflection coefficient ρ defined as $E_{reflected}/E_{incident}$ and the transmission coefficient τ defined as $E_{transmitted}/E_{incident}$.

Description of Light According to Maxwell's Equations

Light can be considered to be electromagnetic waves, as described in Appendix A. It consists of a magnetic and an electric field, $\mathbf{B}$ and $\mathbf{E}$ respectively. They are perpendicular to each other and to the wavevector $\mathbf{k}$, which is pointing in the direction of propagation. The connection between $\mathbf{B}$ and $\mathbf{E}$ is for a monochromatic plane wave given as

$$\mathbf{B} = \frac{\mathbf{k} \times \mathbf{E}}{\omega} \tag{B.1}$$

as described in (A.28). As $\mathbf{E}$ is perpendicular to $\mathbf{k}$, the amplitudes of the electric and magnetic field in (B.1) can be expressed as

$$B = \frac{k}{\omega} E \tag{B.2}$$

or in a media

$$B = \frac{\tilde{n}}{c} E \tag{B.3}$$

where $\tilde{n}$ is the complex index of refraction and c is the speed of light in vacuum. The substitution from (B.2) to (B.3) is carried out using the expression given by (F.5).

Definition of Polarization States

It is convenient to split the polarization state of the incoming wave into two components. These are denoted π- and σ-polarized light[1]. Each case has to fulfill (B.1).

π-**polarized light:** $\mathbf{E}$ is in the plane of incidence, i.e. it is parallel to the plane of incidence. Consequently, $\mathbf{B}$ is perpendicular to the plane of incidence.

σ-**polarized light:** $\mathbf{B}$ lies in the plane of incidence, thus $\mathbf{E}$ is perpendicular to the plane.

An incident linearly polarized plane wave can be described by a linear combination of these components.

Derivation of Boundary Conditions

In the following it will be deduced from Maxwell's equation (A.4c) that the tangential component of $\mathbf{E}$ is continuous across an interface between to media with different index of refraction. The situation is illustrated in Figure B.2. The figure is a two-dimensional illustration, where the interface is marked as a dashed line. A rectangle has been inserted to assist in deriving the condition. The rectangle has the length l_0, which is finite, yet small enough to avoid a difference in the electric field along each of the individual sides. The width Δl of the rectangle is infinitely small ($\Delta l \rightarrow 0$).

The E-fields on the two sides are denoted $\mathbf{E}_1$ and $\mathbf{E}_2$, with their respective tangential component with respect to the interface denoted $\mathbf{E}_{1t}$ and $\mathbf{E}_{2t}$.

---

[1] π and σ are the Greek letters for p and s, where p refer to the term parallel, and s refer to the term senkrecht, which is German for perpendicular [Azzam & Bashara 1977, p. 272].
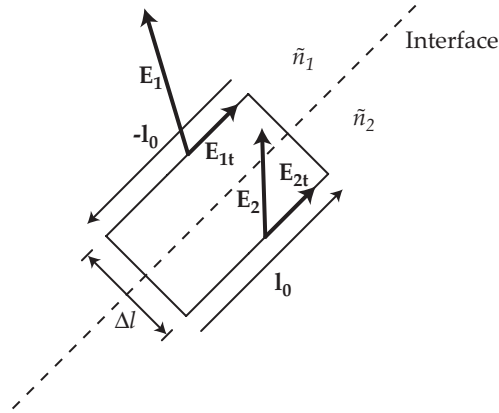
Figure B.2: Depiction of an interface between two media with different index of refraction. A rectangle, which is placed across the interface, is used to derive the tangential condition for the electric field.

(A.4c) is in integral form given by the following as described in Appendix A

$$\oint_k \mathbf{E} \cdot d\mathbf{r} = -\frac{\partial}{\partial t} \int \mathbf{B} \cdot d\mathbf{A} \qquad (B.4)$$

which is applied to the area described by the rectangle in Figure B.2. As the bounded area is infinitely small due to Δl, the integral over $d\mathbf{A}$ is zero. Thus (B.4) is reduced to

$$\oint_k \mathbf{E} \cdot d\mathbf{r} = 0 \qquad (B.5)$$

where the closed curve integral can be divided into four components given by the sides of the rectangle. As the two sides with the length Δl are infinitely small, their contributions to the integral are likewise infinitely small. Thus the curve integral can be expressed by the two parallel sides

$$\mathbf{l_0} \cdot \mathbf{E_2} - \mathbf{l_0} \cdot \mathbf{E_1} = 0 \qquad (B.6)$$

where the tangential parts of $\mathbf{E_1}$ and $\mathbf{E_2}$ can be inserted in order to skip the vector notation

$$l_0 E_{2t} - l_0 E_{1t} = 0 \qquad (B.7)$$

which results in the following

$$E_{1t} = E_{2t} \qquad (B.8)$$

By this, it can be concluded that the tangential part of $\mathbf{E}$ is continuous across an interface.

In a similar way it can be shown that the tangential component of $\mathbf{B}/\mu$ is preserved across an interface.

$$\frac{B_{1t}}{\mu_1} = \frac{B_{2t}}{\mu_2} \qquad (B.9)$$

However, since $\mu \cong \mu_0$ at optical frequencies for all materials [Reitz et al. 1993, p. 415], the simplification

$$B_{1t} = B_{2t} \tag{B.10}$$

is used instead of (B.9).

The boundary conditions for the normal component can likewise be derived as

$$\varepsilon_1 E_{1n} = \varepsilon_2 E_{2n} \tag{B.11}$$

$$B_{1n} = B_{2n} \tag{B.12}$$

Direction of Propagation

The plane of incidence is defined to be the xz-plane, thus

$$\mathbf{k} = (k_x, 0, k_z) \tag{B.13a}$$

The components of the wavevector of the transmitted wave $\mathbf{k}'$ and the wavevector of the reflected wave $\mathbf{k}''$ are given as

$$\mathbf{k}' = (k_x', k_y', k_z') \tag{B.13b}$$

$$\mathbf{k}'' = (k_x'', k_y'', k_z'') \tag{B.13c}$$

It is possible to express (B.8) and (B.10) by the use of the solutions to the wave equations which states

$$\mathbf{E} = \mathbf{E_0} e^{j(\omega t - \mathbf{k} \cdot \mathbf{r} + \phi)} \tag{B.14a}$$

$$\mathbf{B} = \mathbf{B_0} e^{j(\omega t - \mathbf{k} \cdot \mathbf{r} + \phi)} \tag{B.14b}$$

as described in (A.26). However, as the frequency is the same for both the incident, the transmitted and the reflected wave, the term involving ω can be neglected. The same holds for ϕ. Thus by using (B.14), with the notations given by (B.13), it is possible to express (B.8) and (B.10) by the following

$$E_t e^{-jxk_x} + E_t'' e^{-j(xk_x'' + yk_y'')} = E_t' e^{-j(xk_x' + yk_y')} \tag{B.15a}$$

$$B_t e^{-jxk_x} + B_t'' e^{-j(xk_x'' + yk_y'')} = B_t' e^{-j(xk_x' + yk_y')} \tag{B.15b}$$

From (B.15) it follows that

$$k_y'' = k_y' = 0 \tag{B.16}$$

and

$$k_x'' = k_x' = k_x \tag{B.17}$$

It can thus be concluded that both the transmitted and the reflected wave lies in the plane of incidence, i.e. the xz-plane.

Orientation of E and B for σ-polarized Light

From (B.8) it is clear that

$$E_y + E_y'' = E_y' \tag{B.18}$$

and

$$E_x + E_x'' = E_x' \tag{B.19}$$

For σ-polarized light, the incident **E**-field is defined to be strictly perpendicular to the plane of incidence, thus $\mathbf{E} = E_y$. Since the incident light has no x- or z-component, so will neither the reflected nor the transmitted. Thus **E**, **E**′ and **E**″ will all be directed along the y-axis with the following amplitude relation according to (B.18)

$$E + E'' = E' \tag{B.20}$$

As the **E**-fields are strictly tangential to the interface, it can be concluded due to (B.1) that **B**, **B**′ and **B**″ lies in the xz-plane. Thus, the x-component of **B**, **B**′ and **B**″ is the only tangential component of the respective magnetic fields with respect to the interface. Hence from (B.10) it can be concluded that

$$B_x + B_x'' = B_x' \tag{B.21}$$

Reflection and Transmission Coefficient for σ-polarized Light

The purpose of this section is to derive the reflected and transmitted part of σ-polarized light, ρ_σ and τ_σ respectively. The situation where σ-polarized light is incident on a surface is depicted in Figure B.3. The following trigonometrical coherences can be deduced from the figure

$$B_x = -B\cos(\theta) \tag{B.22a}$$
$$B_x' = -B'\cos(\theta') \tag{B.22b}$$
$$B_x'' = B''\cos(\theta) \tag{B.22c}$$

By inserting (B.22) into (B.21), it can be seen that

$$\cos(\theta)(B - B'') = \cos(\theta')B' \tag{B.23}$$

When applying (B.3) on (B.23) it yields

$$\tilde{n}\cos(\theta)(E - E'') = \tilde{n}'\cos(\theta')E' \tag{B.24}$$

By substituting E' in (B.24) with the expression given by (B.20) and isolating the term E''/E, an expression for the reflected component ρ_σ is derived

$$\rho_\sigma \triangleq \frac{E''}{E} = \frac{\tilde{n}\cos(\theta) - \tilde{n}'\cos(\theta')}{\tilde{n}\cos(\theta) + \tilde{n}'\cos(\theta')} \tag{B.25}$$
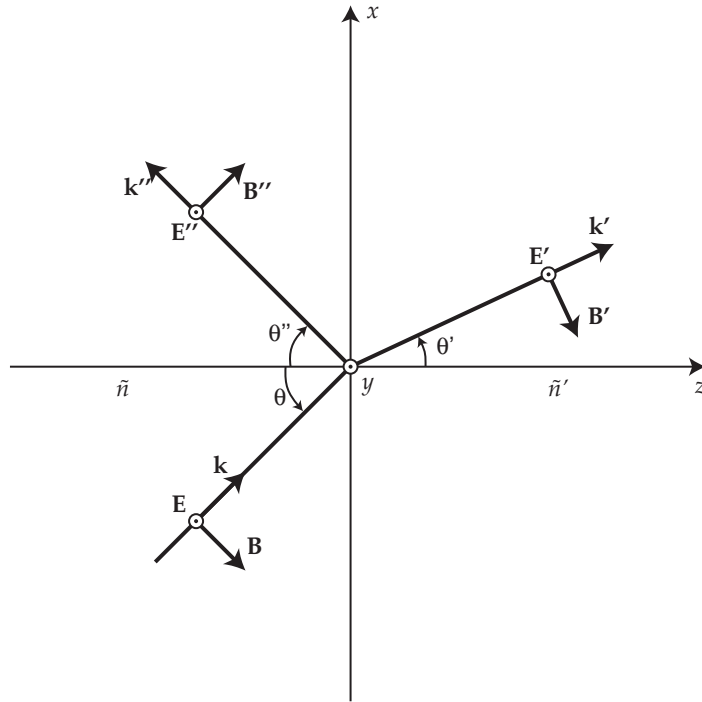
Figure B.3: Depiction of σ-polarized light. [Klein & Furtak 1986, p. 75]

By using (B.20) in order to eliminate E'' in (B.24), an expression for the transmitted part of the **E**-field can be obtained

$$\tau_\sigma \triangleq \frac{E'}{E} = \frac{2\tilde{n}\cos(\theta)}{\tilde{n}\cos(\theta) + \tilde{n}'\cos(\theta')} \tag{B.26}$$

It is, however, in some cases disadvantageous to have θ' included in the expression for ρ_σ and τ_σ, as θ' can be rather difficult to measure. Consequently, $\cos(\theta')$ is replaced by another term derived by Snell's law. Snell's law states that

$$\tilde{n}\sin(\theta) = \tilde{n}'\sin(\theta') \tag{B.27}$$

When modifying (B.27) by means of simple geometrical manipulations, an expression for $\cos(\theta')$ can be deduced

$$\cos(\theta') = \sqrt{1 - \left(\frac{\tilde{n}}{\tilde{n}'}\right)^2 \sin^2(\theta)} \tag{B.28}$$

By inserting this expression for $\cos(\theta')$ into (B.25) and (B.26) respectively, ρ_σ and τ_σ can be defined merely by $\tilde{n}$, $\tilde{n}'$ and θ

$$\rho_\sigma = \frac{\tilde{n}\cos(\theta) - \tilde{n}'\sqrt{1 - \left(\frac{\tilde{n}}{\tilde{n}'}\right)^2 \sin^2(\theta)}}{\tilde{n}\cos(\theta) + \tilde{n}'\sqrt{1 - \left(\frac{\tilde{n}}{\tilde{n}'}\right)^2 \sin^2(\theta)}} \tag{B.29a}$$

$$\tau_\sigma = \frac{2\tilde{n}\cos(\theta)}{\tilde{n}\cos(\theta) + \tilde{n}'\sqrt{1 - \left(\frac{\tilde{n}}{\tilde{n}'}\right)^2 \sin^2(\theta)}} \tag{B.29b}$$

Reflection and Transmission Coefficient for π-polarized Light

Similar calculations can be done for π-polarized light in order to obtain expressions for ρ_π and τ_π. This leads to the following expressions

$$\rho_\pi = \frac{\tilde{n}' \cos(\theta) - \tilde{n}\cos(\theta')}{\tilde{n}' \cos(\theta) + \tilde{n}\cos(\theta')} \tag{B.30a}$$

$$\tau_\pi = \frac{2\tilde{n}\cos(\theta)}{\tilde{n}' \cos(\theta) + \tilde{n}\cos(\theta')} \tag{B.30b}$$

where again $\cos(\theta')$ can be replaced by the expression derived in (B.28).

Three Phase Optical System

<div style="text-align: right">C</div>

This appendix concerns reflection and transmission in an optical system of three phases consisting of medium 0, medium 1 and medium 2. The objective is to relate the electrical field of an incident wave to the electrical field of a resultant reflected and a resultant transmitted wave. The optical system is illustrated in Figure C.1
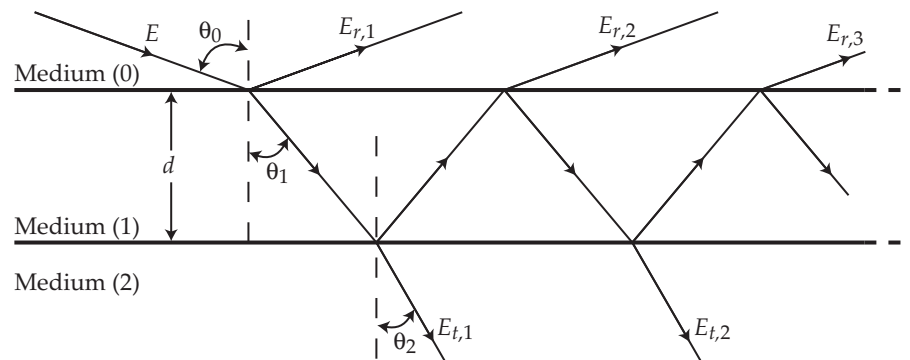
Figure C.1: Illustration of a three phase optical system where an incident wave E is being reflected and transmitted due to the boundaries between the three media. [Azzam & Bashara 1977, p. 283]

In order to simplify the deduction of the relation between the incident wave and the resultant reflected and transmitted wave some assumptions are made:

1. The system is considered to have parallel boundaries between each phase.

2. Medium 1 has lateral dimensions much larger than its thickness d, whereas medium 0 and 2 are of infinite thickness.

3. All three media are considered homogenous and optically isotropic.

4. Medium 1 is not an amplifying medium.

5. Monochromatic plane incident wave.

Each of these assumptions is elaborated in the next sections where the assumptions have direct influence.

Reflection and Transmission of an Incident Wave

The three phase system depicted in Figure C.1 shows an incident wave propagating through medium 0, until it makes contact with medium 1 at an angle of θ_0. The incident wave is

partially reflected at the boundary and partially transmitted through medium 1 at an angle of θ_1. The transmitted part of the incident wave propagates through medium 1 until it makes contact with the boundary between medium 1 and medium 2. At this boundary the wave is again partially reflected and partially transmitted through medium 2 at an angle of θ_2. The connection between the angles θ_0, θ_1 and θ_2 are given by Snell's law

$$\tilde{n}_0 \sin(\theta_0) = \tilde{n}_1 \sin(\theta_1) = \tilde{n}_2 \sin(\theta_2) \tag{C.1}$$

where $\tilde{n}_0$, $\tilde{n}_1$ and $\tilde{n}_2$ are the complex refractive indexes for medium 0, 1 and 2 respectively.

In the following, calculations and considerations are done without regard to the polarization of the incident wave. It is assumed that the incident wave is either σ or π polarized. The subject polarization is treated in the last section of this appendix.

Reflection

By considering Figure C.1 and using the method of calculating reflection and transmission of light waves by use of Fresnel reflection and transmission coefficients (ρ, τ), as described in Appendix B, an expression for the reflected wave can be deducted as

$$E_{r,1} = \rho_{01} \cdot E \tag{C.2a}$$
$$E_{r,2} = \tau_{01} e^{-j\beta} \rho_{12} e^{-j\beta} \tau_{10} \cdot E \tag{C.2b}$$
$$E_{r,3} = \tau_{01} e^{-j\beta} \rho_{12} e^{-j\beta} \rho_{10} e^{-j\beta} \rho_{12} e^{-j\beta} \tau_{10} \cdot E \tag{C.2c}$$

where β denotes the phase change due to propagation of the light wave through medium 1.

Deduction of β

The cause of this phase change is illustrated in Figure C.2. The reflected waves $E_{r,1}$ and $E_{r,2}$ can be considered parts of a total reflected plane wave, hence the phases of the two reflected waves must be compared in the points E and C. Wave $E_{r,1}$ has a phase change due to the

Figure C.2: Illustration of the reflection of an incident monochromatic plane wave E_{in}. The reflected waves $E_{r,1}$ and $E_{r,2}$ constitute a plane by connecting the points E and C as illustrated in the figure.

propagation from A to E, whereas wave $E_{r,2}$ has a phase change due to the propagation from A to C. From Figure C.2 it can be seen that

$$|AD| = \frac{|AE|}{2} \tag{C.3}$$

$$|AB| = \frac{|ABC|}{2} \tag{C.4}$$

and thus the phase difference is considered in points D and B instead, as this will simplify the calculations, while still yielding the same result.

As described in Appendix A a plane wave is described by the equation

$$\mathbf{E}(z,t) = \mathbf{E_0}\cos\left(\omega \cdot t - \mathbf{k} \cdot z + \varphi\right) \tag{C.5}$$

where $\mathbf{k} = \frac{2\pi}{\lambda}\tilde{n}$, λ being the free-space wavelength of the incident wave. The phase of this wave is denoted $\Phi = -\mathbf{k} \cdot z + \varphi$.

The phase change β can be expressed as the difference in phase of the two waves $E_{r,1}$ and $E_{r,2}$ in the points D and B respectively

$$\beta = \Phi_D - \Phi_B \tag{C.6}$$

$$= \mathbf{k_1} \cdot z_1 - \mathbf{k_0} \cdot z_0 \tag{C.7}$$

$$= \frac{2\pi}{\lambda}\left(\tilde{n}_1 \cdot z_1 - \tilde{n}_0 \cdot z_0\right) \tag{C.8}$$

where $z_1 = |AB|$ and $z_0 = |AD|$. By considering Figure C.2 it can be seen that

$$z_1 = \frac{d}{\cos(\theta_1)} \tag{C.9}$$

$$y = \sin(\theta_1) \cdot z_1 = \frac{d \cdot \sin(\theta_1)}{\cos(\theta_1)} \tag{C.10}$$

$$z_0 = \sin(\theta_0) \cdot y = \frac{d \cdot \sin(\theta_1) \cdot \sin(\theta_0)}{\cos(\theta_1)} \tag{C.11}$$

Furthermore it is known by Snell's law that

$$\tilde{n}_0 = \frac{\tilde{n}_1 \cdot \sin(\theta_1)}{\sin(\theta_0)} \tag{C.12}$$

By making substitutions for z_1, z_0 and $\tilde{n}_0$ due to (C.9), (C.11) and (C.12) into (C.8) a reduced expression for the phase change can be obtained

$$\beta = \frac{2\pi}{\lambda}\left(\tilde{n}_1 \cdot \frac{d}{\cos(\theta_1)} - \frac{\tilde{n}_1 \cdot \sin(\theta_1)}{\sin(\theta_0)} \cdot \frac{d \cdot \sin(\theta_0) \cdot \sin(\theta_1)}{\cos(\theta_1)}\right) \tag{C.13}$$

$$= \frac{2\pi \cdot d \cdot \tilde{n}_1}{\lambda}\left(\frac{1 - \sin^2(\theta_1)}{\cos(\theta_1)}\right) \tag{C.14}$$

$$= 2\pi\frac{d}{\lambda}\tilde{n}_1\cos(\theta_1) \tag{C.15}$$

$$= 2\pi\frac{d}{\lambda}\sqrt{\tilde{n}_1^2 - \tilde{n}_0^2\sin^2(\theta_0)} \tag{C.16}$$

If medium 1 is absorbing β is complex i.e. $\beta = \beta' + j\beta''$ [Röseler 1990, p. 31].

Total Reflected Wave

Due to the second assumption made in the beginning of this appendix[1] and (C.2) the total reflected wave E_r can be calculated by adding all the partial reflected waves given in (C.2)

$$E_r = \left(\rho_{01} + \tau_{01}\tau_{10}\rho_{12}e^{-j2\beta} + \tau_{01}\tau_{10}\rho_{10}\rho_{12}^2 e^{-j4\beta} + \tau_{01}\tau_{10}\rho_{10}^2\rho_{12}^3 e^{-j6\beta} + ... \right) \cdot E \tag{C.17}$$

$$P = \rho_{01} + \tau_{01}\tau_{10}\rho_{12}e^{-j2\beta} + \tau_{01}\tau_{10}\rho_{10}\rho_{12}^2 e^{-j4\beta} + \tau_{01}\tau_{10}\rho_{10}^2\rho_{12}^3 e^{-j6\beta} + ... \tag{C.18}$$

where P (uppercase ρ) denotes the total reflection ratio.

Transmission

The deduction of the total transmission ratio T (uppercase τ) is analogous to the deduction of the total reflection ratio and hence will not be described. T is given by

$$T = \tau_{01}\tau_{12}e^{-j\beta} + \tau_{01}\tau_{12}\rho_{10}\rho_{12}e^{-j3\beta} + \tau_{01}\tau_{12}\rho_{10}^2\rho_{12}^2 e^{-j5\beta} + ... \tag{C.19}$$

Rewriting of Infinite Geometric Series

The two series describing P and T can be rewritten in order to achieve expressions that can be used in the further analysis of the reflection and transmission of a light wave due to a three phase optical system. As the principle behind the rewriting is the same, only the total reflected amplitude will be treated. First some manipulations are performed

$$P = \rho_{01} + \tau_{01}\tau_{10}\rho_{12}e^{-j2\beta} + \tau_{01}\tau_{10}\rho_{10}\rho_{12}^2 e^{-j4\beta} + \tau_{01}\tau_{10}\rho_{10}^2\rho_{12}^3 e^{-j6\beta} + ... \tag{C.20}$$

$$= \rho_{01} + \tau_{01}\tau_{10}\rho_{12}e^{-j2\beta} \cdot P'_n \tag{C.21}$$

where P'_n is an infinite geometric series expressed by

$$P'_n = \sum_{k=0}^{n} \left(\rho_{10}\rho_{12}e^{-j2\beta} \right)^k = 1 + \rho_{10}\rho_{12}e^{-j2\beta} + \rho_{10}^2\rho_{12}^2 e^{-j4\beta} + ... + \left(\rho_{10}\rho_{12}e^{-j2\beta} \right)^n \tag{C.22}$$

$$= \sum_{k=0}^{n} q^k = 1 + q + q^2 + ... + q^n \tag{C.23}$$

with $q = \rho_{10}\rho_{12}e^{-j2\beta}$. The task of rewriting the total reflected amplitude now consists of simplifying (C.23). Multiplication by q yields

$$qP'_n = q + q^2 + q^3 + ... + q^{n+1} \tag{C.24}$$

Subtracting (C.24) from (C.23) gives

$$(1-q)P'_n = 1 - q^{n+1}$$

$$P'_n = \frac{1 - q^{n+1}}{1 - q} \tag{C.25}$$

---

[1]Due to the much larger lateral dimensions of medium 1, compared to the thickness, an almost infinite number of partial waves will be reflected

Due to the fourth assumption in the beginning of this appendix $|\rho_{10}\rho_{12}e^{-j2\beta}| < 1$ and thus $|q| < 1$ which entails that

$$P' \equiv P'_\infty = \frac{1 - q^{\infty+1}}{1 - q} \rightarrow \frac{1}{1 - q} \text{ for } n \rightarrow \infty \tag{C.26}$$

[Kreyszig 1999, p. 736], [Eric W. Weisstein, Geometric Series 2004]

By substituting this limit value for P'_n into (C.21) a simplified expression for P is accomplished

$$\begin{aligned} P &= \rho_{01} + \frac{\tau_{01}\tau_{10}\rho_{12}e^{-j2\beta}}{1 - \rho_{10}\rho_{12}e^{-j2\beta}} \\ &= \frac{\rho_{01} - \rho_{01}\rho_{10}\rho_{12}e^{-j2\beta} + \tau_{01}\tau_{10}\rho_{12}e^{-j2\beta}}{1 - \rho_{10}\rho_{12}e^{-j2\beta}} \\ &= \frac{\rho_{01} + \rho_{12}e^{-j2\beta}}{1 + \rho_{01}\rho_{12}e^{-j2\beta}} \end{aligned} \tag{C.27}$$

where the relations $\rho_{10} = -\rho_{01}$ and $\tau_{01}\tau_{10} = 1 - \rho_{01}{}^2$ have been used [Klein & Furtak 1986, p. 80].

Similar rewriting can be done of the total transmission ratio T given by (C.19) which yields

$$T = \frac{\tau_{01}\tau_{12}e^{-j\beta}}{1 + \rho_{01}\rho_{12}e^{-j2\beta}} \tag{C.28}$$

The results in (C.27) and C.28 are the total complex reflection and transmission coefficients of either σ or π polarization.

σ and π Polarized Incident Wave

The information of polarization of the wave is readily restored by adding a subscript to the deducted expressions for P and T

$$P_\sigma = \frac{\rho_{01,\sigma} + \rho_{12,\sigma}e^{-j2\beta}}{1 + \rho_{01,\sigma}\rho_{12,\sigma}e^{-j2\beta}} \tag{C.29a}$$

$$P_\pi = \frac{\rho_{01,\pi} + \rho_{12,\pi}e^{-j2\beta}}{1 + \rho_{01,\pi}\rho_{12,\pi}e^{-j2\beta}} \tag{C.29b}$$

$$T_\sigma = \frac{\tau_{01,\sigma}\tau_{12,\sigma}e^{-j\beta}}{1 + \rho_{01,\sigma}\rho_{12,\sigma}e^{-j2\beta}} \tag{C.29c}$$

$$T_\pi = \frac{\tau_{01,\pi}\tau_{12,\pi}e^{-j\beta}}{1 + \rho_{01,\pi}\rho_{12,\pi}e^{-j2\beta}} \tag{C.29d}$$

With these four equations it is possible to calculate the reflection and transmission of any kind of polarized incident light wave. The incident light wave can be divided into a component perpendicular to the plane of incidence (σ component) and a component parallel to the plane of incidence (π component) and the reflection and transmission of each of

these components can then be treated separately. The β value is not different for the σ and π components due to the third assumption in the beginning of the appendix. However the reflection and transmission coefficients (ρ, τ) are. This is treated in Appendix B. The reflection coefficients are listed in (C.30)

$$\rho_{01,\sigma} = \frac{\tilde{n}_0 \cos(\theta_0) - \tilde{n}_1 \cos(\theta_1)}{\tilde{n}_0 \cos(\theta_0) + \tilde{n}_1 \cos(\theta_1)} \tag{C.30a}$$

$$\rho_{12,\sigma} = \frac{\tilde{n}_1 \cos(\theta_1) - \tilde{n}_2 \cos(\theta_2)}{\tilde{n}_1 \cos(\theta_1) + \tilde{n}_2 \cos(\theta_2)} \tag{C.30b}$$

$$\rho_{01,\pi} = \frac{\tilde{n}_1 \cos(\theta_0) - \tilde{n}_0 \cos(\theta_1)}{\tilde{n}_1 \cos(\theta_0) + \tilde{n}_0 \cos(\theta_1)} \tag{C.30c}$$

$$\rho_{12,\pi} = \frac{\tilde{n}_2 \cos(\theta_1) - \tilde{n}_1 \cos(\theta_2)}{\tilde{n}_2 \cos(\theta_1) + \tilde{n}_1 \cos(\theta_2)} \tag{C.30d}$$

and the transmission coefficients are listed in (C.31)

$$\tau_{01,\sigma} = \frac{2\tilde{n}_0 \cos(\theta_0)}{\tilde{n}_0 \cos(\theta_0) + \tilde{n}_1 \cos(\theta_1)} \tag{C.31a}$$

$$\tau_{12,\sigma} = \frac{2\tilde{n}_1 \cos(\theta_1)}{\tilde{n}_1 \cos(\theta_1) + \tilde{n}_2 \cos(\theta_2)} \tag{C.31b}$$

$$\tau_{01,\pi} = \frac{2\tilde{n}_0 \cos(\theta_0)}{\tilde{n}_1 \cos(\theta_0) + \tilde{n}_0 \cos(\theta_1)} \tag{C.31c}$$

$$\tau_{12,\pi} = \frac{2\tilde{n}_1 \cos(\theta_1)}{\tilde{n}_2 \cos(\theta_1) + \tilde{n}_1 \cos(\theta_2)} \tag{C.31d}$$

[Azzam & Bashara 1977, pp. 283-286]

The Jones Formalism

This appendix describes the Jones Formulation including the Jones vector of a monochromatic plane light wave and the Jones matrix of an optical device. Furthermore the Jones matrix of a cascade coupled optical device and Jones matrixes of different optical devices are described.

The Jones Vector

In order to describe the polarization of a monochromatic plane light wave the entire solution to the wave equation, given in (A.26a) on page 75, is not necessary. As a substitute the Jones vector, which is a more concise mathematical description of the wave, is introduced. The Jones vector is a vector which only contains information about the amplitude and the phase of the field, hence it contains information about the polarization state of the field. The derivation of the Jones vector starts with the equation of the monochromatic plane light wave propagating along the z-axis which is deduced in (A.21) and repeated here

$$\mathbf{E}(z,t) = \mathbf{E_0}\cos\left[\omega\left(t - \frac{z}{c}\right) + \phi\right] \tag{D.1}$$

or written in components

$$\mathbf{E}(z,t) = \left[A_x\cos\left[\omega\left(t - \frac{z}{c}\right) + \phi_x\right]\right]\hat{\mathbf{x}} + \left[A_y\cos\left[\omega\left(t - \frac{z}{c}\right) + \phi_y\right]\right]\hat{\mathbf{y}} \tag{D.2}$$

where A_x and A_y are the amplitudes of the harmonic oscillation of the electric field along the x-axis and the y-axis respectively. ϕ_x and ϕ_y are the phases of the components. The first step towards the Jones vector is to set up the components in a vector

$$\mathbf{E}(z,t) = \begin{bmatrix} E_x(z,t) \\ E_y(z,t) \end{bmatrix} = \begin{bmatrix} A_x\cos\left[\omega\left(t - \frac{z}{c}\right) + \phi_x\right] \\ A_y\cos\left[\omega\left(t - \frac{z}{c}\right) + \phi_y\right] \end{bmatrix} \tag{D.3}$$

Rewriting (D.3) by means of the complex exponential function and knowing that the physical field is the only real part of the complex E-field yields

$$\mathbf{E}(z,t) = e^{j\omega t}e^{-j\frac{\omega z}{c}}\begin{bmatrix} A_x e^{j\phi_x} \\ A_y e^{j\phi_y} \end{bmatrix} \tag{D.4}$$

Regarding the polarization state of the wave the temporal information has no influence and can therefore be suppressed. This yields

$$\mathbf{E}(z) = e^{-j\frac{\omega z}{c}}\begin{bmatrix} A_x e^{j\phi_x} \\ A_y e^{j\phi_y} \end{bmatrix} \tag{D.5}$$

Furthermore the spatial information is of no interest when only the polarization is considered and can therefore also be suppressed which yields

$$\mathbf{E} = \begin{bmatrix} A_x e^{j\phi_x} \\ A_y e^{j\phi_y} \end{bmatrix} \tag{D.6}$$

The vector in (D.6) is known as the Jones vector of the monochromatic plane light wave. The Jones vector can also be written as

$$\mathbf{E} = \begin{bmatrix} E_x \\ E_y \end{bmatrix} \tag{D.7}$$

where $E_x = A_x e^{j\phi_x}$ and $E_y = A_y e^{j\phi_y}$. As can bee seen the Jones vector contains complete information about the amplitudes and the phases of the components of the electrical field, hence it is a vector that describes the polarization of the light. [Azzam & Bashara 1977, pp. 13-15]

The Jones Matrix

In order to describe the modification of the polarization of a monochromatic plane light wave by an optical device, a Jones matrix of the optical system is introduced. The Jones matrix of an optical system relates the polarization of an incident monochromatic plane light wave to the polarization of an outgoing wave. That is, the Jones matrix relates the Jones vector of the incident wave to the Jones vector of the outgoing wave. A schematic drawing of this can be seen in Figure D.1. It is illustrated that the polarization of the incident wave,
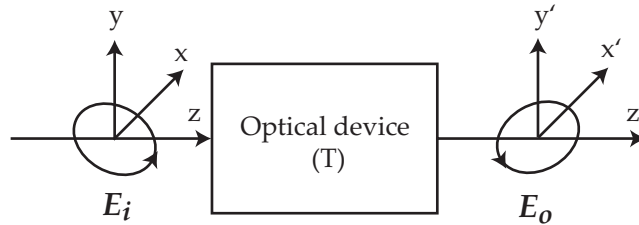
Figure D.1: The polarization of a wave is changed from $\mathbf{E}_i$ to $\mathbf{E}_o$ by an optical device. The two coordinate systems (x,y,z) and (x',y',z') are associated with the incident and the outgoing plane waves respectively. The directions z and z' are parallel to the two wavevectors $\mathbf{k}$ and $\mathbf{k}'$, which need not to be parallel.

described by its Jones vector $\mathbf{E}_i$, is changed due to interaction with the optical device. The polarization of the outgoing wave is described by the Jones vector $\mathbf{E}_o$. The two coordinate systems (x,y,z) and (x',y',z') are associated with the incident and the outgoing waves respectively. The directions z and z' are parallel to the two wavevectors $\mathbf{k}$ and $\mathbf{k}'$ of the incident and outgoing waves respectively. z and z' need not to be parallel. It is seen that change in polarization of the incident light wave due to the interaction with the optical device corresponds to a change of coordinate system from (x,y,z) to (x',y',z') of the incident Jones vector.

That is a change of basis of the incident Jones vector. A change of basis is, in the absence of non-linearities, given as

$$\mathbf{E}_o = \mathbf{T}\,\mathbf{E}_i \tag{D.8}$$

where **T** is the change of coordinate matrix from (x, y, z) to (x', y', z'). **T** is also called the Jones matrix of the optical system. (D.8) describes the law of interaction of the incident wave and the optical system as a matrix transformation of the incident Jones vector. Writing (D.8) i terms of the components of the Jones vectors and the Jones matrix yields

$$\begin{bmatrix} E_{ox} \\ E_{oy} \end{bmatrix} = \begin{bmatrix} T_{11} & T_{12} \\ T_{21} & T_{22} \end{bmatrix} \begin{bmatrix} E_{ix} \\ E_{iy} \end{bmatrix} \tag{D.9}$$

or

$$\begin{bmatrix} E_{ox} \\ E_{oy} \end{bmatrix} = \begin{bmatrix} T_{11}E_{ix} + T_{12}E_{iy} \\ T_{21}E_{ix} + T_{22}E_{iy} \end{bmatrix} \tag{D.10a}$$

It can be seen from (D.10) that the components of the Jones vector of the outgoing wave are given as a linear combination of the components of the Jones vector of the incident wave.

If a cascade of N optical systems is placed in the path of the incident wave, the polarization of the outgoing wave is given as

$$\mathbf{E}_o = \mathbf{T}_N \mathbf{T}_{N-1} \cdots \mathbf{T}_1 \mathbf{E}_i \tag{D.11}$$

or

$$\mathbf{E}_o = \mathbf{T}_C \mathbf{E}_i \tag{D.12}$$

where

$$\mathbf{T}_C = \mathbf{T}_N \mathbf{T}_{N-1} \cdots \mathbf{T}_1 \tag{D.13}$$

(D.12) shows that a cascade of N optical system can be replaced by one system with the overall Jones matrix given as $\mathbf{T}_C$. Note that the order of the Jones matrixes in (D.11) and (D.13) is of importance.

Jones Matrices of Basic Optical Devices

In this section the Jones matrixes of some basic optical devices will be presented. The retarder, the polarizer, the rotator and the reflector. The first three mentioned are of the transmission-type where the polarization of the wave is changed as the wave is propagated through the media. The reflector is a reflection-type medium by which the wave is modified by reflection of the surface of the medium. In the subsequent it is assumed that the light wave propagates in the direction of the z-axis.

Retarder

The Jones matrix describing the effects on a plane wave propagating through an isotropic optical device with real refractive index n over a distance d is given as

$$\mathbf{T} = \begin{bmatrix} e^{-j2\pi nd/\lambda} & 0 \\ 0 & e^{-j2\pi nd/\lambda} \end{bmatrix} \tag{D.14}$$

It can be seen from (D.14) that the plane wave is retarded by $2\pi nd/\lambda$ when the wave has travelled the distance d in the device. The device is called an isotropic retarder. Now introducing a medium which is not isotropic but instead uniaxially[1] linearly birefringent. If the light wave is travelling perpendicular to the optic axis and if the light wave is linearly polarized in a direction parallel to the optic axis then the light wave will be subject to a refractive index n_e. If the light wave is linearly polarized in a direction orthogonal to the optic axis the wave will be subject to another refractive index, namely n_o. As the light wave is travelling in the z-direction and the optical axes is in the x-direction, the refractive index in the x-direction is given as n_e and the refractive index in the y-direction is given as n_o. That is, the Jones matrix of the medium of thickness d is given as

$$\mathbf{T} = \begin{bmatrix} e^{-j2\pi n_e d/\lambda} & 0 \\ 0 & e^{-j2\pi n_o d/\lambda} \end{bmatrix} \tag{D.15}$$

A medium described by the Jones matrix of in (D.15) is a linear retarder. The x-components and y-components of the Jones vector will be retarded differently by a linear retarder.

Polarizer

If a medium is uniaxially linearly dichroic [2], a wave travelling parallel to the optic axis will be attenuated different then a wave travelling orthogonal to the optic axis. The wave polarized parallel to the optic axis will be attenuated with attenuation coefficient K_e and the wave polarized orthogonal to the optic axis will be attenuated with attenuation coefficient K_o. The Jones matrix of a uniaxially linearly dichroic medium is given as

$$\mathbf{T} = e^{-j2\pi nd/\lambda} \begin{bmatrix} e^{-2\pi K_e d/\lambda} & 0 \\ 0 & e^{-2\pi K_o d/\lambda} \end{bmatrix} \tag{D.16}$$

A medium of thickness d described by the Jones matrix of (D.16) is called a linear partial polarizer because unpolarized light will be partially polarized after interaction with the medium. A special case of the linear partial polarizer is the ideal linear polarizer were $K_e = 0$ and $K_o = \infty$ which is described by the Jones matrix

$$\mathbf{T} = e^{-j2\pi nd/\lambda} \begin{bmatrix} 1 & 0 \\ 0 & 0 \end{bmatrix} \tag{D.17}$$

---

[1]There is only one optic axis in the medium. An optic axis is a line in a doubly refracting medium that is parallel to the direction in which all components of plane-polarized light travel with the same speed. [Merriam-Webster Online 2004]

[2]Dichroism is the property of absorbing one of two plane-polarized components of light more that the other. [Merriam-Webster Online 2004]

Rotator

A medium in which linearly polarized light is still linearly polarized light, but the direction of the variation of the electric field changes as the light wave propagates through the medium is called an optical rotator. The Jones matrix of the optical rotator is given as

$$\mathbf{R} = e^{-j2\pi n d/\lambda} \begin{bmatrix} \cos\alpha d & -\sin\alpha d \\ \sin\alpha d & \cos\alpha d \end{bmatrix} \tag{D.18}$$

Where α is the rotation of the polarization per part length and d is the thickness of the material. With the definition of the sign as in (D.18) the rotation of the polarization by the medium will be clockwise if α is positive and counter clockwise if α is negative. If the light is elliptically polarized the major axis of the ellipse is rotated by the optical rotator but the ratio between the major and the minor axes of the ellipse is not changed.

Reflector

If the incident Jones vector is described in the π, σ coordinate system the Jones matrix of a reflector is given as

$$\mathbf{T} = \begin{bmatrix} \rho_\pi & 0 \\ 0 & \rho_\sigma \end{bmatrix} \tag{D.19}$$

Where ρ_π and ρ_σ are the Fresnel reflection coefficients discussed in Appendix B. [Azzam & Bashara 1977, pp. 61-79]

Correlation between the Stokes Parameters and ψ and Δ

<div style="text-align:right">E</div>

This appendix concerns the relation between the three Stokes parameters s_0, s_1, s_2 and the ellipsometric parameters ψ and Δ. This relation is deduced by manipulating the expression for the measured light intensity at the detector of the ellipsometer I_o.

The light intensity measured at the detector is given by (4.18) on page 27, which can be rewritten by inserting expressions for E_π, E_π^*, E_σ and E_σ^*

$$E_\pi = \rho_\pi \cos(\alpha_1)E_i \tag{E.1a}$$

$$E_\pi^* = \rho_\pi^* \cos(\alpha_1)E_i^* \tag{E.1b}$$

$$E_\sigma = \rho_\sigma \sin(\alpha_1)E_i \tag{E.1c}$$

$$E_\sigma^* = \rho_\sigma^* \sin(\alpha_1)E_i^* \tag{E.1d}$$

I_o thus becomes

$$I_o = \cos^2(\alpha_2)E_\pi E_\pi^* + \sin^2(\alpha_2)E_\sigma E_\sigma^* + \cos(\alpha_2)\sin(\alpha_2)\left(E_\pi E_\sigma^* + E_\sigma E_\pi^*\right) \tag{E.2}$$

$$= \rho_\pi \rho_\pi^* \cos^2(\alpha_1)\cos^2(\alpha_2)E_i E_i^* + \rho_\sigma \rho_\sigma^* \sin^2(\alpha_1)\sin^2(\alpha_2)E_i E_i^*$$
$$+ \left(\rho_\pi \rho_\sigma^* E_i E_i^* + \rho_\sigma \rho_\pi^* E_i E_i^*\right)\sin(\alpha_1)\cos(\alpha_1)\sin(\alpha_2)\cos(\alpha_2) \tag{E.3}$$

$$= \frac{1}{2}I_i\left[\rho_\pi \rho_\pi^* \cos^2(\alpha_1)\cos^2(\alpha_2) + \rho_\sigma \rho_\sigma^* \sin^2(\alpha_1)\sin^2(\alpha_2)\right.$$
$$\left. + \left(\rho_\pi \rho_\sigma^* + \rho_\sigma \rho_\pi^*\right)\sin(\alpha_1)\cos(\alpha_1)\sin(\alpha_2)\cos(\alpha_2)\right] \tag{E.4}$$

where $E_i E_i^* = \frac{1}{2}I_i$, I_i being the intensity of the light at the source. From this expression it can be seen that the two polarizers are equivalent. The equations are thus the same for an RAE and an RPE.

(E.4) can be rewritten by utilizing the trigonometric relations [Råde & Westergren 1998, p. 124]

$$\cos(\alpha_2)\sin(\alpha_2) = \frac{1}{2}\sin(2\alpha_2) \tag{E.5a}$$

$$\sin^2(\alpha_2) = \frac{1 - \cos(2\alpha_2)}{2} \tag{E.5b}$$

$$\cos^2(\alpha_2) = \frac{1 + \cos(2\alpha_2)}{2} \tag{E.5c}$$

The intensity thus becomes

$$I_o = \frac{1}{4}I_i\left[\rho_\pi\rho_\pi^*\cos^2(\alpha_1) + \rho_\sigma\rho_\sigma^*\sin^2(\alpha_1) + \cos(2\alpha_2)(\rho_\pi\rho_\pi^*\cos^2(\alpha_1) - \rho_\sigma\rho_\sigma^*\sin^2(\alpha_1))\right.$$

$$\left. + (\rho_\pi\rho_\sigma^* + \rho_\sigma\rho_\pi^*)\sin(\alpha_1)\cos(\alpha_1)\sin(2\alpha_2)\right] \tag{E.6}$$

$$= \frac{1}{4}I_i(\rho_\pi\rho_\pi^*\cos^2(\alpha_1) + \rho_\sigma\rho_\sigma^*\sin^2(\alpha_1))\left[1 + \cos(2\alpha_2)\frac{\rho_\pi\rho_\pi^*\cos^2(\alpha_1) - \rho_\sigma\rho_\sigma^*\sin^2(\alpha_1)}{\rho_\pi\rho_\pi^*\cos^2(\alpha_1) + \rho_\sigma\rho_\sigma^*\sin^2(\alpha_1)}\right.$$

$$\left. + \sin(2\alpha_2)\frac{(\rho_\pi\rho_\sigma^* + \rho_\sigma\rho_\pi^*)\sin(\alpha_1)\cos(\alpha_1)}{\rho_\pi\rho_\pi^*\cos^2(\alpha_1) + \rho_\sigma\rho_\sigma^*\sin^2(\alpha_1)}\right] \tag{E.7}$$

The two fractions in this expression can be rewritten by using the relation $\tan(\psi)e^{j\Delta} = \frac{\rho_\pi}{\rho_\sigma}$. The first fraction becomes

$$\frac{\rho_\pi\rho_\pi^*\cos^2(\alpha_1) - \rho_\sigma\rho_\sigma^*\sin^2(\alpha_1)}{\rho_\pi\rho_\pi^*\cos^2(\alpha_1) + \rho_\sigma\rho_\sigma^*\sin^2(\alpha_1)} = \frac{\frac{\rho_\pi\rho_\pi^*\cos^2(\alpha_1)}{\rho_\sigma\rho_\sigma^*\sin^2(\alpha_1)} - \frac{\rho_\sigma\rho_\sigma^*\sin^2(\alpha_1)}{\rho_\sigma\rho_\sigma^*\sin^2(\alpha_1)}}{\frac{\rho_\pi\rho_\pi^*\cos^2(\alpha_1)}{\rho_\sigma\rho_\sigma^*\sin^2(\alpha_1)} + \frac{\rho_\sigma\rho_\sigma^*\sin^2(\alpha_1)}{\rho_\sigma\rho_\sigma^*\sin^2(\alpha_1)}} = \frac{\frac{\tan^2(\psi)}{\tan^2(\alpha_1)} - 1}{\frac{\tan^2(\psi)}{\tan^2(\alpha_1)} + 1} \tag{E.8}$$

Introduction of a new parameter ψ' that satisfies the equation $\tan(\psi') = \frac{\tan(\psi)}{\tan(\alpha_1)}$ reduces (E.8) to

$$-\frac{1 - \tan^2(\psi')}{1 + \tan^2(\psi')} = -\frac{\cos^2(\psi') + \sin^2(\psi') - \tan^2(\psi')}{1 + \tan^2(\psi')} \tag{E.9}$$

$$= -\frac{\cos^2(\psi') - (1 - \cos^2(\psi'))\tan^2(\psi')}{1 + \tan^2(\psi')} \tag{E.10}$$

$$= -\frac{\cos^2(\psi') - \sin^2(\psi')\tan^2(\psi')}{1 + \tan^2(\psi')} \tag{E.11}$$

$$= -\frac{(\cos^2(\psi') - \sin^2(\psi'))(1 + \tan^2(\psi'))}{1 + \tan^2(\psi')} \tag{E.12}$$

$$= -(\cos^2(\psi') - \sin^2(\psi')) \tag{E.13}$$

$$= -\cos(2\psi') \tag{E.14}$$

Correspondingly the second fraction in (E.7) can be rewritten

$$\frac{(\rho_\pi\rho_\sigma^* + \rho_\sigma\rho_\pi^*)\sin(\alpha_1)\cos(\alpha_1)}{\rho_\pi\rho_\pi^*\cos^2(\alpha_1) + \rho_\sigma\rho_\sigma^*\sin^2(\alpha_1)} = \frac{\frac{1}{\tan(\alpha_1)}\left(\tan(\psi)e^{j\Delta} + \tan(\psi)e^{-j\Delta}\right)}{\frac{\tan^2(\psi)}{\tan^2(\alpha)} + 1} = \cos(\Delta)\frac{2\tan(\psi')}{1 + \tan^2(\psi')} \tag{E.15}$$

This can again be rewritten

$$\cos(\Delta)\frac{2\tan(\psi')}{1 + \tan^2(\psi')} = \cos(\Delta)\frac{2\tan(\psi')(\cos^2(\psi') + \sin^2(\psi'))}{1 + \tan^2(\psi')} \tag{E.16}$$

$$= \cos(\Delta)\frac{2\sin(\psi')\cos(\psi') + 2\tan(\psi')\sin^2(\psi')}{1 + \tan^2(\psi')} \tag{E.17}$$

$$= \cos(\Delta)\frac{2\sin(\psi')\cos(\psi')(1 + \tan^2(\psi'))}{1 + \tan^2(\psi')} \tag{E.18}$$

$$= \cos(\Delta)2\sin(\psi')\cos(\psi') \tag{E.19}$$

$$= \sin(2\psi')\cos(\Delta) \tag{E.20}$$

By substituting (E.14) and (E.20) into (E.7) the intensity at the detector is given as

$$I_o = \frac{1}{4}I_i(\rho_\pi \rho_\pi^* \cos^2(\alpha_1) + \rho_\sigma \rho_\sigma^* \sin^2(\alpha_1))\Big[1 - \cos(2\alpha_2)\cos(2\psi')$$
$$+ \sin(2\alpha_2)\sin(2\psi')\cos(\Delta)\Big] \tag{E.21}$$

By realizing that

$$\frac{1}{2}I_i(\rho_\pi \rho_\pi^* \cos^2(\alpha_1) + \rho_\sigma \rho_\sigma^* \sin^2(\alpha_1)) = E_\pi E_\pi^* + E_\sigma E_\sigma^* = s_0 \tag{E.22}$$

(E.21) can be expressed as

$$\frac{1}{2}s_0\Big[1 - \cos(2\psi')\cos(2\alpha_2) + \sin(2\psi')\cos(\Delta)\sin(2\alpha_2)\Big] \tag{E.23}$$

This equation can be compared to another expression for I_o namely (4.22) on page 27

$$I_o = \frac{1}{2}[s_0 + s_1\cos(2\alpha_2) + s_2\sin(2\alpha_2)] \tag{E.24}$$
$$= \frac{1}{2}s_0\Big[1 + \frac{s_1}{s_0}\cos(2\alpha_2) + \frac{s_2}{s_0}\sin(2\alpha_2)\Big] \tag{E.25}$$

By doing so two important relations between the ellipsometric parameters and the Stokes parameters arises

$$\cos(2\psi') = -\frac{s_1}{s_0} \tag{E.26a}$$
$$\sin(2\psi')\cos(\Delta) = \frac{s_2}{s_0} \tag{E.26b}$$

Remembering that $\tan(\psi') = \frac{\tan(\psi)}{\tan(\alpha_1)}$ these equations make it possible to calculate the ellipsometric parameters ψ and Δ if the three Stokes parameters s_0, s_1 and s_2 are known.

Index of Refraction

*This appendix will explain the mathematical foundations of the refractive index and give a simple understanding of the interpretation of it. The concept of permittivity is introduced by means of the Fourier transform of the electric field **E** and the electric displacement **D**. Then, the Drude-Lorentz theory will be used to model the microscopic nature of the material and thereby give an explanation of the complex index of refraction.*

Defining the Index of Refraction

The term "refraction" deals with the deflection of electromagnetic waves e.g. light from a straight path when passing obliquely from one medium to another, see Figure F.1. The index of refraction is a means of describing an optical property of a medium. If the medium is fully transparent, the index of refraction is purely real and denoted n. If the medium is absorbing light, the index of refraction becomes complex and is denoted $\tilde{n}$.
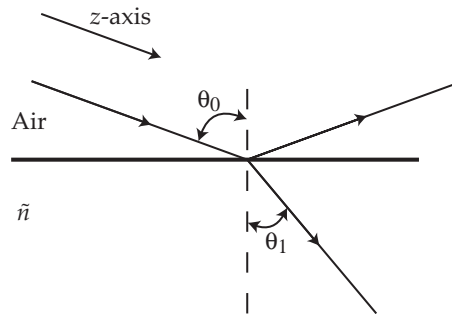
Figure F.1: Refraction at an oblique angle of incidence into a medium with a complex index of refraction $\tilde{n}$.

The mathematical foundation is given by the Maxwell equations. By using (A.10) in linear, isotropic matter instead of in free-space, we get the wave-equation for an electrical field

$$\nabla^2 \mathbf{E} - \mu\varepsilon\frac{\partial^2 \mathbf{E}}{\partial t^2} = 0 \tag{F.1}$$

Here μ and ε are complex quantities and not as in the free-space equations, where they are named the free-space permeability μ_0 and permittivity ε_0 and are both real numbers. The solution for (F.1) is given by (A.26a) and rewritten here

$$\mathbf{E}(\mathbf{r},t) = \mathbf{E}_0 e^{j(\omega t - \mathbf{k}\cdot\mathbf{r} + \varphi)} \tag{F.2}$$

Substituting (F.2) into (F.1) yields

$$k^2 = \mu\varepsilon\omega^2 \tag{F.3}$$

where k is the wave-number and ω is the angular frequency of the light. We then define the complex index of refraction

$$\tilde{n}^2 \triangleq (n - jK)^2 \triangleq \mu\varepsilon c^2 = \frac{\mu\varepsilon}{\mu_0\varepsilon_0} \tag{F.4}$$

such that the dispersion relation for the medium is given by [Reitz et al. 1993, p. 426]

$$k = \tilde{n}\frac{\omega}{c} \tag{F.5}$$

where

$$c = \frac{1}{\sqrt{\mu_0\varepsilon_0}} \tag{F.6}$$

Notice that the imaginary part K used in (F.4) is not directly related to the wave-number k used in the dispersion relation in (F.5). The complex index of refraction is sometimes also written as

$$\tilde{n} \triangleq (n - jK) = n(1 - j\kappa) \tag{F.7}$$

where κ (kappa) is called the absorption index [Azzam & Bashara 1977, p. 270]. To show the effect of the two real optical constants n and K, the dispersion relation (F.5) is inserted into (F.2), assuming the direction of propagation is along the z-coordinate axis yields

$$\mathbf{E}(z,t) = \mathbf{E}_0 e^{j(\omega t + \varphi)} e^{-jkz} \tag{F.8}$$

$$= \mathbf{E}_0 e^{j(\omega t + \varphi)} e^{-j\tilde{n}\frac{\omega}{c}z} \tag{F.9}$$

$$= \mathbf{E}_0 e^{-K\frac{\omega}{c}z} e^{j(\omega t - n\frac{\omega}{c}z + \varphi)} \tag{F.10}$$

As can be seen from (F.10), the first term $E_0 e^{-K\frac{\omega}{c}z}$ is a function of z and affects only the amplitude of the wave. The wave is attenuated in the medium with this factor as the wave moves along the z-axis. E_0 is constant and the term $K\frac{\omega}{c}$ is called the attenuation constant. The reciprocal $\delta = \frac{c}{K\omega}$ is called the skin depth and is a measurement of the distance to which the field is at $\frac{1}{e}$ of the original value.

The velocity in a medium is found by evaluating the solution to the wave-equation (F.10). When measuring velocity, the total phase can be taken as constant.

$$\omega t - n\frac{\omega}{c}z + \varphi = \text{constant} \tag{F.11}$$

This just means that the velocity is defined as following a certain value through the wave propagation. The velocity v can then be found by isolating z and taking the derivative with respect to time

$$v = \frac{dz}{dt} = \frac{c}{n} \tag{F.12}$$

So far, the complex index of refraction has been defined as a constant. This is a crude simplification, as it is very frequency-dependent. This dependency relates to the permittivity. [Klein & Furtak 1986, p. 68-70]

Permittivity as a frequency-dependent concept

When dealing with permittivity, the Fourier transform can be used to understand the dependency on frequency in the medium. The Fourier transform of a function (a signal, field, excitation etc.) is defined as

$$X_F(\omega) = \frac{1}{\sqrt{2\pi}} \int_{-\infty}^{\infty} X(t)e^{j\omega t} dt \tag{F.13}$$

where $X(t)$ is the time-dependent signal, $X_F(\omega)$ is the Fourier transform of this signal, ω is the angular frequency, t is the time and $1/\sqrt{2\pi}$ is introduced to restore symmetry of the transform. The inverse Fourier transform is likewise defined as

$$X(t) = \frac{1}{\sqrt{2\pi}} \int_{-\infty}^{\infty} X_F(\omega)e^{-j\omega t} d\omega \tag{F.14}$$

One of the fundamental preconditions for the media that are under investigation is that the medium is linear. When this holds, the medium can be considered to be a system with an input, response and output function to which the convolution theorem can be applied. This also implies that the system is causal, but all real physically systems are causal. Causality is that the cause comes before the effect. In a physical system this implies that the output only appears after the input.

The convolution theorem relates the input function $X(t)$, the response function $R(t)$ and the output function $Y(t)$ as

$$Y(t) = \frac{1}{\sqrt{2\pi}} \int_{-\infty}^{\infty} R(t-\tau)X(\tau)d\tau \tag{F.15}$$

If the convolution theorem can be applied to the medium, the Fourier transform of the input, response and output function are denoted $X_F(\omega)$, $R_F(\omega)$ and $Y_F(\omega)$, respectively, and are related as

$$Y_F(\omega) = R_F(\omega)X_F(\omega) \tag{F.16}$$

This relation is a consequence of the Fourier transform. It shows that if the output function can be found as the convolution of the input and response function in the time domain, it can conversely be found as the multiplication of the Fourier transform of the individual functions in the frequency domain. If the convolution is mathematically difficult to achieve, the functions can be Fourier transformed individually, multiplied in the frequency domain and then inverse Fourier transformed.

The consequences of (F.16) are important because it shows that if the input function is an impressed field in the form of a monochromatic wave, the resulting field (the output function) is proportional to the impressed field, because $R_F(\omega)$ is constant. The proportionality factor is, however, frequency dependent if the full spectrum is considered.

Another consequence of the Fourier transform is that the relation between the input and output function can be written as a linear, inhomogeneous differential equation of N'th order with constant coefficients, namely

$$\sum_{n=0}^{N} a_n \frac{d^n}{dt^n} Y(t) = bX(t) \tag{F.17}$$

where a_n and b are constant coefficients and N is the order of the differential equation. Generally, the right-hand side of (F.17) can also be written as a sum of derivatives of $X(t)$ each with a coefficient b_n, but this will not be used in the following. By use of the definition for the inverse Fourier transformation, the response function can be written as

$$R_F(\omega) = \frac{b}{\sum_{n=0}^{N} a_n(-j\omega)^n} \tag{F.18}$$

which will be useful later when recognizing the response function.

The theory mentioned here can be used on real media, with some assumptions. When impressing an electric field $\mathbf{E}$ on a linear time-invariant dielectric medium (LTI-system), the electric displacement $\mathbf{D}$ is coupled to $\mathbf{E}$ via the convolution theorem from (F.15) as

$$\mathbf{D}(\mathbf{r},t) = \frac{1}{\sqrt{2\pi}} \int_0^{\infty} R(\mathbf{r},\tau)\mathbf{E}(\mathbf{r},t-\tau)d\tau \tag{F.19}$$

Due to causality, the integral needs only to be evaluated from 0 to ∞. The response function does not depend on $\mathbf{E}$ and the relationship between $\mathbf{D}$ and $\mathbf{E}$ is assumed spatially local. This means that $\mathbf{D}$ only depends on $\mathbf{E}$ at the same point in space. If R is assumed independent of $\mathbf{r}$, meaning that R only changes at an interface between two media, then (F.19) can be reduced to

$$D(t) = \frac{1}{\sqrt{2\pi}} \int_0^{\infty} R(\tau)E(t-\tau)d\tau \tag{F.20}$$

which is identical with the convolution theorem in (F.15). It can hereby be seen that the relation between the $\mathbf{D}$- and $\mathbf{E}$-field, called the permittivity ε, in the time domain is not just dependant on the time t, but also of all past times because of τ. This can be interpreted as a time delay, as the $\mathbf{D}$-field at a given time does not only depend on the $\mathbf{E}$-field at this time, but on all previously values of the $\mathbf{E}$-field. However, in the frequency domain the permittivity is a proportionality factor dependant only on the frequency ω. [Reitz et al. 1993, pp. 484-489]

This yields the constitutive equation for a linear, isotropic dielectric

$$\mathbf{D}(\omega) = \tilde{\varepsilon}(\omega)\varepsilon_0\mathbf{E}(\omega) \tag{F.21}$$

where $\tilde{\varepsilon}(\omega)$ is the dimensionless complex dielectric coefficient. By using the definition of the electric displacement given in [Reitz et al. 1993, p. 107]

$$\mathbf{D}(\omega) = \varepsilon_0\mathbf{E}(\omega) + \mathbf{P}(\omega) \tag{F.22}$$

where $\mathbf{P}(\omega)$ is the electric polarization of the dielectric material, another constitutive equation is given as

$$\mathbf{P}(\omega) = \chi(\omega)\mathbf{E}(\omega) \tag{F.23}$$

where

$$\chi(\omega) = (\tilde{\varepsilon}(\omega) - 1)\varepsilon_0 \tag{F.24}$$

is the electric susceptibility. The susceptibility can completely describe the electrical behavior of the material, but often $\tilde{\varepsilon}$ is used instead. It relates the complex index of refraction as [Reitz et al. 1993, p. 425]

$$\tilde{\varepsilon}(\omega) = (\tilde{n}(\omega))^2 \tag{F.25}$$

where

$$\tilde{\varepsilon}(\omega) = \varepsilon_{re}(\omega) + j\varepsilon_{im}(\omega) \tag{F.26}$$

giving

$$n(\omega) = \sqrt{\frac{1}{2}\left(\varepsilon_{re}(\omega) + \sqrt{(\varepsilon_{re}(\omega))^2 + (\varepsilon_{im}(\omega))^2}\right)} \tag{F.27}$$

$$K(\omega) = \sqrt{\frac{1}{2}\left(-\varepsilon_{re}(\omega) + \sqrt{(\varepsilon_{re}(\omega))^2 + (\varepsilon_{im}(\omega))^2}\right)} \tag{F.28}$$

This is the basis for introducing a model, in which the susceptibility relates the complex index of refraction to some fundamental properties of the electrons in the material.

The Drude-Lorentz Model

This section relates the macroscopic optical constants with the microscopic electric-dipole excitations in the material. This is done through the Drude-Lorentz harmonic oscillator model, which was stated in the beginning of the 20th century and the electrons are therefore seen as classical particles. The idea is to replace the atoms and molecules in a material by a set of harmonically bound electrons, oscillating at some resonant frequency ω_0. The term "harmonically bound" indicates that the electrons are bound to an equilibrium by a linear restoring force, as in a harmonic spring. The electrons are modeled as damped by a damping device. Furthermore, a field called the molecular field $E_m(t)$ is impressed on the electrons, yielding the driving force $eE_m(t)$. This yields a forced, damped harmonic oscillator to model the motion of the electrons. Even though quantum mechanics is not considered in this model, it still works well when dealing with conductivity-related terms, but fails to model e.g. heat capacity.

The standard second-order linear differential equation representing the one-dimensional motion of the forced, damped harmonic oscillator can be found by Newton's second law

$$F_{res} = m\frac{d^2x}{dt^2} \tag{F.29}$$

$$-Cx(t) - G\frac{dx}{dt} + eE_m(t) = m\frac{d^2x}{dt^2} \tag{F.30}$$

where $x(t)$ is the displacement of the electron from an equilibrium, m is the mass of the electron, $-Cx(t)$ is the linear restoring force (spring force), $-G\frac{dx}{dt}$ is the damper force and $eE_m(t)$ is the driving force due to the impressed field $E_m(t)$. An illustration of this can be seen in Figure F.2. By introducing a damping constant as $\gamma = \frac{G}{m}$ and the square of the natural
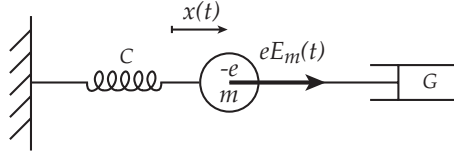
Figure F.2: Illustration of a forced, damped harmonic oscillating electron. C is the spring constant, G is the damping constant, $E_m(t)$ is the impressed molecular field, e^- and m are the electron charge and mass, respectively and $x(t)$ is the displacement of the electron from its equilibrium.

frequency of the undamped oscillator as $\omega_0^2 = \frac{C}{m}$, the fundamental differential equation of this model appears as

$$\frac{d^2x}{dt^2} + \gamma\frac{dx}{dt} + \omega_0^2 x = \frac{eE_m(t)}{m} \tag{F.31}$$

For free electrons, the restoring force is not present which yields $\omega_0 = 0$. If the displacement of the electrons in the material is static, the derivatives of $x(t)$ is 0 and the natural frequency of the undamped oscillator can be found as[1]

$$\omega_0^2 = \frac{e^2}{4\pi\varepsilon_0 mR_0^3} \tag{F.32}$$

where R_0 is the atomic radius. Two substitutions are needed to eliminate the mechanical displacement $x(t)$ and the molecular field $E_m(t)$. First, the polarization is calculated by the number of charged particles N per unit volume times the dipole moment $ex(t)$ due to the displacement $x(t)$ of the charge e

$$P(t) = Nex(t) \tag{F.33}$$

An illustration of this can be seen in Figure F.3.

Second, the molecular field is calculated. It is produced by all external sources and all polarized molecules in the material, with the exception of the one molecule under consideration [Reitz et al. 1993, pp. 127-131]. In isotropic material this yields

$$E_m(t) = E(t) + \frac{\nu}{\varepsilon_0}P(t) \tag{F.34}$$

where $E(t)$ is the E-field of the wave and ν is a constant that effects the local field.

The two equations (F.33) and (F.34) are now used to rewrite (F.31) into

$$\frac{d^2P}{dt^2} + \gamma\frac{dP}{dt} + (\omega_0^2 - \nu\omega_p^2)P(t) = \varepsilon_0\omega_p^2 E(t) \tag{F.35}$$

where the plasma frequency ω_p is given as

$$\omega_p^2 = \frac{Ne^2}{\varepsilon_0 m} \tag{F.36}$$

---

[1]By using (5-12) in [Reitz et al. 1993, pp. 131-132] concerning induced dipoles
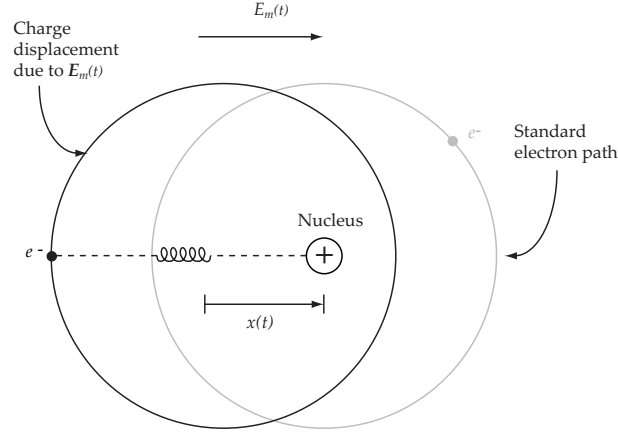
Figure F.3: An illustration of the dipole moment created due to the driving field $E_m(t)$. The field causes the electron charge to be displaced and thereby creating an electrical dipole.

As described in (F.16), this inhomogeneous second-order differential equation can be written as

$$P_F(\omega) = R_F(\omega)E_F(\omega) \tag{F.37}$$

where $R_F(\omega)$ is the response function that represents the system and relates E to P. From (F.18) the response function can be easily calculated and from (F.23) it is seen that this response function can be regarded as the susceptibility

$$\chi_F(\omega) = R_F(\omega) = \frac{\varepsilon_0\omega_p^2}{\omega_0^2 - \omega^2 - j\gamma\omega - \nu\omega_p^2} \tag{F.38}$$

Rewriting this while including the definition of the electric susceptibility from (F.24) yields

$$\frac{\tilde{\varepsilon}(\omega) - 1}{1 + \nu(\tilde{\varepsilon}(\omega) - 1)} = \frac{\omega_p^2}{\omega_0^2 - \omega^2 - j\gamma\omega} \tag{F.39}$$

which is the general relation between the dielectric coefficient of the material, and thereby the index of refraction, and the microscopic properties of the material. From this relationship it can also be seen that $\tilde{\varepsilon}(\omega)$ is complex and is a function of the frequency.

Some assumption to this result has to be made. Different particles in different distances to their equilibrium have different restoring forces. This consideration leads to the problem that they have different natural frequencies and damping. Restricting the term "particles" to electrons, thereby assuming no ions in the material, allow the mass and charge to be fixed. To simplify the model, it is restricted to valence electrons, thereby making the distance to equilibrium fixed.

Furthermore, ν is set to 0, which reduces (F.39) to

$$\tilde{\varepsilon}(\omega) - 1 = \frac{\omega_p^2}{\omega_0^2 - \omega^2 - j\gamma\omega} \tag{F.40}$$

which is often used to model most metals. When plotting this, the real and imaginary part is drawn independently. The real and imaginary parts of (F.40) are

$$\varepsilon_{re}(\omega) = 1 + \frac{\omega_p^2(\omega_0^2 - \omega^2)}{(\omega_0^2 - \omega^2)^2 + (\gamma\omega)^2} \tag{F.41a}$$

$$\varepsilon_{im}(\omega) = \frac{\omega_p^2 \gamma\omega}{(\omega_0^2 - \omega^2)^2 + (\gamma\omega)^2} \tag{F.41b}$$

Knowing that the square of the complex refractive index $\tilde{n}(\omega)$ is the complex dielectric coefficient $\tilde{\varepsilon}(\omega)$, yields that the real n and imaginary K part of the complex index of refraction can be calculated as

$$n(\omega) = \mathrm{Re}\left(\sqrt{1 + \frac{\omega_p^2}{\omega_0^2 - \omega^2 - j\gamma\omega}} \right) \tag{F.42a}$$

$$K(\omega) = \mathrm{Im}\left(\sqrt{1 + \frac{\omega_p^2}{\omega_0^2 - \omega^2 - j\gamma\omega}} \right) \tag{F.42b}$$

This model can be simplified in metals, where the valence electrons are free to move around and contribute to dc conduction. This is called the Drude free-electron model. That the valence electrons are free to move means that these electrons are not affected by any restoring force. Putting $C = 0$ in (F.30) causes $\omega_0 = 0$ in (F.40) which then can be calculated as

$$\tilde{\varepsilon}(\omega) = 1 - \frac{\omega_p^2}{\omega(\omega + j\gamma)} \tag{F.43}$$

where it is enough to estimate the plasma frequency ω_p and the damping coefficient γ in the simulation of the complex index of refraction. These parameters can be calculated from material parameters given in various optical books. The plasma frequency is as already stated in (F.36) given as

$$\omega_p^2 = \frac{Ne^2}{\varepsilon_0 m} \tag{F.44}$$

and the damping coefficient γ is given as

$$\gamma = \frac{1}{\tau} \tag{F.45}$$

where τ is a time constant for the decay of a current with no driving field. This will be used in the simulation of the metals.

Index of Refraction and Band Structures of Crystals $\;\;$ G

The purpose of this appendix is to explain the coherence between the index of refraction and the energy band structure of a solid. First the origin of energy gabs in solids is explained by means of the nearly free electron model and the Bragg diffraction condition. Afterwards the band structures of silicon and copper are presented and related to the calculated refractive indexes of silicon and copper in Appendix H.

Energy Bands in Solids

In order to describe the energy band structure of a solid the nearly free electron model is used. In the nearly free electron model the electrons are described as waves propagating through the crystal. The probability of finding an electron at a certain location can be calculated by means of the single-particle time independent Schrödinger equation

$$\left(-\frac{\hbar^2}{2m}\nabla^2 + V(\mathbf{r})\right)\psi(\mathbf{r}) = E\psi(\mathbf{r}) \tag{G.1}$$

where $\hbar$ is Planck's constant divided with 2π, m is the mass of the electron and E is the energy of the electron, $V(\mathbf{r})$ is the potential energy, ∇ is the nabla operator, $\psi(\mathbf{r})$ is a solution to the wave equation and $\mathbf{r}$ is a position vector. The energy E of the electron is the sum of the kinetic energy and potential energy

$$E = -\frac{\hbar^2}{2m}\nabla^2 + V(\mathbf{r}) = \frac{\mathbf{p}^2}{2m} + V(\mathbf{r}) = \frac{1}{2}m\mathbf{v}^2 + V(\mathbf{r}) \tag{G.2}$$

where $\mathbf{v}$ is the velocity of the electron and $\mathbf{p}$ is the linear momentum of the electron given as

$$\mathbf{p} = -j\hbar\nabla \tag{G.3}$$

To solve the Schrödinger equation we must impose some boundary conditions. The bulk properties are not very sensitive to the boundary conditions. The bulk means everything else than the last few atomic layers on the surface. The most convenient conditions will be used which are the periodic boundary conditions. The solutions to the Schrödinger equation that satisfy periodic boundary conditions are in the form of traveling plane waves

$$\psi(\mathbf{r}) = e^{j\mathbf{k}\cdot\mathbf{r}} \tag{G.4}$$

where the components of the wavevector $\mathbf{k}$ are given as

$$k_x = k_y = k_z = \frac{2\pi n}{L} \tag{G.5}$$

where n is a positive or negative integer and L is the period, that is

$$\psi(x+L, y+L, z+L) = \psi(x, y, z) \tag{G.6}$$

The probability density of an electron is given as

$$\psi^*(\mathbf{r})\psi(\mathbf{r}) = |\psi(\mathbf{r})|^2 \tag{G.7}$$

For a traveling wave the probability density is given as

$$e^{j\mathbf{k}\cdot\mathbf{r}}e^{-j\mathbf{k}\cdot\mathbf{r}} = 1 \tag{G.8}$$

(G.8) shows that the charge density of a traveling electron is constant.

When a wave propagates in a crystal it is disturbed by Bragg reflection. At Bragg reflection, no wavelike solutions to the Schrödinger equation exist.

Bragg Diffraction Condition

In order to set up the condition of Bragg reflection a few important concepts of crystals must be introduced. The lattice of a crystal is defined by means of three translation vectors $\mathbf{a_1}$, $\mathbf{a_2}$ and $\mathbf{a_3}$ such that the set of points $\mathbf{r}$ defined as

$$\mathbf{r} = u_1\mathbf{a_1} + u_2\mathbf{a_2} + u_3\mathbf{a_3} \tag{G.9}$$

for all integers u_1, u_2 and u_3 define the lattice. A translation in the lattice is defined by means of a translation vector

$$\mathbf{T} = u_1\mathbf{a_1} + u_2\mathbf{a_2} + u_3\mathbf{a_3} \tag{G.10}$$

All points in a lattice can be connected by means of $\mathbf{T}$. A lattice is a regular periodic array of points in 3 dimensions. The lattice is a mathematical construction. Given a lattice and a basis of atoms, the crystal is given when the basis of atoms is attached to every point in the lattice. Figure G.1 shows an illustration of the lattice, the crystal and the basis.

In order to set up the Bragg diffraction condition an expression for the electron number density $n(\mathbf{r})$ is necessary. It is used that the electron number density is periodic in $\mathbf{r}$ with the period $\mathbf{T}$. That is

$$n(\mathbf{r} + \mathbf{T}) = n(\mathbf{r}) \tag{G.11}$$

An arbitrary periodic function can be described as an infinite sum of complex exponential function in a complex Fourier series. This yields

$$n(\mathbf{r}) = \sum_{\mathbf{G}} n_{\mathbf{G}} e^{j\mathbf{G}\cdot\mathbf{r}} \tag{G.12}$$

where $\mathbf{G}$ is a set of vectors such that the electron number density is invariant under all crystal translations $\mathbf{T}$.

Two lattices are connected to a crystal, the direct lattice and the reciprocal lattice. The reciprocal lattice is defined as the Fourier transform of the lattice. The reciprocal lattice is

(a) The lattice.

(b) The crystal structure is the lattice with the basis of atoms attached to all lattice points.

(c) The basis atoms, in this case two ions.
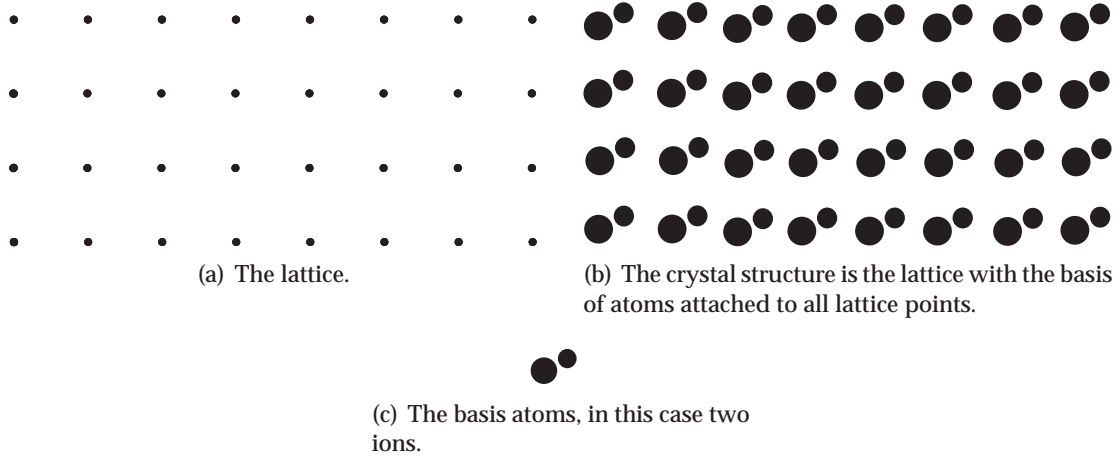
Figure G.1: Illustration of a lattice, a crystal and a basis in 2 dimensions. [Kittel 1986, p. 6]

called the Fourier space of the crystal. Points in the reciprocal lattice are described by $\mathbf{G}$. $\mathbf{G}$ is given as

$$\mathbf{G} = v_1\mathbf{b_1} + v_2\mathbf{b_2} + v_3\mathbf{b_3} \tag{G.13}$$

where v_1, v_2 and v_3 are arbitrary integers and $\mathbf{b_1}$, $\mathbf{b_2}$ and $\mathbf{b_3}$ are the axis vectors. The coherence between the axis vectors in the lattice and the axis vectors in the reciprocal lattice is given from [Kittel 1986, p. 33] as

$$\mathbf{b_1} = 2\pi\frac{\mathbf{a_2} \times \mathbf{a_3}}{\mathbf{a_1} \cdot \mathbf{a_2} \times \mathbf{a_3}} \tag{G.14a}$$

$$\mathbf{b_2} = 2\pi\frac{\mathbf{a_3} \times \mathbf{a_1}}{\mathbf{a_1} \cdot \mathbf{a_2} \times \mathbf{a_3}} \tag{G.14b}$$

$$\mathbf{b_3} = 2\pi\frac{\mathbf{a_1} \times \mathbf{a_2}}{\mathbf{a_1} \cdot \mathbf{a_2} \times \mathbf{a_3}} \tag{G.14c}$$

The Bragg diffraction condition is set up by means of Figure G.2 Contemplating the figure yields that the difference in phase factor of waves scattered of volume elements $\mathbf{r}$ apart is given as $e^{j(\mathbf{k_1}-\mathbf{k_2})\cdot\mathbf{r}}$. The electron density number of the volume element $n(\mathbf{r})$ is proportional to the amplitude of a wave scattered from the volume element dV. The total amplitude A of the scattered wave is therefore given as

$$A = \int n(\mathbf{r})e^{j(\mathbf{k_1}-\mathbf{k_2})\cdot\mathbf{r}}dV \tag{G.15}$$

which by (G.12) yields

$$A = \sum_{\mathbf{G}} n_{\mathbf{G}} \int e^{j(\mathbf{G}-\Delta\mathbf{k})\cdot\mathbf{r}}dV \tag{G.16}$$

where

$$\Delta\mathbf{k} = \mathbf{k_2} - \mathbf{k_1} \tag{G.17}$$

111
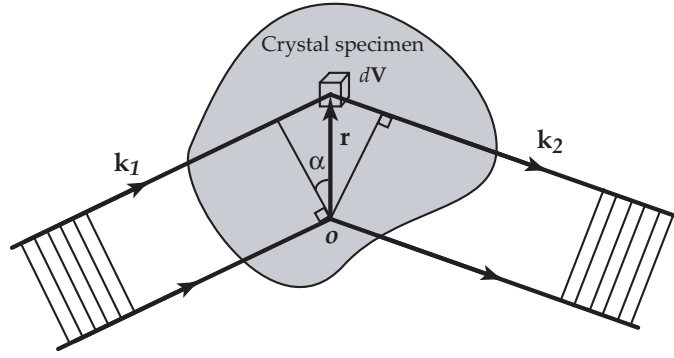
Figure G.2: Illustration of Bragg scattering. The difference in phase factor of waves scattered from volume elements $\mathbf{r}$ apart is given as $e^{j(\mathbf{k}_1-\mathbf{k}_2)\cdot\mathbf{r}}$. The length in part that the incident wave must travel longer to the point $\mathbf{r}$ then to the point o is given as $\sin\alpha r$. This give rise to a phase $2\pi\sin\alpha r/\lambda$ which is equal to $\mathbf{k}_1\cdot\mathbf{r}$. The phase difference from $\mathbf{r}$ and o of the scattered wave $\mathbf{k}_2$ is $-\mathbf{k}_2\cdot\mathbf{r}$. The overall phase difference is therefore given as $(\mathbf{k}_1-\mathbf{k}_2)\cdot\mathbf{r}$ which yields a difference in phase factor of $e^{j(\mathbf{k}_1-\mathbf{k}_2)\cdot\mathbf{r}}$. [Kittel 1986, p. 35]

From (G.16) it is seen that when $\Delta\mathbf{k}=\mathbf{G}$ then $A=Vn_\mathbf{G}$ where V is the volume of the crystal. When $\Delta\mathbf{k}$ differs significantly from any $\mathbf{G}$, A is negligibly small and amplitude of the electric and magnetic field vector in the electromagnetic wave scattered is therefore negligibly small. That is, a wave is only scattered when the Bragg diffraction condition is satisfied namely

$$\Delta\mathbf{k}=\mathbf{G} \tag{G.18}$$

It is seen from (G.18) that it is the set of reciprocal lattice vectors that determines the possible reflections. When an electron is scattered the energy $\hbar\omega$ is conserved. Thus the frequency of the incident wave is equal to the emergent wave $\omega_1=\omega_2$ or $ck_1=ck_2$ or $k_1=k_2$ or $k_1^2=k_2^2$. Combining this with (G.18) and (G.17) yields

$$\mathbf{k}_1+\mathbf{G}=\mathbf{k}_2 \Rightarrow (\mathbf{k}_1+\mathbf{G})^2=\mathbf{k}_2^2 \Rightarrow (\mathbf{k}_1+\mathbf{G})^2=k_1^2 \tag{G.19}$$

[Kittel 1986, 29-36]

Origin of Energy Gabs

In order to describe the origin of energy gabs a 1-dimensional linear crystal of lattice constant a is used. When the Bragg diffraction condition is met, no wavelike solutions to the Schrödinger equation exist. The Bragg condition is given in (G.19) which in 1-dimension yields

$$(k+G)^2=k^2 \Rightarrow k=\pm\frac{1}{2}G \Rightarrow k=\pm\frac{n\pi}{a} \tag{G.20}$$

where $G=(n2\pi)/a$. The Bragg reflection condition is met for $k=\pm(n\pi)/a$. The zone between $\pm\pi/a$ is called the first Brillouin zone. When a wavevector of a traveling wave is equal to the Bragg condition $k=\pm\pi/a$, a wave traveling to the right is Bragg reflected to travel to the left and a wave traveling left is Bragg reflected to travel to the right. All the following

Bragg reflections will reverse the direction of the wave and a standing wave will therefore be formed. Two standing waves can arise from the two traveling waves. One of them is the wave traveling to the left and the other is the one traveling to the right, namely

$$\psi(x) = e^{(\pm j\pi x/a)} \tag{G.21}$$

The two possible standing waves can arise as

$$\psi_1(x) = e^{(j\pi x/a)} + e^{(-j\pi x/a)} = 2\cos(\pi x/a) \tag{G.22a}$$

$$\psi_2(x) = e^{(j\pi x/a)} - e^{(-j\pi x/a)} = 2j\sin(\pi x/a) \tag{G.22b}$$

Where the standing waves both are a sum of a right and a left traveling wave. The probability densities of the two possible standing waves are given as

$$|\psi_1(x)|^2 = 4\cos^2(\pi x/a) \tag{G.23a}$$

$$|\psi_2(x)|^2 = 4\sin^2(\pi x/a) \tag{G.23b}$$

From (G.23) it can be seen that the two different standing waves pile up electrons at different zones. The potential energy of a traveling electron in the field of the positive ion cores in a periodic lattice is not constant over distance and the two standing waves will therefore have different values of potential energy. Figure G.3 shows the potential energy of a conducting electron in a field of ion cores of a 1-dimensional linear lattice together with the distribution of probability density for the two possible standing waves and a traveling wave. It can be
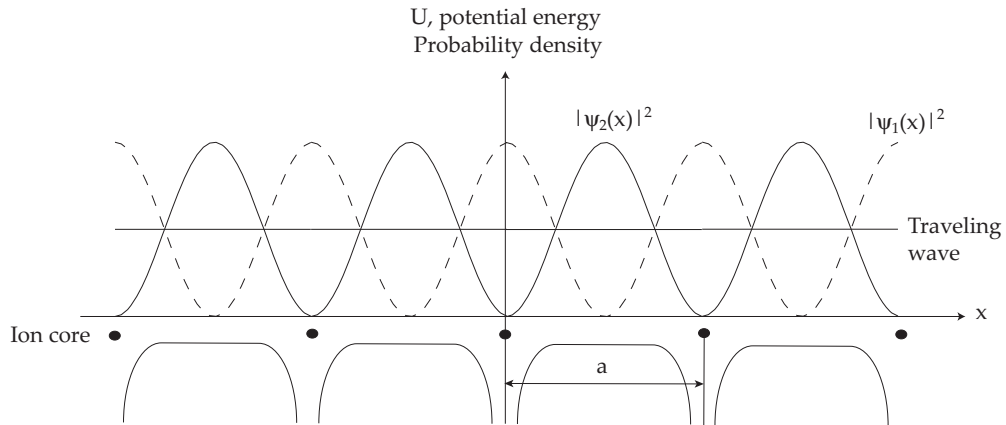
Figure G.3: The potential energy of a conducting electron in a field of ion cores of a 1-dimensional linear lattice together with the distribution of probability density for the two possible standing waves and a traveling wave. [Kittel 1986, p. 162]

seen from Figure G.3 that when the average potential energy over the three charge distributions is calculated, a different answer arises. The average potential energy of $|\psi_1(x)|^2$ is lower than the average potential energy of the traveling wave. The average potential energy of $|\psi_2(x)|^2$ is higher than the average potential energy of the traveling wave. The energy gab E_g is given as the difference in average potential energy of $|\psi_2(x)|^2$ and $|\psi_1(x)|^2$, that is

$$E_g = <V(x)_{|\psi_2(x)|^2}> - <V(x)_{|\psi_1(x)|^2}> \tag{G.24}$$

where $<>$ denotes the time-average value. [Kittel 1986, pp. 159-163]

Wave Equation of the Electron

(G.24) describes the energy gab if the wavevector $\mathbf{k}$ is at $k = \pm\pi/a$. In order to describe the wave equation of an electron in a general 1-dimensional periodic potential at general values of k the 1-dimensional version of single-particle time independent Schrödinger equation from (G.1) is used. Furthermore it is used that the potential energy is invariant under any crystal translation $V(x) = V(x+a)$. Because of this the potential energy may be expanded as a Fourier series in the reciprocal lattice scalars G

$$V(x) = \sum_G V_G e^{jGx} \tag{G.25}$$

The 1-dimensional version of single-particle time independent Schrödinger equation now yields

$$\left(-\frac{\hbar^2}{2m}\frac{d^2}{dx^2} + \sum_G V_G e^{jGx} \right)\psi(x) = E\psi(x) \tag{G.26}$$

The solution $\psi(x)$ to (G.26) can also be expanded as a Fourier series in the permitted wavevectors k given by (G.5)

$$\psi(x) = \sum_k C(k) e^{jkx} \tag{G.27}$$

Substituting (G.27) into (G.26) yields

$$\sum_k \frac{\hbar^2}{2m} k^2 C(k) e^{jkx} + \sum_k \sum_G C(k) V_G e^{j(G+k)x} = E \sum_k C(k) e^{jkx} \tag{G.28}$$

Rearranging terms yields

$$\left(\frac{\hbar^2 k^2}{2m} - E \right)\sum_k C(k) e^{jkx} + \sum_G V_G \sum_k C(k-G) e^{jkx} = 0 \tag{G.29}$$

or

$$(\lambda_k - E)C(k) - \sum_G V_G C(k-G) = 0 \tag{G.30}$$

where

$$\lambda_k = \frac{\hbar^2 k^2}{2m} \tag{G.31}$$

(G.30) is called the central equation, and it presents a set of linear equations. The number of equations is given as the number coefficients C. When all the C's are determined the wavefunction in (G.27) is given as

$$\psi(x) = \sum_G V_G C(k-G) e^{j(k-G)x} \tag{G.32}$$

In order to show how (G.30) can be used, an approximate solution near the first Bragg reflection condition is calculated. First a wavevector exactly at the Bragg reflection condition is considered. That is $k^2 = (1/2G)^2$ according to (G.20). This yields that the important coefficients in the solution $\psi(x)$ is $C(1/2G)$ and $C(-1/2G)$, all the other coefficients are neglected. The solution to the Schrödinger equation is approximated as

$$\psi(x) = C(1/2G)e^{j1/2Gx} + C(-1/2G)e^{j(-1/2G)x} \tag{G.33}$$

If it is assumed that the potential energy contains only a single Fourier component, here denoted V, two equations are now given according to the central equation (G.30), namely

$$(\lambda_k - E)C(1/2G) + VC(-1/2G) = 0 \tag{G.34}$$
$$(\lambda_k - E)C(-1/2G) + VC(1/2G) = 0 \tag{G.35}$$

where $C(-3/2G)$ is transferred into first Brillouin zone by adding a suitable reciprocal lattice vector of $2G$ [Kittel 1986, p. 173]. The two equations have solutions if the determinant of the coefficients is zero

$$\begin{vmatrix} \lambda_k - E & V \\ V & \lambda_k - E \end{vmatrix} = 0 \tag{G.36}$$

which yields the energy as

$$E = \lambda \pm V = \frac{\hbar^2}{2m}(1/2G)^2 \pm V \tag{G.37}$$

It can be seen that the energy has two roots at $k = \pm\frac{\pi}{a}$.

In order to solve the wave equation of k near the Bragg diffraction condition, a two component approximation to the solution is used again. Now given as

$$\psi(x) = C(k)e^{ikx} + C(k-G)e^{j(k-G)x} \tag{G.38}$$

All other components of the solution are neglected. By the central equation in (G.30) this yields two equations

$$(\lambda_k - E)C(k) + VC(k-G) = 0 \tag{G.39}$$
$$(\lambda_{k-G} - E)C(k-G) + VC(k) = 0 \tag{G.40}$$

where $C(k-2G)$ is transferred into first Brillouin zone by adding a suitable reciprocal lattice vector of $2G$. These equations have solutions if the determinant is zero

$$\begin{vmatrix} \lambda_k - E & V \\ V & \lambda_{k-G} - E \end{vmatrix} = 0 \tag{G.41}$$

or

$$E^2 - E(\lambda_{k-G} + \lambda_k) + \lambda_{k-G}\lambda_k - V^2 = 0 \tag{G.42}$$

Solving this second order equation yields two roots of the energy, namely

$$E = \frac{1}{2}(\lambda_{k-G} + \lambda_k) \pm \sqrt{\frac{1}{4}(\lambda_{k-G} + \lambda_k)^2 - \lambda_{k-G}\lambda_k + V^2} \tag{G.43}$$

Figure G.4 shows a plot of the two roots of the energy as a function of the wavevector k. The energies are plotted with $\frac{\hbar^2}{m} = 1$, $G = 2$ and $V = 0.2$. It can be seen from Figure G.4 that each energy root describes an energy band. [Kittel 1986, pp. 167-179]
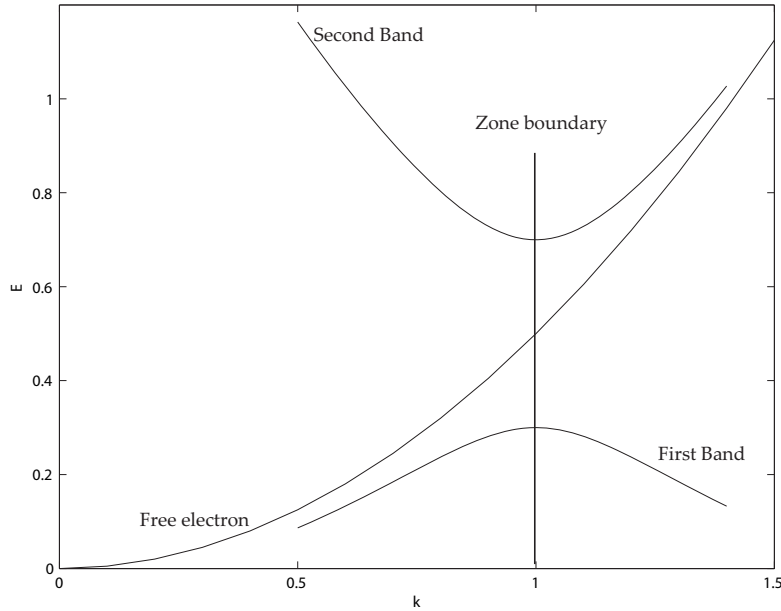
Figure G.4: Plot of energy bands near the Bragg diffraction condition $1/2G$. The kinetic energy of the free electron is drawn in order to compare the energy levels of an electron in a periodic lattice with the energy of a free electron. After Figure 9 in [Kittel 1986, p. 176]. [CD 2004, matlab/Bandgab/energyband.m]

Band Structures and Refractive Indexes of Silicon and Copper

In order to related the refractive indexes to the band structures, the plots of the calculated refractive indexes in appendix H is the starting point. By contemplating Figure H.2 on page 121, it can be seen that an abrupt change in the refractive index is found only in the case of silicon and copper. As it is these abrupt changes of the refractive index which can be related to the energy band structure of the materials, only the band structure of silicon and copper will be related to the refractive indexes.

By contemplating Figure H.2(a) it can be seen that an abrupt change in both the real and imaginary part of the refractive index for silicon can be found approximately at $\lambda = 385$ nm. The energy of the photon corresponding to the wavelength $\lambda = 385$ nm can be found as

$$E = \hbar\omega = \hbar\frac{2\pi c}{\lambda} = 3.22 \text{ eV} \tag{G.44}$$

where $\hbar = 6.583 \cdot 10^{-16}$ eVs is Planck's constant divided by 2π and the speed of light is $c = 3.0 \cdot 10^8$ m/s. The corresponding wavenumber k can be found as

$$k = \frac{2\pi}{\lambda} = 1.632 \cdot 10^7 \text{ m}^{-1} \tag{G.45}$$

By contemplating Figure H.2(b) the wavelength of the abrupt changes in the refractive index for copper can approximately be found at $\lambda = 580$ nm. The corresponding photon energy

and wavenumber is given as

$$E = 2.17 \text{ eV} \tag{G.46}$$

$$k = 1.083 \cdot 10^7 \text{ m}^{-1} \tag{G.47}$$

The lattice constants of silicon and copper are given as

$$a_{Si} = 0.543 \text{ nm} \tag{G.48}$$

$$a_{Cu} = 0.361 \text{ nm} \tag{G.49}$$

[Kittel 1986, p. 23]. The zone boundary of the first Brillouin zone in the 1-dimensional case of silicon and copper is given as

$$k_{Si} = \frac{\pi}{a_{Si}} = 5.79 \cdot 10^9 \text{ m}^{-1} \tag{G.50}$$

$$k_{Cu} = \frac{\pi}{a_{Cu}} = 8.70 \cdot 10^9 \text{ m}^{-1} \tag{G.51}$$

This shows that the wavenumbers of the photons are small compared with the first zone boundaries of the crystals. Figure G.5 shows the calculated band structures of silicon and copper. When the band structures are plotted in k-space in the first Brillouin zone the k-
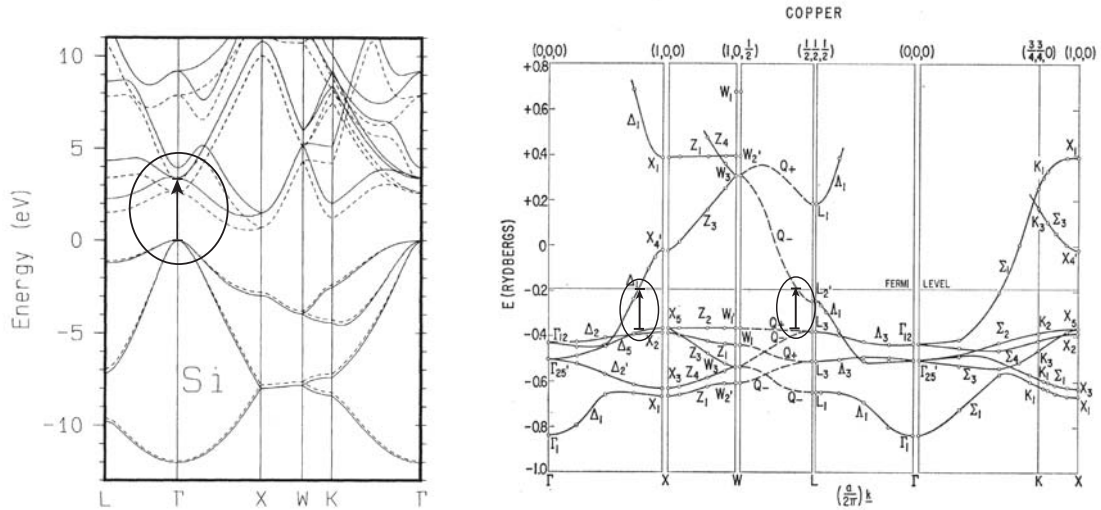
(a) Calculated electronic bands along lines of high symmetry for Si in eV. Γ is at $\mathbf{k} = \mathbf{0}$ and all the other points in k-space is inside the first Brillouin zone [Rohlfing et al. 1993].

(b) The calculated energy band of copper in the first Brillouin zone. Γ is at $\mathbf{k} = \mathbf{0}$ [Ehrenreich & Philipp 1962].

Figure G.5: The calculated band structures of silicon and copper.

values of the photons are small compared with the k-values of the zone boundaries. This means that a transition of an electron between two bands, due to a photon, will be an almost vertical transition in k-space due to the conservation of wavevector. The conservation

of wavevector is due to the conservation of linear momentum because the linear momentum is given as $\mathbf{p} = \hbar\mathbf{k}$. In Figure G.5(a) the direct band gab[1] of silicon is drawn and is approximately equal to 3.4 eV. Comparing this energy with the energy of the photon of 3.22 eV yields a good correspondence. It is therefore seen that the abrupt change in refractive index of silicon at $\lambda = 385$ nm can be connected to the direct energy gab in silicon of 3.4 eV. When the energy of the photon is equal to the band gab energy, the photon can excite an electron into a higher energy band and the photon will thereby be absorbed or slowed. When photons are slowed down or absorbed the refractive index is changed significantly from unity.

Contemplating Figure G.5(b), the band structure of copper, shows that the energy scale is in Rydberg. The Rydberg is an energy unit defined as the ground-state energy of an electron in the hydrogen atom.

$$1 \text{ Ry} = \frac{m_e e^4}{2\hbar^2} = 13.6 \text{ eV} \tag{G.52}$$

The energy of the photon corresponding to the wavelength $\lambda = 580$ nm in Rydberg is given as

$$E = \frac{2.17\text{eV}}{13.6\text{eV}} = 0.16 \text{ Ry} \tag{G.53}$$

On Figure G.5(b) the thresholds for transitions from the d-band, under the Fermi energy[2], to the conducting band are drawn. It can be seen that these energy gabs are approximately of 0.16 Ry which is approximately equal to the energy of the photon, corresponding to the wavelength of abrupt change in refractive index of copper. It is therefore concluded that the abrupt change in refractive index of copper around the wavelength 580 nm can be connected to the transitions from the d-band to the conducting band in the band structure of copper.

In general, it is observed that the abrupt changes in the refractive index at given wavelengths are closely related to the band gaps of the band structure of the materials. The band gap energy can be directly converted to the wavelength of the corresponding change in the refractive index.

---

[1]The direct band gab is the band gab between the valence band and the conducting band at $\mathbf{k} = 0$.

[2]The Fermi energy of a material is the energy boundary between the occupied orbitals and the vacant orbitals at 0 K.

Test Report of Refractive Index of Crystals

<div style="text-align: right; font-size: xx-large;">H</div>

This appendix is the test report describing the experiment where the ψ and Δ angles of silicon, copper, aluminum and silver are measured and the refractive indexes of these crystals are calculated. All discussion of the test results and conclusions drawn about the test results are found in Chapter 7 in the main report.

Purpose

The purpose of this test is to measure the ellipsometric parameters of several crystals by means of an ellipsometer and from these calculate the refractive index as a function of the wavelength. The calculated values are then compared to the table values of the refractive indexes. The crystals under investigation are silicon, silver, copper and aluminum.

Equipment and Materials

The equipment used during the experiment is:

- SENTECH Instruments - UV-VIS-NIR spectroscopic ellipsometer SE 850
- SENTECH Instruments - Spectraray II Software
- Silicon sample
- Copper sample
- Aluminum sample
- Silver sample

Procedure

The experiment was performed on Skjernvej 4C in room 1.109 on the 20th of October 2004. The ellipsometer was powered up, the xenon lamp was turned on, the incident angle was set to 70° on the ellipsometer and the program Spectraray II was initiated. The sample was placed on the ellipsometer sample stage and the sample stage was adjusted such that the reflected light hit the detector inside the ellipsometer precisely, which was done by measuring the intensity. This is important in order to get proper measurements. The ψ-Δ spectrum was measured by means of Spectraray II from 350 nm to 825 nm with the UV-VIS setting in Spectraray II. The data was stored on a floppy disk.

Results

The data can be found on [CD 2004, /matlab/test_surface_201004]. The measured ψ-Δ spectrums for the surfaces used are shown in Figure H.1
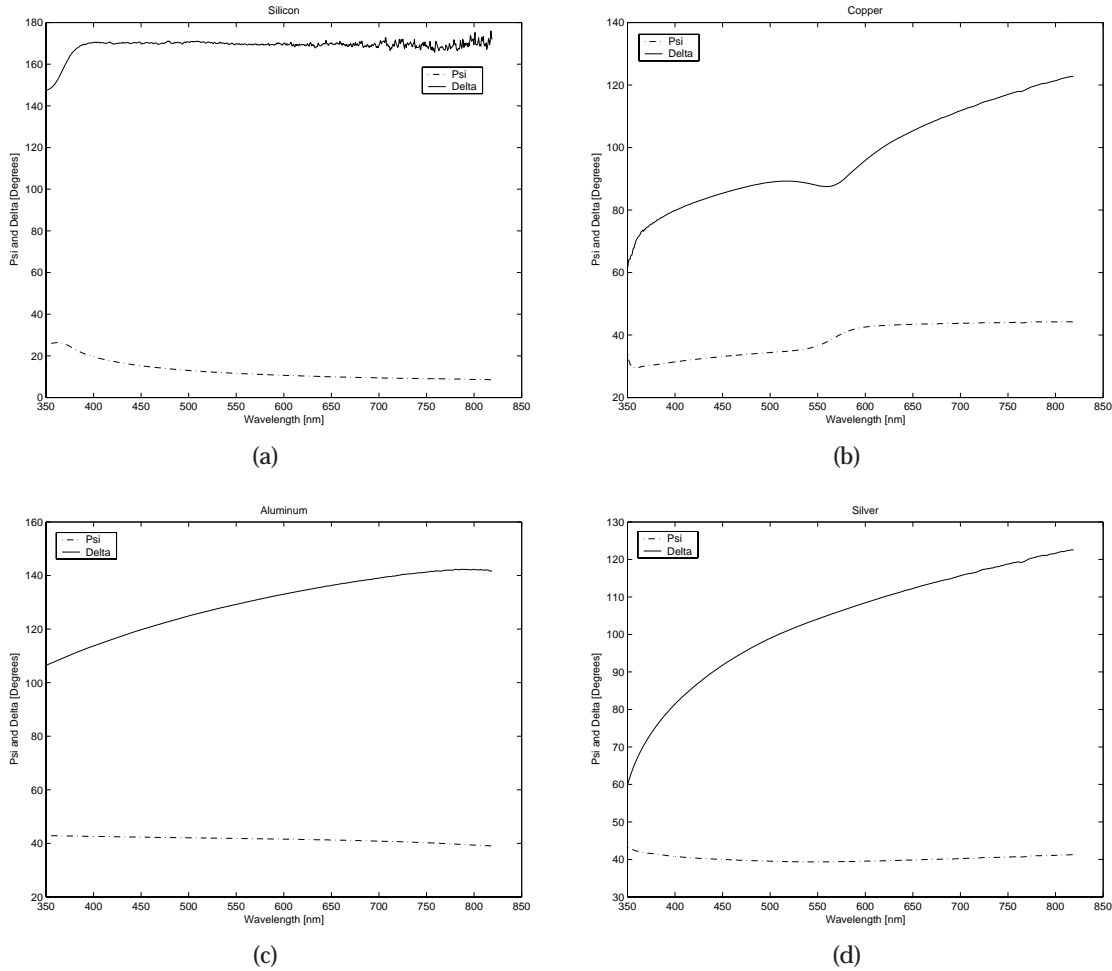
(a)

(b)

(c)

(d)

Figure H.1: ψ and Δ as a function of wavelength measured with Sentech UV-VIS-NIR spectroscopic ellipsometer SE 850 on silicon, copper, aluminum and silver. [CD 2004, matlab/surface_test/RefractiveIndex.m]

It is seen from Figure H.1 that the curves of ψ and Δ, for all the surfaces, in general are smooth curves. The only exception is the Δ angle of silicon which fluctuates at wavelengths longer than 600 nm. None of them are subject to a considerable amount of random noise. This is to be expected due to the nature of ellipsometric measurements.

Data Processing

In order to convert the measured ellipsometric parameters ψ and Δ into the refractive index $\tilde{n}$ the relation (5.4) on page 33 is used, namely

$$\tilde{n} = \frac{\left[\sqrt{1 - 4\sin^2\theta\tan(\psi)\,e^{j\Delta} + 2\tan(\psi)\,e^{j\Delta} + \tan^2(\psi)\,e^{j\Delta}}\right] n_0 \sin\theta}{\cos\theta\left[1 + \tan(\psi)\,e^{j\Delta}\right]} \qquad (\text{H.1})$$

where θ is the incident angles, n_0 is the refractive index of the ambient, in this case air. Using (H.1), the refractive index is calculated as a function of wavelength by means of the measured ψ-Δ spectrum. A plot of the real and the imaginary part of the refractive index as a function of the wavelength for the four surfaces together with the table values of the real and imaginary part of the refractive index is shown in Figure H.2 and H.3.

(a)   (b)
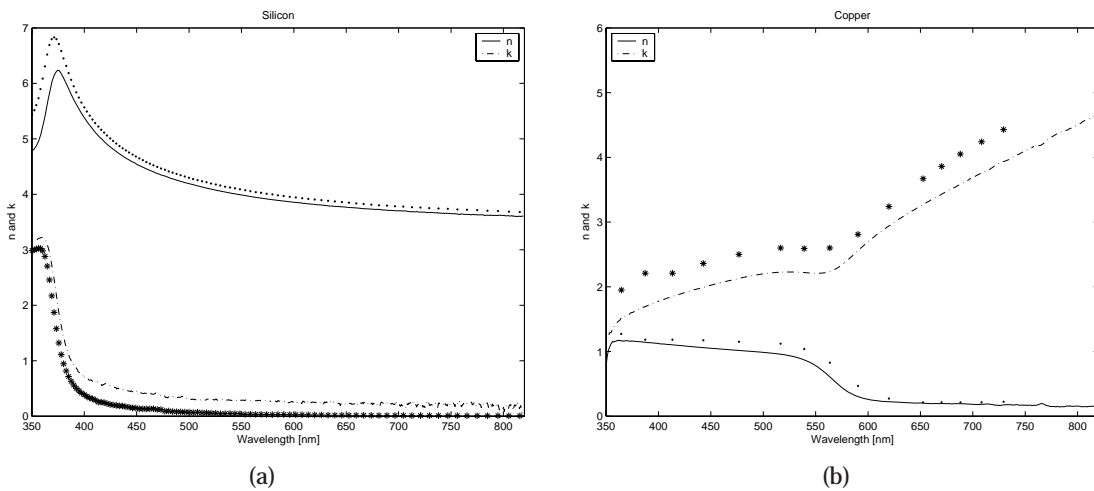
Figure H.2: The calculated real n and imaginary k part of the refractive index as a function of wavelength together with table values of the real and imaginary part of the refractive index of silicon and copper. The real part of the table values are dots and the imaginary part are asterisks. The table values are found in [Palik 1998] and [Klein & Furtak 1986]. [CD 2004, matlab/surface_test/RefractiveIndex.m]
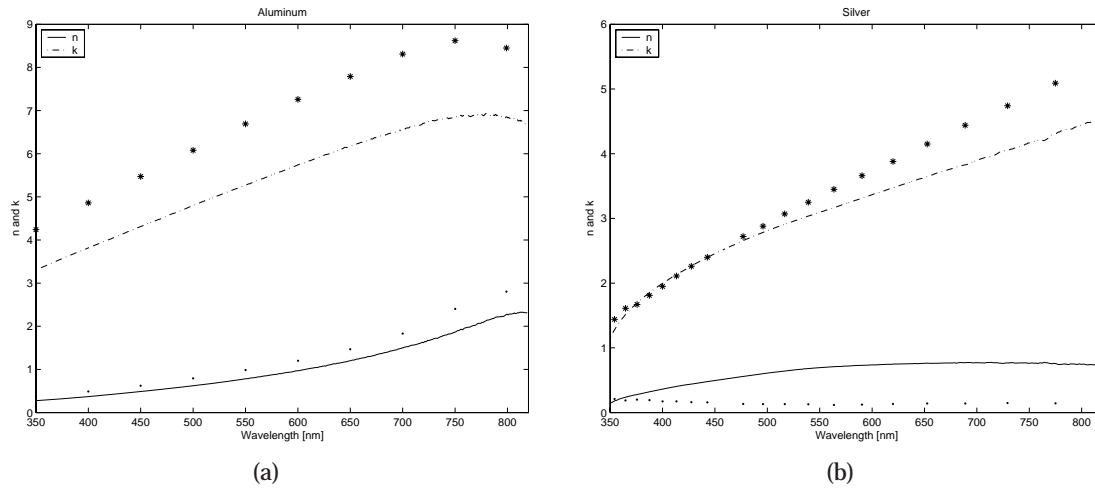
Figure H.3: The calculated real n and imaginary k part of the refractive index as a function of wavelength together with table values of the real and imaginary part of the refractive index of aluminum and silver. The real part of the table values are dots and the imaginary part are asterisks. The table values are found in [Palik 1998]. [CD 2004, matlab/surface_test/RefractiveIndex.m]

Test Report of the Thickness of an SiO$_2$ Film on Si

<div style="text-align: right">I</div>

This appendix is the test report describing the measurement of the silicon dioxide film thickness. All discussion of the test results and conclusions drawn about the test results are found in Chapter 8 in the main report.

Purpose

The purpose of this test is to measure the ellipsometric parameters in order to enable calculation of the thickness of a silicon dioxide layer on a silicon substrate as a function of the wavelength by means of an ellipsometer.

Equipment and Materials

The equipment used during the experiment:

- SENTECH Instruments - UV-VIS-NIR spectroscopic ellipsometer SE 850

- SENTECH Instruments - Spectraray II Software

- SENTECH Silicon wafer with a silicon dioxide film

Procedure

The experiment was performed on Skjernvej 4C in room 1.109 on the 2nd of November 2004. The ellipsometer was powered up, the xenon lamp was turned on, the incident angle was set to 70° on the ellipsometer and the program Spectraray II was initiated. The sample was placed on the ellipsometer sample stage and the sample stage was adjusted such that the reflected light hit the detector inside the ellipsometer precisely, which was done by measuring the intensity. This is important in order to get proper measurements. The ψ-Δ spectrum was measured by means of Spectraray II from 350 nm to 825 nm with the UV-VIS setting in Spectraray II. The data was stored on a floppy disk.

Results

The measured ψ-Δ spectrum for the sample used is shown in Figure I.1.
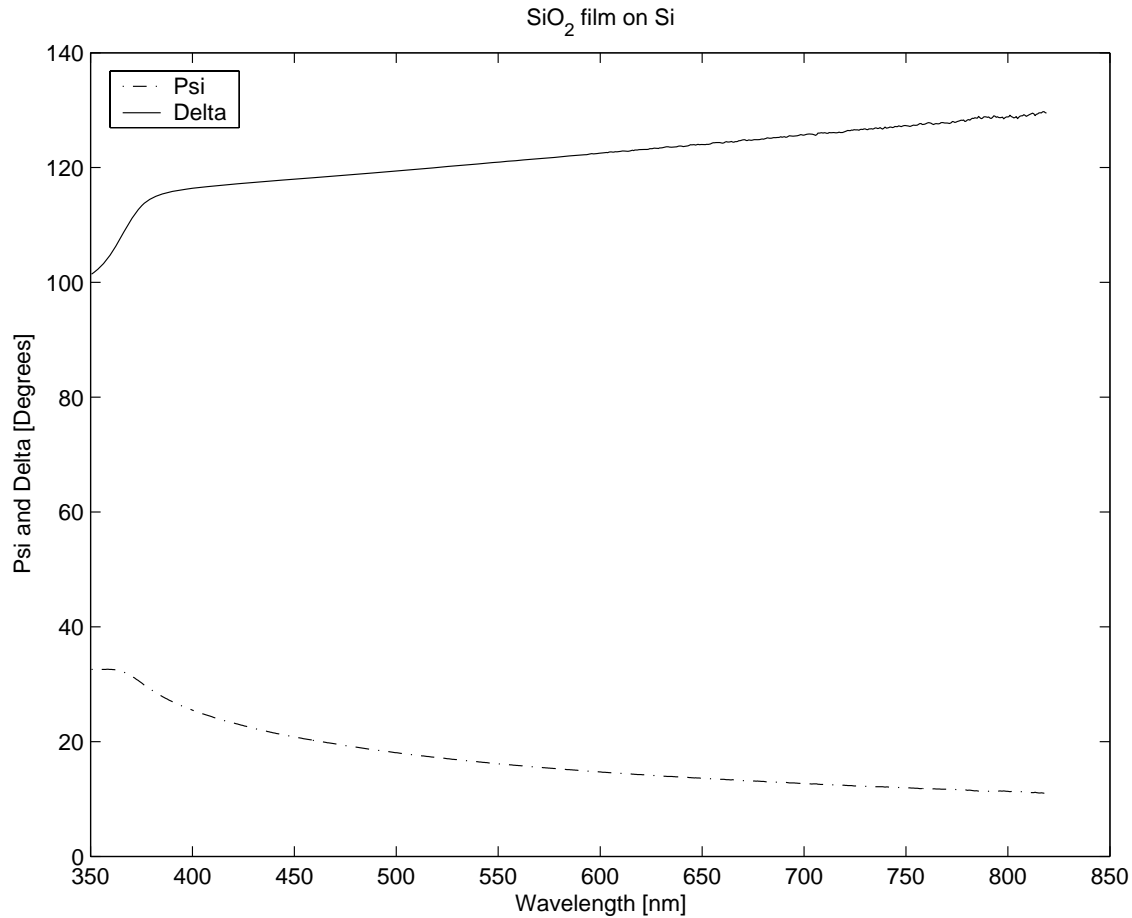
Figure I.1: ψ and Δ as a function of wavelength measured with Sentech
UV-VIS-NIR spectroscopic ellipsometer SE 850.

It is seen from the figure that the curves of ψ and Δ are relative smooth curves. Some small fluctuations do however exist in the higher wavelength region for Δ.

The measurement is not subject to a considerable amount of random noise. This is to be expected due to the nature of ellipsometric measurements.

Data Processing

The calculation of the SiO$_2$ film thickness is done by utilizing the method described in Section 5.2. In this calculation the angle of incidence, the free-space wavelength of the light, the ellipsometric parameters ψ and Δ and the refractive indexes for air, SiO$_2$ and Si must be known in order to determine the film thickness. Values for the refractive index of Si and SiO$_2$ are found by use of [Palik 1998, I: pp. 563-565] and [Index of Refraction Values and Photonics Calculations 2004] respectively.

Solving (5.14) leads to two solutions, both complex. The solution with a positive real part and the smaller imaginary part is chosen. The result of these calculations is presented in Figure I.2
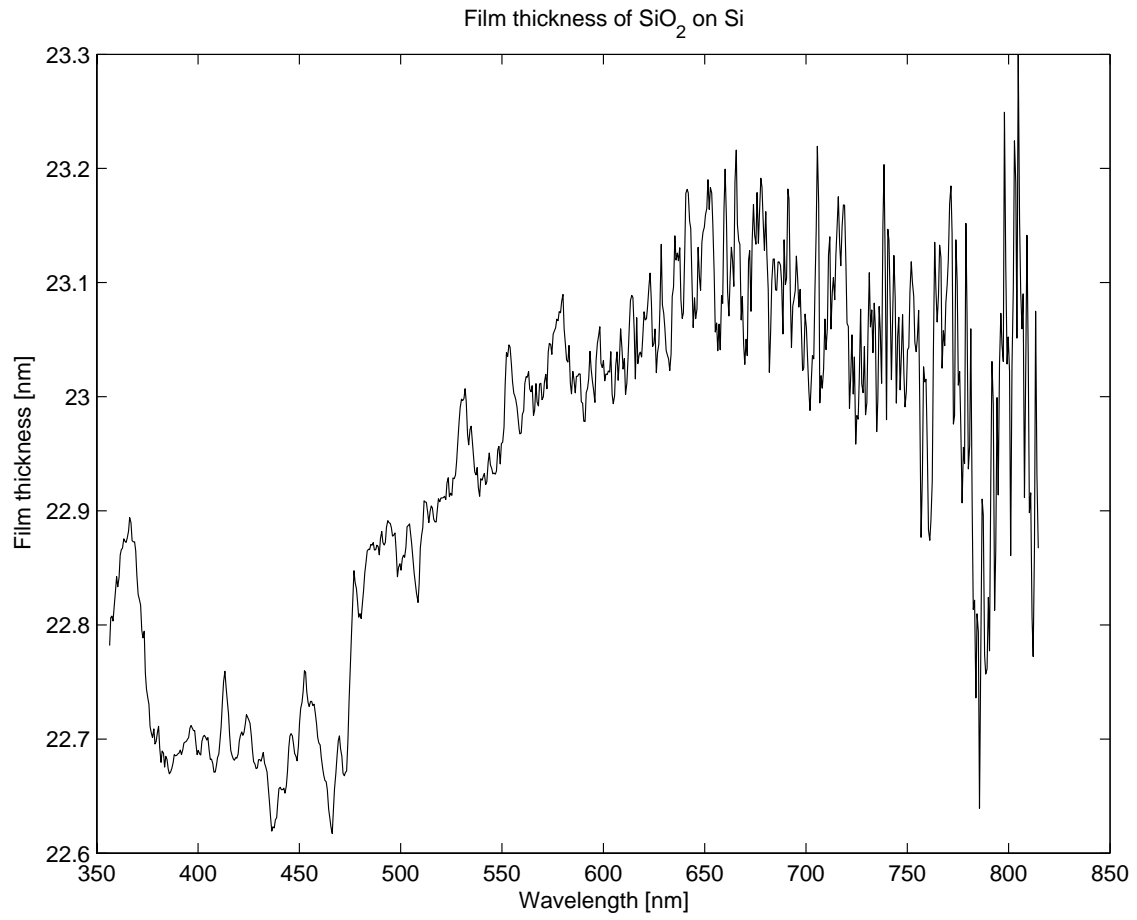
Figure I.2: The calculated thickness of the SiO$_2$ film as a function of wavelength. [CD 2004, matlab/thickness/film_thickness_sio_2.m]

Test Report of the Thickness of a Polymer Film on Si

J

This appendix is the test report describing the experiment where ψ and Δ of the polymer PI-5878G from HD MicroSystems are measured and the thickness of the polymer is calculated. The polymer was spin coated on a silicon wafer by NanoNord. Two silicon wafers with polymer film were made. The two polymers were spin coated with the same angular velocity, namely 4000 RPM. The wafers were however spin coated for different time periods, namely 1 and 5 minutes.

All discussion of the test results and conclusions drawn about the test results are found in Chapter 9 in the main report.

Purpose

The purpose of this test is to determine the thickness, in the center of the sample, of the two polymers by means of a ψ-Δ measurement performed with the ellipsometer. Another purpose is to investigate the uniformity of the thickness of the two polymer films on the wafers by means of a sequence of ψ-Δ measurements.

Equipment and Materials

The equipment used during the experiment:

- SENTECH Instruments - UV-VIS-NIR spectroscopic ellipsometer SE 850

- SENTECH Instruments - Spectraray II Software

- Two silicon wafers with a spin coated PI-5878G polymer film

Procedure

The procedure of the two experiments is almost the same. In both experiments the ellipsometer was powered up, the xenon lamp was turned on, the incident angle was set to 70° on the ellipsometer and the program Spectraray II was initiated. The sample was placed on the ellipsometer sample stage and the sample stage was adjusted such that the reflected light hit the detector inside the ellipsometer precisely, which was done by measuring the intensity. This is important in order to get proper measurements. The rest of the procedure of the two experiments is not alike and will therefore be described separately.

Thickness

The experiment was performed on Skjernvej 4C in room 1.109 on the 9th of December 2004. Two ψ-Δ spectrums were measured, one for each wafer. The ψ-Δ spectrums were measured from 350 nm to 825 nm at the middle of the two polymers and they were stored on a floppy disk.

Uniformity of Film Thickness

The experiment was performed on Skjernvej 4C in room 1.109 on the 12th of December 2004. In this experiment 68 ψ-Δ spectrums were measured, 34 for each wafer. Figure J.1 depicts wafer. The figure shows four axes, an x-axis, a y-axis, a u-axis and a v-axis. These are the
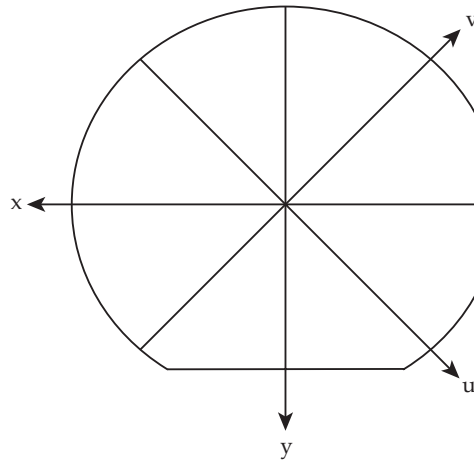
Figure J.1: The axes on the wafer along which the ψ-Δ spectrums are measured. In case of the thickest polymer film the spectrums are measured along x and y. In case of the thinnest polymer film the spectrums are measured along u and v.

axes along which the ψ-Δ spectrums are measured. In the case of the silicon wafer with the thickest polymer layer imposed the ψ-Δ spectrums were measured along the x-axis and the y-axis. 17 spectrums were measured along each axis, with the positive direction along the axis. The measurements were performed from -40 mm to 40 mm with a step of 5 mm between each measurement. In the case of the thinnest polymer film the ψ-Δ spectrums were measured along the u-axis and the v-axis. 17 spectrums were also measured along each axis, with the positive direction along the axis. The measurements were again performed from -40 mm to 40 mm with a step of 5 mm between each measurement.

All the ψ-Δ spectrums were measured from 350 nm to 825 nm by means of the UV-VIS setting in Spectraray II. All the spectrums were stored on a floppy disk.

Results

In this section the ψ-Δ spectrums of the measurements are shown. In the experiment where the uniformity of the two polymer films are tested there are 68 ψ-Δ spectrums and they will

therefore not be shown in this appendix. For reference to these spectrums see [CD 2004, matlab/polymer_thickness/uniformity/]. In the experiment were the thicknesses of the two polymer films is determined, only one ψ-Δ spectrum for each wafer were measured and they are presented in the following subsection.

Thickness

The measured ψ-Δ spectrums of the polymer films on the silicon wafers are shown in Figure J.2 and J.3. It can be seen from the figure that due to the large thickness of the films, an
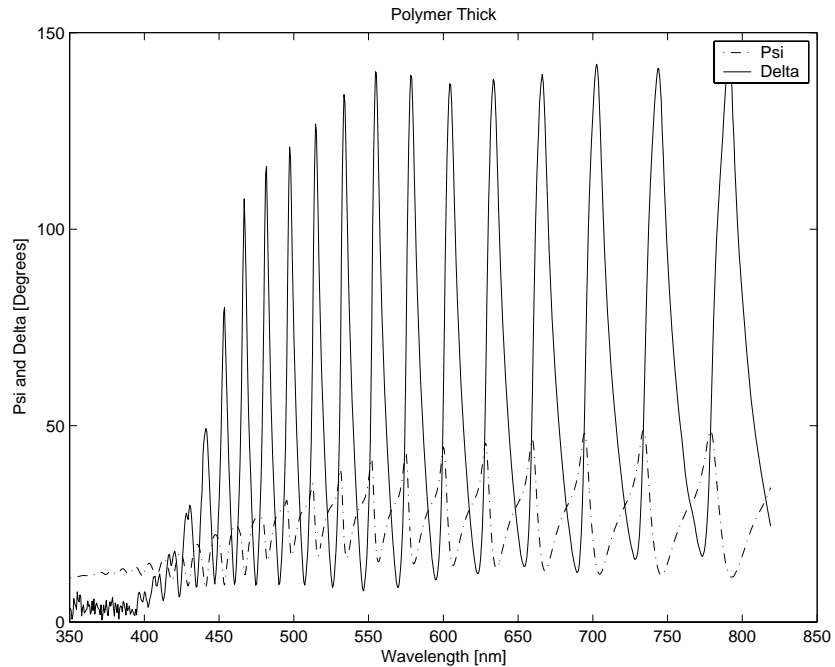
Figure J.2: ψ-Δ spectrums of the thickest polymer film. [CD 2004, matlab/polymer_thickness/psidelta_plotter.m]

interference pattern is seen in ψ and Δ. It can also be seen that the period between peaks is larger for the thin film, indicating that it in fact is thinner.

Uniformity of Film Thickness

See [CD 2004, matlab/polymer_thickness/uniformity/].
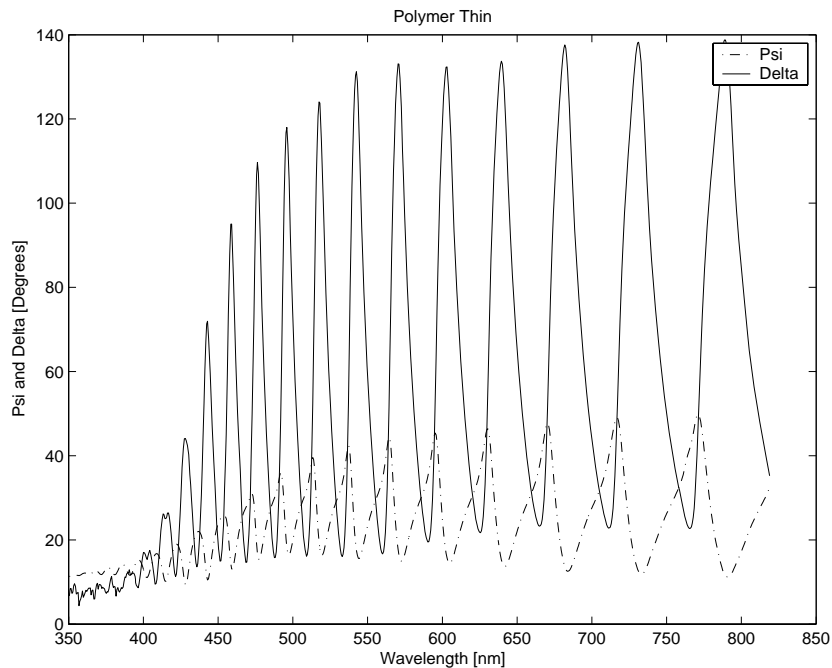
Figure J.3: ψ-Δ spectrums of the thinner polymer film. [CD 2004, mat-lab/polymer_thickness/psidelta_plotter.m]

Data Processing

Thickness

The calculation of the two polymer film thicknesses is done by utilizing the method described in Section 5.3. In this method the interference pattern in ψ and Δ is used to estimate the thickness of the film imposed on the surface. In order to perform the calculation, the index of refraction of both the polymer and the silicon wafer must be know. The index of refraction of the polymer is found in [MicroSystems 2003], and the index of refraction of the silicon wafer is found by use of [Index of Refraction Values and Photonics Calculations 2004].

The result of these calculations is presented in Figure J.4(a) for the thick polymer and in Figure J.4(b) for the thin polymer. The ψ-Δ spectrum between 350 nm and 450 nm does not contain adequate information to determine the thickness as a function of wavelength.

Uniformity of Film Thickness

In order to determine the uniformity of the thickness of the two polymer films, the thickness of all the points on the surface where the ψ-Δ spectrums are measured must be determined. It is chosen to calculate the thickness in the wavelength interval from 650 nm to 825 nm. The thickness in the point where the ψ-Δ spectrum is measured is then found as the average value of the thickness over the wavelength interval. Figure J.5 depicts the thickness of the thick polymer film measured over the *x*- and the *y*-axis as depicted on Figure J.1. Figure J.6 shows the thickness of the thin polymer film measured over the *u*- and the *v*-axis as shown on Figure J.1.
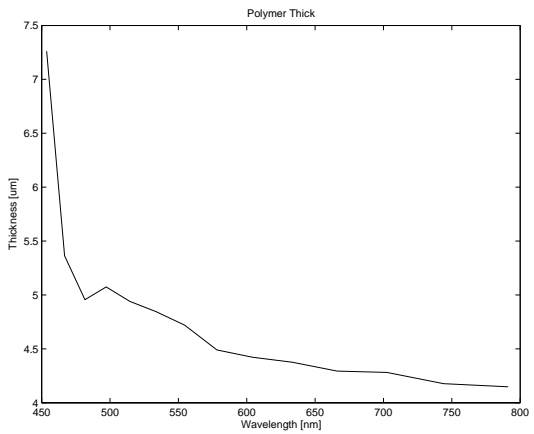
(a) Thickness of the thick polymer at the middle, as a function of wavelength.
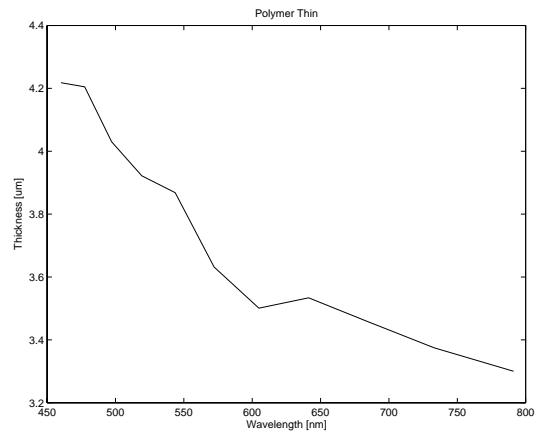
(b) Thickness of the thin polymer at the middle, as a function of wavelength.

Figure J.4: Polymer thickness at the middle of the wafer, as a function of wavelength. [CD 2004, matlab/polymer_thickness/film_thickness_polymer_spectrum.m]
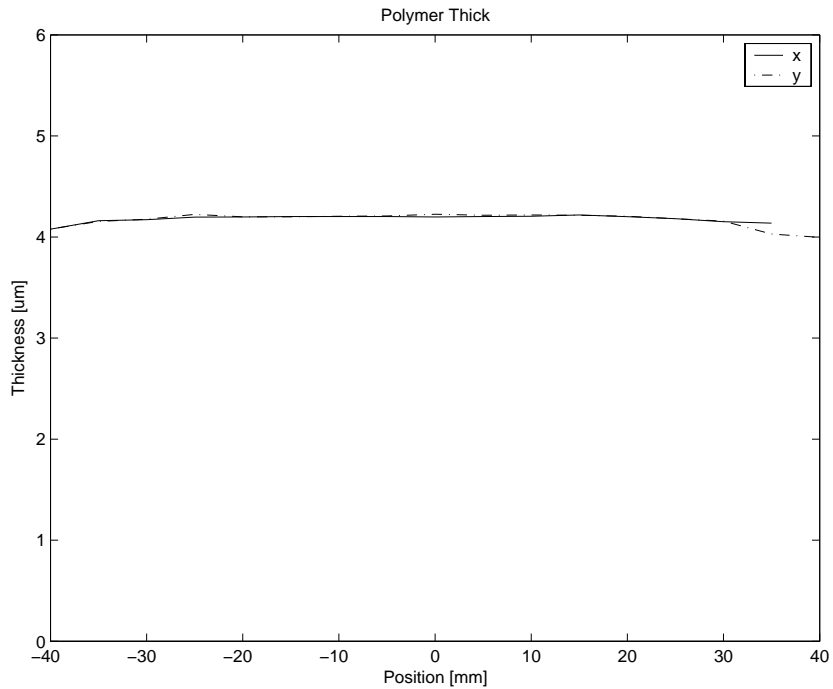
Figure J.5: Thickness of the thick polymer film measured over the *x*- and the *y*-axis as depicted in Figure J.1. [CD 2004, matlab/polymer_thickness/film_thickness_polymer.m]
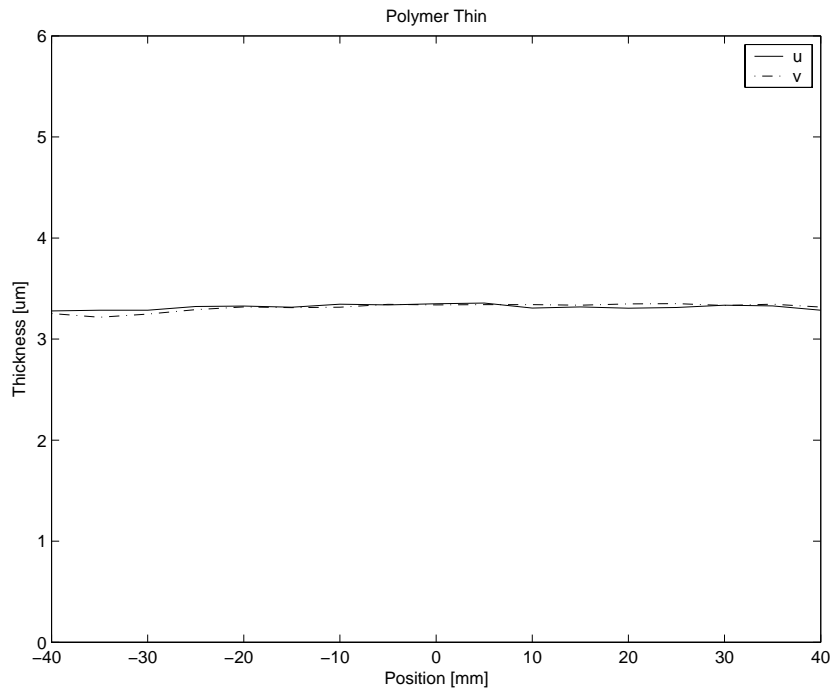
Figure J.6: Thickness of the thin polymer film measured over the *u*- and the *v*-axis as depicted in Figure J.1. [CD 2004, matlab/polymer_thickness/film_thickness_polymer.m]